MicroRNAs as therapeutic targets in heart diseases

Cover Design: Patrizio Raso e Andrea Raso
Printing: ProefschriftMaken || www.proefschriftmaken.nl

ISBN/EAN: 978-94-6380-300-7

MicroRNAs as therapeutic targets in heart diseases

DISSERTATION

to obtain the degree of Doctor at Maastricht University,
on the authority of the Rector Magnificus
Prof.dr. Rianne M. Letschert,
in accordance with the decision of the Board of Deans,
to be defended in public
on Thursday 2 May 2019 at 14.00 hours

by

Andrea Raso

Supervisor:
Prof. dr. L.J de Windt .

Co-Supervisor:
Dr. P. da Costa Martins .

Assessment Committee:
Prof. dr. B.L.M. Schroen (Chair) ;
Prof. dr. G. Condorelli, Milan, Italy ;
Prof. dr. S. Engelhardt, Technische Universität München, Germany ;
Prof. dr. M. Stoll .

Financial support for the publication of this thesis as provided by Maastricht University is gratefully acknowledged.

TABLE OF CONTENTS

CHAPTER 1

GENERAL INTRODUCTION

The study of the heart, of its symbolic value and its (patho)physiology, represented from the antiquity a mystic point of contact between philosophy, art and science.

A multidisciplinary genius as Leonardo da Vinci ascribed to the heart admirable properties suggesting even divine origins:

"Core, instrumento mirabile, invenzionato dal sommo Maestro"

In fact, the heart is a remarkable organ, the first to form and function in developing vertebrates already from early embryonic phase [1]. The cardiac muscle beats incessantly during our entire life span and any heart insult can have dramatic consequence on the whole organism.

Being able to understand and control this precious power, especially when its activity is altered, is a challenge that has fascinated mankind from the dawn of time.

The heart failure syndrome

Heart failure (HF) is a syndrome occurring under conditions of sustained cardiac dysfunction, or rather, when the heart is not able anymore to carry out its task: pump enough blood to satisfy the metabolic needs of the tissues in the body. As a syndrome, HF is characterized by symptoms and signs [2]. Weakness, dyspnea, edema and rapid/irregular heartbeats are some of the indications that appear as soon as the protective neurhormal systems, activated by the organism to contain the progression of heart diseases, cease to be efficient.

The clinical classification of HF patients can be performed applying different strategies; based on stages of disease progression, as suggested by American College of Cardiology and American Heart Association (ACC/AHA) [3], or on limitations during physical activity, as proposed by the New York Heart Association (NYHA) and used by the European Society of Cardiology (ESC) [4]. Historically, the percentage of blood pumped out by the left ventricle each contraction, the ejection fraction (EF), was used as an important parameter for the syndrome evaluation. Considering this measurement, it is possible to distinguish two main classes of heart failure:

- Heart Failure with reduced Ejection Fraction (HFrEF): comprises patients with an EF <40%. The myocardium is not able to contract effectively because of a contraction problem. Previously, this class was referred as "systolic HF"; nevertheless some HFrEF patients can present also diastolic dysfunction (the left ventricle can not relax or fill completely). Today HFrEF patients are the only one showing beneficial treatment effects from the current pharmacotherapy [5].
- Heart Failure with preserved Ejection Fraction (HFpEF): more challenging to diagnose compared with HFrEF, it refers to patients with an EF ≥ 50%. They present elevated levels of natriuretic peptides (BNP.35 pg/ml and/or NT-proBNP.125 pg/m) and/or diastolic

dysfunction [4]. Epidemiological reports show an increase of the prevalence of HFpEF compared to HFrEF [6].

There is a third class, considered as a "grey area" between the mentioned two, the Heart Failure with mid-range Ejection Fraction (HFmrEF). This group of patients has an intermediate EF value of 40-49%. They appear to have mild systolic dysfunction with characteristics of diastolic dysfunction [4], and show reduced mortality compared to HFrEF, but their rates of rehospitalization can be analogous [7].

Heart diseases

The HF syndrome is the common final endpoint of diverse diseases. The origins of these pathological conditions are different. Their causes can affect in concurrence or singularly and can lead to the structural and functional alterations of the heart:

- Coronary artery disease: the thrombotic occlusion of a coronary represents the origin of most cases of myocardial infarction (heart attack)[8]. The event of thrombosis is the main trigger following the rupture of an atherosclerotic plaque. Stress conditions of the coronaries can promote processes of vessel wall alterations. The consequence is a site-accumulation of lipid and lipid-laden macrophages (foam cells) deposits with the constitution of an atherosclerotic plaque. The destabilization of this plaque induces the formation of a thrombus causing the obstruction of the vessel. The final result is a necrotic damage of the cardiac muscle due to a lack of blood perfusion of the myocardium.
- Hypertensive heart disease: many patients with heart failure have a history of high blood pressure. In this condition, the heart has to pump harder in order to guarantee an adequate circulation of the blood throughout the entire organism [9]. As a consequence of this excessive workload, during the complete progression of the pathology, the cardiac muscle becomes first too stiff and later too weak. The end-stage is the overload of the organ with a volume enlargement and reduced function.
- Cardiomyopathies: primary diseases of the myocardium, their etiology is variable and often unknown [10]. Also referred as "non-coronary cardiomyopathies", they can be acquired or inherited [11]. The origin of the acquired ones can be found in other diseases (as diabetes and thyroid disease), conditions (as infections or complication during the last months of pregnancy) or factors (such as cocaine or alcohol abuse). The inherited cardiomyopathies are a important topic of biomedical research [12]. We distinguish three main categories of cardiomyopathies: hypertrophic (HCM), dilated (DCM) and restrictive (RCM) cardiomyopathy. More recently, a new category, the arrhythmogenic cardiomyopathy (ACM), has been included and generally refers to arrhythmogenic right ventricular dysplasia[12-14].
- Other diseases: this last category includes different diseases such as faulty heart valves, congenital heart defects and *takotsubo* syndrome, also known as broken heart

syndrome. The latter consists in a transient apical ballooning of the left ventricle caused by catecholamine release following a stressful event [15]. Usually, it is a reversible heart failure condition, but in acute cases can lead to cardiac death due to arrhythmia, myocardial infarction or cardiac rupture.

Pathological cardiac remodeling and molecular mechanisms

Pathological cardiac remodeling is the result of cardiac injuries translated in molecular, cellular and interstitial modifications with a clinical outcome of changes in size, shape and function of the heart [16]. We already described that cardiac injuries have variable etiologies; the consequence is the remodeling of the heart, mainly influenced by hemodynamic load, neurohormal activation and genetic factors. On the cellular level, the cardiomyocyte compartment is highly compromised.

The ischemic shock induced by myocardial infarction can have the devastating consequence of an extended loss of cardiomyocytes reaching up to 25% of the total amount present in the left ventricle [17]. Even if recent studies reported a temporally privileged period of regenerative repair also in human newborns [18], in adulthood the proliferative capacity of cardiomyocytes fails to repair the myocardial damage, giving place to the formation of a scar, elastic but not functional [19].

On the other side, surviving cardiomyocytes, including the ones subjected to a long stress of a hypertensive condition or of cardiomyopathies, move to hypertrophic modifications that lead to structural subcellular reorganizations that is then reflected on heart morphology [20].

- Cardiomyocyte proliferation: cardiomyocytes proliferation is a topic that has generated, and still generates, many discussions in the scientific community. In the last decade, it was established that also in human, as in other species, cardiomyocytes conserve an extremely reduced, but still present, capacity to proliferate. It was reported that cardiomyocytes are able to renew with a rate of 1% year till the age of 25. This rate decreases to 0,45% at the age of 75 [21]. Almost 50% of cardiomyocytes is exchanged during the entire life span, but as said, this proliferative capacity is not efficient enough to repair the consequence of cardiac injury in adulthood. For this reason, much work focuses on understanding the main pathways controlling the process of cardiomyocyte proliferation to clarify the low incidence of proliferation. Specific cyclin-dependent protein kinases (CDKs) are sequentially activated during different phases of the cell cycle by the oscillating synthesis and degradation of their cyclin partners. Several works reported that the modulation of the CDKs activity promotes cardiomyocyte cell cycle progression *in vitro* and *in vivo*. In particular, the overexpression of the cyclin A2 and D2 showed to induce cardiomyocyte proliferation and lead to cardiac recovery in animal models of ischemic injury [22, 23]. On the other side, the modulation of MEIS1, a

transcriptional activator that regulates the expression of the CDK inhibitors p15, p16 and p21, appears to be efficient enough to boost mitosis and production of cytokines by cardiomyocytes in the adult heart without having any negative consequences on cardiac function [24]. The Hippo pathway is another important player in cell cycle modulation. This pathway controls cell proliferation and organ-size growth through a phosphorylation cascade affecting the activity of the two transcriptional co-activators YAP and TAZ. Briefly, Mst1/2, combined with SAV1, activates trough phosphorylation LATS1/2. The activated LATS1/2, associated with Mob1, inactivates trough phosphorylation YAP. In resting cardiomyocytes, phosphorylated YAP cannot migrate from the cytoplasm to the nucleus. Transgenic mice overexpressing a constitutively active form of YAP or expressing an unfunctional form of Mst1 showed cardiac regeneration after myocardial injury through cardiomyocyte proliferation [25, 26]. It was reported that in non-regenerative cardiomyocytes YAP is blocked by destroglycan1 (Dag1), a component of a transmembrane multiprotein complex connecting actin cytoskeleton to the extracellular matrix. During neonatal life the extracellular matrix protein agrin binds Dag1 leading to myofibril disassembly and YAP activation. Recent studies reported that the overexpression of agrin promotes dedifferentiation and sarcomere disassembly in adult cardiomyocytes *in vitro*. Moreover, a single injection of recombinant agrin induces cardiac regeneration in a murine model of myocardial infarction[27, 28]. In conclusion, specific growth factors have been identified to have a positive effect on cardiomyocyte proliferation. The overexpression of neuregulin1 (NRG1), combined with the tyrosine kinase receptor ERBB2, induces mononucleated cardiomyocyte division. Moreover, the administration of NRG1β3 to chronic heart failure patients showed safety of treatment and improvement of left ventricular function at 90 days [29, 30].

- Cardiomyocyte hypertrophy: pathological cardiac hypertrophy is characterized by reactivation of a fetal gene program. Skeletal α-actin and β-myosin heavy chain (βMHC) are overexpressed proteins together with stress hallmarks such as atrial natriuretic factor (ANF) and brain natriuretic peptide (BNP)[31]. Two different phenotypes of pathological cardiac hypertrophy can be classified based on the geometry of the heart and the organization of the sarcomeres into the individual cardiomyocytes. Concentric pathological hypertrophy is mainly the result of pathological conditions (i.e. hypertension, aortic valve stenosis) leading to pressure overload situations on the heart. The geometry of the heart is modified towards thicker walls and smaller cavities. These are the consequences of the parallel addition of sarcomeres into wider cardiomyocytes. Conversely, eccentric pathological hypertrophy is associated with pathological conditions (i.e. valve disease, myocardial infarction) causing volume overload. The walls get thinner and the cavities enlarge. Cardiomyocytes increase in length due to a serial addition of sarcomeres [20]. The concentric condition can progress to eccentric remodeling leading to dilatation of the heart and subsequently heart failure. The molecular mechanisms involved in this transition remain still poorly defined, so it is important to know which main pathways are involved in the process of hypertrophy. G protein-couple receptors

(GPCRs) are fundamental player in the process of cardiac hypertrophy. In the myocardium, the most important GPCRs are the α- and β-adrenergic- and muscarinic receptors. They transduce agonist- or antagonist signals through the activation of three classes of G-protein: Gs, Gi and Gq/ G11 [32]. Adrenalin and noradrenaline exert their function trough Gs activation. Interacting with β-adrenergic receptors, these catecholamines increase heart rate and contractility. In particular, the β1-subtype appears to be almost exclusive on cardiomyocytes showing also a significative decrease of expression in failing hearts [33, 34]. Transgenic mice overexpressing the β1-adrenergic receptor present at a young age a strong hypertrophic response (with an 3.5-fold increase of cardiomyocyte cell area) accompanied by a sustained cardiac contractility. Subsequently, on the long run, a progressive heart failure condition reveals that is characterized by characteristic morphological and histological modifications [35]. Gi proteins are coupled by both β2-adrenergic and muscarinic receptors directly opposing to the Gs-dependent signaling. This G-protein class appears to be involved in decompensation since it is unregulated in hypertensive hypertrophy before the evolution towards failure [32]. Gq/G11 signaling is activated by the interaction of the α-adrenergic receptors with hormones and vasoactive factors resulting from pathological stimuli as pressure overload. Angiotensin 2 (ANGII) is one of these vasoactive effectors. It belongs to the Renin-Angiotensin-Aldosterone system and in the cardiovascular system expresses two different α-adrenergic receptors: AT1 and AT2. It was reported that the over activation of AT1 result in cardiac hypertrophic remodeling in transgenic mice [36]. Moreover, AT1 is able to directly transduce mechanical stress signals trough the involvement of Gq/G11 and mitogen-activated protein kinases (MAPKs) even without ANGII stimulation [37].

The calceneurin-NFAT pathway is playing a pivotal role in the process of cardiac hypertrophy. Stimuli including ANGII or norepinephrine (NE) or phenylephrine (PE) induce the increase of intracellular Ca^{2+} with subsequent activation of the calcineurin (CaN). This calcium–dependent phosphatase dephosphorylates NFAT (nuclear factor of activated T cells) leading to its translocation into the nucleus. In the nucleus, NFAT promotes the expression of several hypertrophic response genes in cooperation with cofactors as GATA4 and MEF2. Transgenic murine models overexpressing active forms of CaN or NFAT show cardiac hypertrophy evolving towards heart failure [38].

MAPK signaling shows to be involved in several pathways leading to hypertrophic and/or survival effects [39]. In particular, the IL6 cytokine-family acting through the receptor subunit gp130 can initiate signaling cascades in cardiomyocytes combined with stress stimuli such as stretch [40, 41]. Transgenic mice overexpressing the mitogen-activated protein kinase kinase 1 (MEK1) show concentric hypertrophy not accompanied by any indication of cardiac dysfunction. This phenotype was ascribed to ERK1/2, but not p38 or JNK, direct activation [42]. Conversely, the constitutive expression of MEK5 leads to the specific activation of ERK5. The result is a hypertrophic elongation of cardiomyocytes and

the configuration of an eccentric hypertrophic phenotype due to serially assembled sarcomeres [43].

In conclusion, although the reported knowledge regarding effectors and pathways driving the processes of cardiomyocytes proliferation and hypertrophy, we still miss the understanding of essential regulators of all these molecular mechanisms. The investigation on the promising field of non-coding RNA research can give us the opportunity to unveil these mysteries.

MicroRNAs and their power

The opportunity to catch the intrinsic potential of the human genome attracts many scientific groups around the word. The improvement of RNA profiling technologies combined with the enormous amount of information derived from the Human Genome Project (HGP) allowed us to understand that around three-quarters of the human genome can be transcribed [44]. Nevertheless, just ~1.5% is represented by coding sequences that are effectively translated [45]. The rest constitutes the compartment of non-coding RNA, nowadays recognized as powerful regulators of gene expression.

MicroRNAs (miRNAs) belong to this class of transcripts. Of note, miRNAs are small RNA molecules, with a length of ~21-23 nucleotides, able to interact and interfere in the process of translation of specific messenger RNA (mRNA) targets [46]. This interaction is exerted trough a small portion of 6-7 nucleotides, named “seed-sequence”. The location of the seed-sequences was mostly considered exclusive of the 3’ untranslated region (3’UTR) of the mRNA target [47]. Nevertheless, recent publications highlight the presence of frequent non-canonical binding sites located also into other parts of the mRNA sequence [48]. Notoriously, a microRNA can target different mRNAs; conversely a mRNA can be targeted by several miRNAs**.,** The wide effect of miRNAs on gene expression can be proficiently investigated through bioinformatics analyses. The network analysis application on the significant variations of the transcriptome is a precious tool for the identification of the pathways involved in a specific phenotype. Futhermore, recent works indicate a gradient of effective regulation among potential targets [49]. In this scenario the hierarchical organization of miRNA direct and undirected targets leads to a more complete perception of the sensitive points where a specific therapy could succeed. Moreover, the approach offered by this wide vision better clarify the molecular dynamics governing specific biological responses of our organism.

The number of the human miRNA sequences stored in miRBase reaches two thousand [50]. MiRNAs can be independently transcribed by RNA polymerase II/III but mostly result from polycistronic transcripts giving rise to more than one type of miRNA or of miRNAs and coding mRNAs [51]. The product is a long-hairpin (~60-80 nucleotides) named pri-miRNA. The pri-miRNA is processed and shortened directly into the nucleus through the cooperation

of Drosha (RNase III enzyme) and two DGCR8 (dsRNA-binding protein). Drosha performs the cleavage at the hairpin base recognizing the double-strand RNA-single-strand RNA junction [52]. Binding the hairpin stem, the two DGCR8 ensure the correct location of Drosha. Depending on the cleavage point this process could lead to alternative isomiRs. At this stage the shorted pri-miRNA, now named pre-miRNAs, is exported from nucleus to cytoplasm by Exportin-5. The knockout of the Exportin-5 gene (XPO5) in human cell line showed a reduction but not an elimination of pre-miRNA nuclear export suggesting the coexistence of alternative process exerting this process [53]. In the cytoplasm the RNase III Dicer catalyzes the cleavage of the terminal loop. Also at this level the different location of Dicer cleavage can give origin to alternative isomiRs [54]. As a next step, the double-stranded pre-miRNA (~21-23 nucleotides long) is loaded into the RISC (RNA-induced silencing complex) complex interacting with Argonaute proteins (Ago). Next follows the separation of the miRNA-duplex. The ejection of the other strand (passenger or "*" strand), rather than the retention of the leading strand (guide or "G" strand), is an event heavily affected by the thermodynamic instability of the double-stranded RNA [55, 56]. In the specific case of miRNA-duplex, this process occurs in a slicer-independent manner and it is primarily moved by parameters as temperature and Mg^{2+} with the involvement of functional domains of the Ago proteins [57]. Finally, the assembly product of guide miRNAs and Ago proteins gives place to the RISC complex (RNA-induced silencing complex). RISC is the functional machinery exerting the RNA-interference (RNAi) process [46].

The mechanisms used by miRNAs to control gene expression in a post-transcriptional manner are different and not all completely understood. We can mention two main pathways: A) Endonuclease cleavage by Agonaute type 2 (Ago2). In humans Ago2 is the only isoform of the Ago protein able to induce RNA cleavage of recognized mRNA [58]. As a consequence, the cleaved targets are exposed to exonuclease action leading to mRNA degradation. B) The second mechanism is based on pure interference on recruitment and progression of the translational process. RISC can compete with the subunits composing the translational machinery on binding the 5'cap of the mRNA target [59]. Alternatively, the RISC interaction can induce ribosomal premature dissociation repressing further steps of peptide synthesis. In conclusion, RNAi can either indeed lead to mRNA degradation but it is always exerted as protein silencing [60].

Aim of the thesis

The Diagnosis of HF still represents, unfortunately, an invariable end-point for many patients. Despite impressive progress on scientific knowledge and technological applications the only curative approach remains heart transplantation. Nevertheless the gap between the number of patients on waiting lists and the availability of hearts is extensive.

Despite the variability in heart disease etiology, contemporary therapy is generic and non-curative, aiming to suppress the progression of the diverse heart diseases.

The identification of novel medications suitable for tailored therapeutic strategies represents a primary objective in cardiovascular field. This ambition is accompanied by a better understanding of the molecular mechanisms underlying the causes and evolutions of diverse cardiac pathologies.

The work described in this thesis focuses on miRNAs as potential therapeutic targets in cardiac injuries. In **chapter 2** we review the state of art how miRNAs are exploited in the cardiac regenerative field. We also describe some of the most promising delivery strategies aimed to specifically target the heart. In **chapter 3** we report a study highlighting the role of cluster miRNA-106b~25 as a molecular switch between the condition of cardiomyocyte hyperplasia and hypertrophy. Furthermore we show that the overexpression of this cluster induces near complete heart regeneration in adult animals with myocardial infarction. **Chapter 4** describes our findings related to the molecular regulation induced by miRNA-148a between concentric and eccentric cardiac hypertrophy. We also reported the cardiac functional rescue effect induced by miRNA-148a overexpression in pressure overload models of HF. In conclusion, **chapter 5** summarizes the major findings of the reported experimental work with a general discussion and consideration regarding value, applications and future prospective of the gained information in the cardiovascular field.

References

1. Moorman, A., et al., *Development of the heart: (1) formation of the cardiac chambers and arterial trunks.* Heart, 2003. **89**(7): p. 806-14.
2. Mudd, J.O. and D.A. Kass, *Tackling heart failure in the twenty-first century.* Nature, 2008. **451**(7181): p. 919-28.
3. Writing Committee, M., et al., *2013 ACCF/AHA guideline for the management of heart failure: a report of the American College of Cardiology Foundation/American Heart Association Task Force on practice guidelines.* Circulation, 2013. **128**(16): p. e240-327.
4. Ponikowski, P., et al., *2016 ESC Guidelines for the diagnosis and treatment of acute and chronic heart failure: The Task Force for the diagnosis and treatment of acute and chronic heart failure of the European Society of Cardiology (ESC). Developed with the special contribution of the Heart Failure Association (HFA) of the ESC.* Eur J Heart Fail, 2016. **18**(8): p. 891-975.
5. Metra, M. and J.R. Teerlink, *Heart failure.* The Lancet, 2017. **390**(10106): p. 1981-1995.
6. Owan, T.E., et al., *Trends in prevalence and outcome of heart failure with preserved ejection fraction.* N Engl J Med, 2006. **355**(3): p. 251-9.
7. Basuray, A., et al., *Heart failure with recovered ejection fraction: clinical description, biomarkers, and outcomes.* Circulation, 2014. **129**(23): p. 2380-7.
8. Mackman, N., *Triggers, targets and treatments for thrombosis.* Nature, 2008. **451**(7181): p. 914-8.
9. Messerli, F.H., S.F. Rimoldi, and S. Bangalore, *The Transition From Hypertension to Heart Failure: Contemporary Update.* JACC Heart Fail, 2017. **5**(8): p. 543-551.
10. Braunwald, E., *Cardiomyopathies: An Overview.* Circ Res, 2017. **121**(7): p. 711-721.
11. Brigden, W., *Uncommon myocardial diseases; the non-coronary cardiomyopathies.* Lancet, 1957. **273**(7007): p. 1179-84.
12. National Heart, L., and Blood Istitute. *Cardiomyopathy*. U.S. Department of Health & Human Services 2018; Available from: https://www.nhlbi.nih.gov/health-topics/cardiomyopathy.
13. Corrado, D., C. Basso, and D.P. Judge, *Arrhythmogenic Cardiomyopathy.* Circ Res, 2017. **121**(7): p. 784-802.
14. Akdis, D., et al., *Arrhythmogenic Cardiomyopathy: Electrical and Structural Phenotypes.* Arrhythm Electrophysiol Rev, 2016. **5**(2): p. 90-101.
15. Lyon, A.R., et al., *Current state of knowledge on Takotsubo syndrome: a Position Statement from the Taskforce on Takotsubo Syndrome of the Heart Failure Association of the European Society of Cardiology.* Eur J Heart Fail, 2016. **18**(1): p. 8-27.
16. Cohn, J.N., R. Ferrari, and N. Sharpe, *Cardiac remodeling--concepts and clinical implications: a consensus paper from an international forum on cardiac remodeling. Behalf of an International Forum on Cardiac Remodeling.* J Am Coll Cardiol, 2000. **35**(3): p. 569-82.
17. Murry, C.E., H. Reinecke, and L.M. Pabon, *Regeneration gaps: observations on stem cells and cardiac repair.* J Am Coll Cardiol, 2006. **47**(9): p. 1777-85.
18. Haubner, B.J., et al., *Functional Recovery of a Human Neonatal Heart After Severe Myocardial Infarction.* Circ Res, 2016. **118**(2): p. 216-21.
19. Sutton, M.G. and N. Sharpe, *Left ventricular remodeling after myocardial infarction: pathophysiology and therapy.* Circulation, 2000. **101**(25): p. 2981-8.
20. Bernardo, B.C., et al., *Molecular distinction between physiological and pathological cardiac hypertrophy: experimental findings and therapeutic strategies.* Pharmacol Ther, 2010. **128**(1): p. 191-227.
21. Bergmann, O., et al., *Evidence for cardiomyocyte renewal in humans.* Science, 2009. **324**(5923): p. 98-102.

22. Chaudhry, H.W., et al., *Cyclin A2 mediates cardiomyocyte mitosis in the postmitotic myocardium.* J Biol Chem, 2004. **279**(34): p. 35858-66.
23. Pasumarthi, K.B., et al., *Targeted expression of cyclin D2 results in cardiomyocyte DNA synthesis and infarct regression in transgenic mice.* Circ Res, 2005. **96**(1): p. 110-8.
24. Mahmoud, A.I., et al., *Meis1 regulates postnatal cardiomyocyte cell cycle arrest.* Nature, 2013. **497**(7448): p. 249-253.
25. Xin, M., et al., *Hippo pathway effector Yap promotes cardiac regeneration.* Proc Natl Acad Sci U S A, 2013. **110**(34): p. 13839-44.
26. Heallen, T., et al., *Hippo signaling impedes adult heart regeneration.* Development, 2013. **140**(23): p. 4683-90.
27. Morikawa, Y., et al., *Dystrophin-glycoprotein complex sequesters Yap to inhibit cardiomyocyte proliferation.* Nature, 2017. **547**(7662): p. 227-231.
28. Bassat, E., et al., *The extracellular matrix protein agrin promotes heart regeneration in mice.* Nature, 2017. **547**(7662): p. 179-184.
29. Bersell, K., et al., *Neuregulin1/ErbB4 signaling induces cardiomyocyte proliferation and repair of heart injury.* Cell, 2009. **138**(2): p. 257-70.
30. Lenihan, D.J., et al., *A Phase I, Single Ascending Dose Study of Cimaglermin Alfa (Neuregulin 1beta3) in Patients With Systolic Dysfunction and Heart Failure.* JACC Basic Transl Sci, 2016. **1**(7): p. 576-586.
31. Rajabi, M., et al., *Return to the fetal gene program protects the stressed heart: a strong hypothesis.* Heart Fail Rev, 2007. **12**(3-4): p. 331-43.
32. Frey, N. and E.N. Olson, *Cardiac hypertrophy: the good, the bad, and the ugly.* Annu Rev Physiol, 2003. **65**: p. 45-79.
33. Buxton, I.L. and L.L. Brunton, *Direct analysis of beta-adrenergic receptor subtypes on intact adult ventricular myocytes of the rat.* Circ Res, 1985. **56**(1): p. 126-32.
34. Ungerer, M., et al., *Altered expression of beta-adrenergic receptor kinase and beta 1-adrenergic receptors in the failing human heart.* Circulation, 1993. **87**(2): p. 454-63.
35. Engelhardt, S., et al., *Progressive hypertrophy and heart failure in beta1-adrenergic receptor transgenic mice.* Proc Natl Acad Sci U S A, 1999. **96**(12): p. 7059-64.
36. Paradis, P., et al., *Overexpression of angiotensin II type I receptor in cardiomyocytes induces cardiac hypertrophy and remodeling.* Proc Natl Acad Sci U S A, 2000. **97**(2): p. 931-6.
37. Zou, Y., et al., *Mechanical stress activates angiotensin II type 1 receptor without the involvement of angiotensin II.* Nat Cell Biol, 2004. **6**(6): p. 499-506.
38. Molkentin, J.D., et al., *A calcineurin-dependent transcriptional pathway for cardiac hypertrophy.* Cell, 1998. **93**(2): p. 215-28.
39. Kodama, H., et al., *Significance of ERK cascade compared with JAK/STAT and PI3-K pathway in gp130-mediated cardiac hypertrophy.* Am J Physiol Heart Circ Physiol, 2000. **279**(4): p. H1635-44.
40. Heineke, J. and J.D. Molkentin, *Regulation of cardiac hypertrophy by intracellular signalling pathways.* Nat Rev Mol Cell Biol, 2006. **7**(8): p. 589-600.
41. Sugden, P.H. and A. Clerk, *"Stress-responsive" mitogen-activated protein kinases (c-Jun N-terminal kinases and p38 mitogen-activated protein kinases) in the myocardium.* Circ Res, 1998. **83**(4): p. 345-52.
42. Bueno, O.F., et al., *The MEK1-ERK1/2 signaling pathway promotes compensated cardiac hypertrophy in transgenic mice.* EMBO J, 2000. **19**(23): p. 6341-50.
43. Nicol, R.L., et al., *Activated MEK5 induces serial assembly of sarcomeres and eccentric cardiac hypertrophy.* EMBO J, 2001. **20**(11): p. 2757-67.
44. Djebali, S., et al., *Landscape of transcription in human cells.* Nature, 2012. **489**(7414): p. 101-8.
45. Lander, E.S., *Initial impact of the sequencing of the human genome.* Nature, 2011. **470**(7333): p. 187-97.

46. Bartel, D.P., *MicroRNAs: target recognition and regulatory functions.* Cell, 2009. **136**(2): p. 215-33.
47. Lai, E.C., *Micro RNAs are complementary to 3' UTR sequence motifs that mediate negative post-transcriptional regulation.* Nat Genet, 2002. **30**(4): p. 363-4.
48. Helwak, A., et al., *Mapping the human miRNA interactome by CLASH reveals frequent noncanonical binding.* Cell, 2013. **153**(3): p. 654-65.
49. Werfel, S., et al., *Preferential microRNA targeting revealed by in vivo competitive binding and differential Argonaute immunoprecipitation.* Nucleic Acids Res, 2017. **45**(17): p. 10218-10228.
50. http://www.mirbase.org/, m. *microRNA annotation and deep-sequencing data*. 24 February 2019.
51. Kim, Y.K. and V.N. Kim, *Processing of intronic microRNAs.* EMBO J, 2007. **26**(3): p. 775-83.
52. Gebert, L.F.R. and I.J. MacRae, *Regulation of microRNA function in animals.* Nat Rev Mol Cell Biol, 2019. **20**(1): p. 21-37.
53. Kim, Y.K., B. Kim, and V.N. Kim, *Re-evaluation of the roles of DROSHA, Export in 5, and DICER in microRNA biogenesis.* Proc Natl Acad Sci U S A, 2016. **113**(13): p. E1881-9.
54. Neilsen, C.T., G.J. Goodall, and C.P. Bracken, *IsomiRs--the overlooked repertoire in the dynamic microRNAome.* Trends Genet, 2012. **28**(11): p. 544-9.
55. Nakanishi, K., *Anatomy of RISC: how do small RNAs and chaperones activate Argonaute proteins?* Wiley Interdiscip Rev RNA, 2016. **7**(5): p. 637-60.
56. Yoda, M., et al., *ATP-dependent human RISC assembly pathways.* Nat Struct Mol Biol, 2010. **17**(1): p. 17-23.
57. Park, J.H. and C. Shin, *Slicer-independent mechanism drives small-RNA strand separation during human RISC assembly.* Nucleic Acids Res, 2015. **43**(19): p. 9418-33.
58. Liu, J., et al., *Argonaute2 is the catalytic engine of mammalian RNAi.* Science, 2004. **305**(5689): p. 1437-41.
59. Mathonnet, G., et al., *MicroRNA inhibition of translation initiation in vitro by targeting the cap-binding complex eIF4F.* Science, 2007. **317**(5845): p. 1764-7.
60. Cimmino, A., et al., *miR-15 and miR-16 induce apoptosis by targeting BCL2.* Proc Natl Acad Sci U S A, 2005. **102**(39): p. 13944-9.

CHAPTER 2

Cardiac regenerative medicine: At the crossroad of microRNA function and biotechnology

Andrea Raso and Ellen Dirkx

Department of Cardiology, CARIM School for Cardiovascular Disease, Maastricht University, 6229ER Maastricht, The Netherlands.

[Non-coding RNA research, 2(1), 27-37. doi:10.1016/j.ncrna.2017.03.001]

Abstract

There is an urgent need to develop new therapeutic strategies to stimulate cardiac repair after damage, such as myocardial infarction. Already for more than a century scientist are intrigued by studying the regenerative capacity of the heart. While moving away from the old classification of the heart as a post-mitotic organ, and being inspired by the stem cell research in other scientific fields, mainly three different strategies arose in order to develop regenerative medicine, namely; the use of cardiac stem cells, reprogramming of fibroblasts into cardiomyocytes or direct stimulation of endogenous cardiomyocyte proliferation. MicroRNAs, known to play a role in orchestrating cell fate processes such as proliferation, differentiation and reprogramming, gained a lot of attention in this context the latest years. Indeed, several research groups have independently demonstrated that microRNA-based therapy shows promising results to induce heart tissue regeneration and improve cardiac pump function after myocardial injury. Nowadays, a whole new biotechnology field has been unveiled to investigate the possibilities for efficient, safe and specific delivery of microRNAs towards the heart.

Introduction

Heart failure remains the primary cause of hospitalization and mortality in Europe, United States and in the developed nations [1, 2]. Currently, the only therapeutic option for end-stage heart failure is transplantation, but since the number of heart failure patients is rising dramatically, there is a lack of hearts available for this procedure. Therefore, there is a dire need to develop a therapeutic approach coping with the damage after cardiac injury.

Already within a time-frame of a few hours after ischemic damage, a loss of 25% of the total amount of cardiomyocytes present in the left ventricle could be observed [3]. Aiming at maintenance of the ventricular structural integrity, a reparative process is initiated to rebuild the damaged myocardium, which unfortunately only results in formation of a scar [4]. Since this scar is non-functional, cardiac muscle contractility will decrease and heart failure will develop. Taken this into account, regeneration of the heart muscle is a main goal for many researchers within the field and during the last decade new approaches have been developed to identify the (cell) source responsible for the newly formed cardiomyocytes in the adult heart. The applications range from *ex vivo* cell therapy strategies based on the direct delivery of regenerative cells isolated from different sources (e.g. induced pluripotent stem cells, embryonic stem cells, bone marrow, liposuction or heart biopsies), tissue engineering implantations of functional patches or *in vivo* stimulation of resident cell sources by delivery of reprogramming factors or inducers of cardiomyocyte cell-cycle re-entry [5-11].

From the molecular point of view, many scientists have turned their focus on the role of microRNAs (miRNAs, miRs) in order to unravel unknown and overlapping signaling cascades necessary for cardiac regeneration [12, 13]. MiRNAs, small non-coding RNA molecules of about 18-22 nucleotides long and highly conserved among species, have been shown to fine-tune gene regulatory networks via post-transcriptional regulation of different mRNAs, functioning in similar pathways. This molecular biological approach, combined with the development of smart technology for specific and controlled delivery will open the door to bring a novel and efficient therapeutic strategy to the heart failure patient.

The regenerative capacity of the heart muscle: An historical perspective

Already since the 19th century scientists have been intrigued by the regenerative capacity of the human heart. An intense and controversial discussion about whether increase of the heart mass in the postnatal phase was due to hypertrophic growth or cardiomyocyte proliferation has been going on for more than 100 years. Back in the late 1800s, Goldenberg was one of the first to report that although longitudinal splitting of cardiomyocytes might take place, growth of the heart muscle was mostly due to hypertrophy of muscle fibers [14]. In that period, other scientists confirmed there was a lack of evidence of myocardial mitotic figures and thus they concluded that the increase of the heart mass after birth was largely

achieved by hypertrophic growth rather than hyperplasia. In the early 1900s, researchers start to investigate the relationship between the amount of muscle fibers and nuclei. In this context, human hearts were studied and a comparison between normal, hypertrophic and atrophic status was made. Based on these finding, Karsner et al. published that enlargement of the heart in the hypertrophic state was due to hypertrophy of the muscle fibers without an actual increase in the number of fibers [15]. On the other hand, decreased heart size in atrophy was caused by both a reduction in muscle fiber size and fiber number, while the number of nuclei was clearly increased. Back then it was concluded that there might have been an attempt for the heart muscle to regenerate, however no mitotic figures were observed [15]. Interestingly, when comparing the myocardium of children versus adults, it became clear that mitotic figures in the hearts of children were present, while this was difficult to observe in the adult hearts [16]. These data indicated that cardiomyocytes were able to proliferate during the early postnatal phase but lose their capacity to proliferate at later ages In the 60s and 70s, evaluation of DNA synthesis in cardiomyocyte nuclei was shown to be negligible and people started to classify the human heart as a post-mitotic organ, incapable to self-regenerate [17, 18] . However, the atomic weapon testing during the Cold War followed by termination of these tests in 1963 let to the idea to use the measure of carbon-14 (14C) in genomic DNA of human cardiomyocytes to determine when these cells were born. Since the concentration of 14C in the human body mirrors that in the atmosphere at any given time, and given the fact that 14C incorporates in our DNA, these measurements could be used to retrospectively birth date cells in humans. The nuclear bombing tests let to a drastic increase in 14C concentrations in the atmosphere, and using mass spectrometry on extracted DNA coming from humans born before this atmospheric 14C peak, it became clear that cardiomyocyte DNA was synthesized even many years after birth. This geopolitical pulse-chase experiment let to the conclusion that in young adults, cardiomyocyte renewal was about 1% per year, while in elderly this was about 0.45% [19]. At that time, the self-repair capacity of the human heart after injury was not investigated yet, however given the fact that coronary artery disease leads to heart failure in patients, it was clear that even if the cardiomyocytes were able to proliferate, this was not sufficient to compensate the tremendous loss of cardiomyocytes after ischemic injury.

MicroRNAs: Directors of cell fate

Development of regenerative medicine for the heart muscle could be addressed via several approaches targeting cell fate processes such as proliferation, differentiation and reprogramming. Interestingly, miRNA-dependent regulatory networks seem to be able to affect all the biological processes implicated in cardiac regeneration (Figure 1). For example, miR-1 knockout in Drosophila has been shown to alter myofiber structure and muscle growth, causing larval paralysis and death [20]. Furthermore, the muscle-specific microRNAs, miR-1 and miR-133, appear to be potent repressors of non-muscle gene expression and cell fate in mouse and human pluripotent embryonic stem (ES) cells

differentiation. Under the control of cardiogenic and myogenic transcription regulators, such as the serum response factor (SRF), miR-1 and miR-133 promote mesodermal differentiation from ES cells but act partially in opposition on further differentiation to the cardiac lineage [21].

Furthermore, researchers have been describing the molecular characterization of the postnatal maturating cardiomyocytes, isolated from mice at postnatal day 1 up to 1 year old [22]. Zhang et al. reported decreased expression of several cyclins, cyclin-dependent kinases (CDKs) and positive cell cycle modulators and increased expression on CDK inhibitors and negative cell cycle modulators. These data were associated with the upregulation of miR-29a, miR-30a and miR-141. Moreover, downregulation of these miRNAs in neonatal rat cardiomyocytes promoted cell cycle re-entry, which was partly explained by the induction of Cyclin A2 (CCNA2) expression. Cao et al. reported similar observations in rats [23]. Next, also miR-133 has been demonstrated to play a role in cardiomyocyte cell cycling. The levels of miR-133 are strongly downregulated during the process of heart regeneration in zebrafish. Upon miR-133 overexpression, several cell cycling genes are downregulated and the reparative capacity of the heart muscle is reduced. In mice, the double knockout (dKO) of miR-133a-1 and miR-133a-2 causes lethal ventricular-septal defects in approximately half of double-mutant embryos or neonates. Double-mutant mice that did survive up to adulthood developed severe dilated cardiomyopathy and heart failure due to ectopic smooth muscle genes expression and aberrant cardiomyocyte proliferation [24]. The direct downstream targets of miR-133a, namely SRF and Cyclin D2 (CCND2), showed to be upregulated in these dKO mice, which could (at least partly) explain the observed phenotype. These findings reveal an essential role for miR-133a-1 and miR-133a-2 in orchestrating cardiac development and cardiomyocyte cell fate and point to these miRNAs as critical components of an SRF-dependent myogenic transcriptional circuit. Whether manipulation of these miRNAs, involved in cell differentiation and cardiomyocyte cell cycling, could help to regenerate the adult injured heart needs further investigation. However, the indications that these miRNAs play a role in cardiac cell fate determination, suggests their involvement in biological processes important for cardiac regeneration. In light of these findings, it became clear that it would be a merit to develop tools to target miRNAs for tissue regeneration purposes. Consequently, the last decade there has been a considerable increase in the number of patent applications filed. Although most miRNA-based therapeutics are still in pre-clinical stadium for various diseases, miravirsen, a miR-122 agonist inhibiting hepatitis C virus infection (HCV), seems to be promising and is the first miRNA-based therapeutics to reach clinical phase IIb. [25]. Miravirsen dosing in chronic hepatitis C patients results in decreased microRNA-122 levels without affecting other microRNAs in plasma [26].

Here we further review the different approaches to generate cardiac regenerative applications in which the role of microRNAs have been studied, and showing *in vivo* proof of improved cardiac pump function after myocardial injury.

The role of Cardiac Stem Cells in cardiac regeneration

While moving away from the old classification of the heart as a post-mitotic organ, and being inspired by the stem cell research in other scientific fields, a new challenge in the field arose to identify the stem cell population present in the heart. The concept that stem cells could be a source for cardiomyocyte renewal arose from initial research which demonstrated that administration of bone-marrow-derived c-Kit-positive (c-Kit+) hematopoietic stem cells led to restoration of the heart muscle after a myocardial infarction (MI) [27].

Next, several investigators came up with different approaches to identify resident Cardiac Stem Cells/Progenitor Cells (CSCs, CPCs) in the postnatal heart. These methods varied from the ability to form multicellular spheres or to efflux a fluorescent dye towards the expression of different surface markers, such as cardiac KIT Proto-Oncogene Receptor Tyrosine Kinase (c-Kit), Stem cells antigen-1 (Sca-1), Multi-drug resistance gene 1 (Mdr-1) and islet-1 (Isl-1) [28-31]. In mouse hearts, Sca-1-positive (Sca-1+) CPCs have been demonstrated to be implicated in cardiomyocyte formation and showed almost 100% co-expression with c-Kit [32-34]. However, In contrast to mouse hearts, Sca-1+ CPCs are not present in large mammals and humans. As a consequence, these data are not translatable to humans and so far CPCs showing expression of the tyrosine kinase receptor c-Kit are the most widely studied and characterized. During development, cardiomyocytes have been shown to express c-Kit, however in the adult human, c-Kit is only expressed in telocytes, thymic epithelium and mature circulating cells (e.g. hematopoietic cells and mast cells) [35]. Nevertheless, in the perivascular compartment of the adult heart, a particular small round shaped cell type has been identified to express c-Kit as well. Moreover, in the adult failing heart these c-Kit expressing cells seem to increase in abundance [36].

In meanwhile around 2004, subsequent studies demonstrated that c-Kit+ hematopoietic stem cells possessed essentially no ability to make cardiomyocytes, calling into question the earlier reports that these cells would lead to restoration of the heart muscle after injury [37, 38]. At that time, opinions were divided and while some research groups reported these c-Kit+ cells as CPCs, others point out that it are mast cells that reside in clusters in the perivascular space and that increase in number in the adult failing heart [39]. In 2007, using double-transgenic mice to track the fate of adult cardiomyocytes in a 'pulse-chase' fashion, Hsieh et al. reported that after injury, in areas bordering a MI, about 15% of newly formed cardiomyocytes were derived from stem cells or precursor cells [40]. Whether these stem cells or CPCs do express c-Kit was not investigated. Later on, in 2014, van Berlo et al. generated two genetic approaches in mice to examine whether endogenous c-Kit+ cells contribute to cardiomyocyte differentiation during development, with ageing or after injury in the adult heart. These c-Kit lineage tracing experiments showed that endogenous c-Kit+ cells did only produce new cardiomyocytes within the heart at a percentage of 0.03 or less [41]. In line, one year later, work of Sultana et al. demonstrated that c-Kit expression rarely co-localizes with the expression of the cardiac progenitor marker Nkx2.5, or the myocardial

marker cardiac troponin T [42]. Based on their observations, both research groups independently drew the conclusion that c-Kit predominantly labels a cardiac endothelial cell population in developing and adult hearts [41, 42]. Recently, Liu et al. independently addressed the same issue using a *Kit-CreER* mouse line for inducible lineage tracing [43]. This instant lineage tracing approach identifies Kit-expressing cardiomyocytes that are labeled during tamoxifen treatment. In combination with long-term lineage tracing experiments, the authors concluded that the large majority of long-term labeled cardiomyocytes in MI hearts are derived from pre-existing cardiomyocytes, expressing Kit [43]. Thus, the latest work within this field does not support the interpretation that most of the labeled cardiomyocytes in lineage tracing are formed *de novo* from c-Kit+ CSCs.

Besides the debate whether or not c-Kit+ cells exist in the adult heart, investigators have tested the potential of c-Kit+ CSCs transplantation into the injured myocardium. In this context, the clinical trials CADUCEUS, SCIPIO and ALCADIA, which are based on the isolation, expansion and transplantation of differently derived regenerative cardiomyocytes, gave promising results, as reviewed by Yacoub and Terrovitis [44]. From a molecular point of view, exogenous treatment of high-mobility group box 1 protein has been shown to boost the activation, proliferation and differentiation of c-Kit+ CSCs into a cardiomyocyte-like phenotype and improved cardiac function in infarcted mouse hearts [45]. This effect of myocardial regeneration was linked to the increased levels of metalloproteinases MMP-2 and MMP-9 and an increased expression of miR-206 [46]. In line, one of the validated targets of miR-206 is Tissue Inhibitor of Metalloproteinase-3 (TIMP-3). The downregulation of this inhibitor may enhance the activity of the MMPs promoting the cardiac regeneration by the migration of the active CSCs into the scar. Furthermore, it has been demonstrated that overexpression of miR-499 induces *in vitro* commitment of human c-Kit+ CSCs to mature functional cardiomyocytes [47]. MiR-499 was suggested to play a role in c-Kit+ CSCs differentiation by affecting the formation of gap-junctions via direct downregulation of SRY (sex determining region Y)-box 6 (Sox6) and regulator of differentiation 1 (Rod1). Indeed, Sox6 and Rod1 have previously been reported to be involved in the modulation of cell differentiation [48, 49]. *In vivo,* using a MI rat model, the transplantation of c-Kit+ CSCs overexpressing miR-499 showed a restoration of myocardial mass and contractile function related to an enhanced myocyte differentiation. These findings were in line with the work of Sluijter et al. [50], which demonstrated the differentiation of human fetal Sca-1+ CPCs into beating cardiomyocytes, showing a strong upregulation of miR-1 and miR-499. Transient transfection of miR-1 and miR-499 in human CPCs indeed led to a reduction of the proliferation rate for about 25% and 15%, respectively, likely via the repression of Histone deacetylase 4 and Sox6 proteins. Similar work on miR-10a has shown that when human CPCs are transfected with miR-10a, a reduction of 5-ethynyl-2´-deoxyuridine (EdU) incorporation into the cardiomyocytes nucler DNA during active DNA synthesis, was observed. This effect was abolished with a co-transfection of GATA Binding Protein 6

(Gata6), a direct downstream target of miR-10a [51]. On the other hand, miR-155 has been shown to be able to inhibit the differentiation of Sca-1+ CSCs, by directly targeting β-arrestin2 (Arrb2). However, these data could not be confirmed *in vivo*. In fact, in a MI mouse model, transplanted Arrb2-KO-CSCs did not show any protective effect [52]. Nevertheless, a different study suggests miR-155 as a useful tool to improve the engraftment for cells *in vivo*. This suggestion was based on the fact that miR-155 could repress necrotic death of CPCs by targeting the receptor interacting protein 1 (RIP1), independently from Akt (Protein kinase B) pro-survival pathway activation [53]. Also, the miR-17/92 cluster (harboring miR-17, -18, -19a, -19b, -20a, -92a) has been demonstrated to play an important role in regulating the proliferation rate of c-Kit+ CPCs. Indeed, overexpression of the mir-17/92 cluster both *in vitro* and *in vivo* induced an increase in proliferation rate of mouse CPCs with two fold. This effect was shown to be associated with an increased expression of the cell cycle regulator retinoblastoma-like 2 (Rbl2/p130) protein [54].

Taken together, driven by the clinical need, scientists have explored the possibility of identifying and using CPCs as therapeutic strategy to repair the injured heart. Most of the studies and clinical trials have been focusing on cell culture and transplantation of these cells, however there rules a huge controversy within this research field since a good characterization of these cells and their role *in vivo* remains unclear.

Direct reprogramming of fibroblasts into cardiomyocytes

Another possible method to boost generation of new cardiomyocytes is the reprogramming of the non-cardiomyocyte cell types present in the heart, namely fibroblasts, endothelial cell and vascular smooth muscle cells. Of these cell types, fibroblasts appear to be the most ideal candidate for this direct reprogramming approach. Cardiac fibroblasts are fully differentiated somatic cells, representing the largest proportion of the total cell population in the human heart, ranging from 40% up to 60% [55, 56]. Furthermore this cell type provides a supportive structure, secrete signals, and contribute to scar formation upon cardiac damage [57].

Two decades ago, it was demonstrated that fibroblasts could be stimulated to transdifferentiate into skeletal muscle cells by overexpressing the myogenic transcription factor, MyoD. However, back then a similar transcription factor to promote cardiac transdifferentiation was not found. Later on, the discovery of induction of pluripotent stem (iPS) cells suggested that a specific combination of defined factors, rather than a single factor would be necessary to reactivate a regulatory gene network of the desired cell type. In this context, an experiment was designed to systematically screen 14 different transcription factors simultaneously in order to reprogram cardiac-derived fibroblasts into cardiomyocytes. 13 of these factors were selected based on the severe developmental cardiac defects and embryonic lethality that was developed upon mutation of these factors. Additionally Mesp1 was selected based on a previous publication showing cardiac

transdifferentiation capacities in Xenopus [58].

Out of the selection of these 14 factors, a cocktail of three transcription factors was shown to be essential for transdifferentiating fibroblasts into cardiomyocytes. A cocktail of GATA Binding Protein (Gata4), Myocyte Enhancer Factor 2c (Mef2c), and T-Box 5 (Tbx5) reprogrammed postnatal fibroblasts directly into differentiated, spontaneously contracting cardiomyocyte-like cells. Furthermore, also *in vivo* transplantation of fibroblasts, transduced for one day with these three factors, into mouse hearts differentiated into cardiomyocyte-like cells [57]. Inclusion of the basic helix–loop–helix transcription factor Hand2 within this cocktail further increased reprogramming efficiency. Introduction of either transcription factor cocktail into cardiac fibroblasts of mice following MI resulted in the formation of cardiomyocytes associated with an improved cardiac function and diminished fibrosis [59, 60]. In the meantime, Efe et al. showed conventional reprogramming towards cardiogenesis through overexpression of Octamer-binding transcription factor 4 (Oct4), Sox2, Krueppel-Like Factor 4 (Klf4) and proto-oncogene c-Myc. Within 4 days of transgenic expression of these factors, mouse embryonic fibroblasts (MEFs) showed to be reprogrammed to spontaneously contracting patches of differentiated cardiomyocytes over a period of 11–12 days [61]. The same group also reported that small molecules could enable cardiac transdifferentiation of mouse fibroblasts with only one transcription factor Oct4 [62]. One of the advantages of these reprogramming approaches is that it seems to avoid an intermediate pluripotent stage, theoretically obviating a potential tumorigenic effect. However, the limitations related to an *ex vivo* treatment persist, namely the timing from the cell isolation, *ex vivo* expansion until the final cell delivery may affect the success of this kind of treatments [63].

Nevertheless, based on the potential of miRNAs in regulating gene regulatory networks during development, researchers began to investigate their role in redirecting cell fate [64-67]. In this context Jayawardena and coworkers were the first to develop a strategy in order to identify miRNAs capable of reprogramming cardiac fibroblasts into a cardiomyocyte lineage [68]. Candidate miRNAs were selected based on previous reports demonstrating their roles in cardiac muscle development and differentiation [24, 69-72]. By using a combined transfection of synthetic, chemically modified mimics of the selected miRNAs the authors showed an induction of direct differentiation of mouse adult fibroblast to cardiomyocytes-like cells. Top candidates identified included miR-1 alone; miRs-1, -133, -206; miRs-1, -133, -208; miRs-133, -206, -208; miR-1, -138; and miRs-1, -138, -208. This was further demonstrated *in vivo* using transient transfection of the microRNAs in neonatal cardiac fibroblasts isolated from double-transgenic mice carrying both the Fibroblast-specific protein-1 (Fsp1)-driven Cre recombinase gene and a floxed tdTomato reporter (Fsp1-Cre/tdTomato). The fibroblastic origin of miRNA-induced cardiomyocyte-like cells was shown by a co-localization of the tdTomato marker with heart muscle-specific markers; cardiac Troponin I or α-actinin. Interestingly, miRNA-mediated reprogramming was enhanced 10-fold on Janus kinase (JAK) inhibitor 1 treatment. Furthermore, administration

of lentivirus encoding miR-1 or a combination of 4 lentiviruses encoding the miRNA combo (miR-1, -133, -208, -499) into ischemic mouse myocardium resulted in evidence of direct conversion of cardiac fibroblasts to cardiomyocytes *in situ*. Genetic tracing analysis using Fsp1Cre-traced fibroblasts from both cardiac and non-cardiac cell sources strongly suggests that induced cells are most likely of fibroblastic origin. Moreover the authors could associate these results with an improvement of cardiac function on up to 3 months after MI [73]. Simultaneously, another research group highlighted the importance of MyoD in the reprogramming of fibroblasts into a cardiomyocyte-like phenotype. They demonstrated more effective induction of reprogramming with MyoD in combination with Mef2c and Tbx5, compared with any other combination of three factors from 10 candidate, including the ones previously described in literature. The cocktail of Mef2c, Tbx5 and MyoD expressed cardiac contractile proteins, had cardiac-like potassium and sodium currents and action potentials could be elicited [74]. In 2013, Nam and colleagues investigated whether human adult fibroblasts could be reprogrammed into cardiac-like myocytes by the cardiac transcription factors and muscle-specific miRNAs previously reported to reprogramme mouse fibroblasts into cardiomyocytes. The authors showed that four human cardiac transcription factors, including Gata4, Heart And Neural Crest Derivatives Expressed 2 (Hand2), T-box5, and MyoD, combined with miR-1 and miR-133, activated cardiac marker expression in neonatal and adult human fibroblasts. After maintenance in culture up to 11 weeks, human fibroblasts reprogrammed with this cocktail displayed sarcomere-like structures and calcium transients, and a small subset of such cells exhibited spontaneous contractility [75].

To avoid genetic insertion and carcinogenicity by viral based methods, Fu et al. tested a small-molecule combination CRFVPTZ (C, CHIR99021; R, RepSox; F, Forskolin; V, VPA; P, Parnate; T, TTNPB; and Z, DZnep), previously developed by Hou et al. [76]. Using this chemical cocktail it was possible to generate automatically beating cardiomyocyte-like cells from mouse fibroblasts. These chemical-induced cardiomyocyte-like cells express cardiomyocyte-specific markers, exhibit sarcomeric organization, and possess typical cardiac calcium flux and electrophysiological features [77]. Bypassing the use of viral-derived factors for *in vivo* cardiac transdifferentiation with pharmacological agents could open a new avenue towards regenerative medicine for heart failure patients. Although research in this field has made tremendous progress during the latest years, further optimization of this process and the eventual generation of more mature and homogeneous populations of the generated cardiomyocyte-like cells is necessary. In order to be able to do this, further research unraveling the underlying molecular mechanisms of all these strategies would be indispensable.

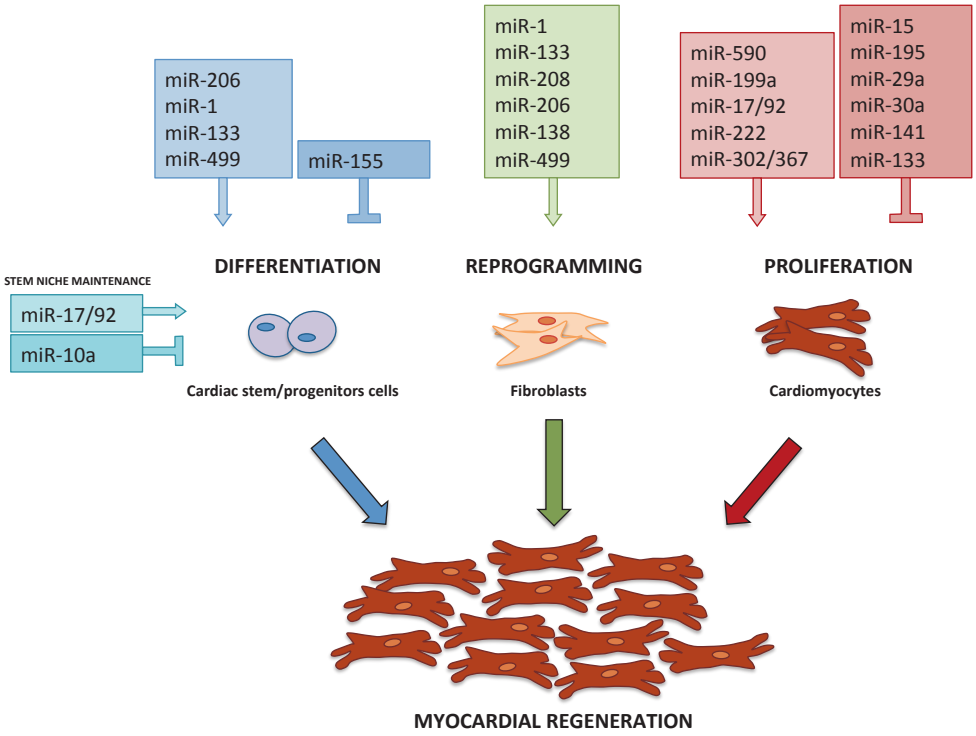

Figure 1. The role of miRNAs in three strategies leading to myocardial regeneration, namely by regulating cardiac stem/progenitors cells differentiation, reprogramming of fibroblasts into a cardiomyocyte phenotype and stimulation of pre-existing cardiomyocyte proliferation.

Endogenous cardiomyocytes as target for the development of regenerative medicine

Shortly after birth, the majority of human cardiomyocytes shift from a proliferate state towards a terminally differentiated phenotype, unable to re-enter the cell cycle. Consequently, adult mammalian cardiomyocytes possess a restricted proliferative capacity, insufficient to rebuild the ventricular wall and restore cardiac function after injury [19]. However, since the mid 50s a number of reports indicated that a few replicating cardiomyocytes could be detected after cardiac injury. These were the first suggestions that cardiomyocytes by themselves underwent an attempt to regenerate the damaged myocardium [78-81]. Although these reports were published by independent research groups, the scientific community kept on being skeptic about the fact that certain cardiomyocytes are still able to proliferate during adult life. The latest years, research methods have improved and by combining genetic fate-mapping and stable isotope labeling techniques, researchers again showed that the dominant source of cardiomyocyte replacement during myocardial homeostasis, and even more after myocardial injury, is

represented by pre-existing cardiomyocytes [82]. Furthermore, it was demonstrated that pre-existing cardiomyocytes preferably in a hypoxic state, which is a typical feature of proliferating cells in diverse organs, displayed a significant contribution in the generation of new cardiomyocytes in the adult heart. This finding confirms that the heart contains a small population of cardiomyocytes, which keep their prenatal proliferative nature, even during adulthood [83]. The recognition of endogenous cardiomyocytes as a source for new cardiomyocytes, even at a very low percentage, raises the possibility of stimulating this process for developing cardiac regenerative therapies.

In contrast to mammals, lower vertebrates like the teleost fish are able to intrinsically regenerate the heart muscle after induction of myocardial injury. As well as Jopling et al., as well as Kikucki et al., reported pre-existing cardiomyocytes as major source of the newly formed cardiomyocytes during the regenerative process in zebrafish. This was demonstrated by enhanced green fluorescent protein (EGFP) labeling of the pre-existing cardiomyocytes trough an inducible Cre recombinase system. 30 days after ventricular sectioning, the majority of the newly formed cardiomyocytes showed to be EGFP positive [84, 85]. Moreover, in 2007, a technology was developed to designate ~90 color labels to murine neurons [86]. This technology, termed brainbow, facilitated the visualization of adjacent neurons and their connections in the brain with high resolution. This technology enabled the potential to assign many colors to different cells in a population, and thus investigate cell proliferation and lineage decisions. Using this brainbow technology to study the zebrafish heart, it was demonstrated that 14 days after injury, cortical muscle regeneration is the primary component of the newly formed wall, whereas the primordial muscle was regenerated much later (30 day after injury). Interestingly, these events occur in a temporally reversed manner compared to initial morphogenesis during cardiac development [87].

In 2008, the regenerative capacity of the mammalian fetal heart was investigated by Drenckhahn et al. [88]. They introduced a cardiomyocyte-lethal mutant gene in the X chromosome, which became conditionally expressed at embryonic day 12.5 (E12.5) in half of the cardiomyocytes in female embryos (due to random X inactivation). Fetal hearts that had undergone this genetic ablation were able to restore approximately 50% of lost cardiomyocyte mass. These data indicate that the embryonic environment facilitates cardiomyocyte repopulation of the heart [88]. This repopulation capacity of the heart muscle ability was even reported to be maintained during the early postnatal phase. After partial surgical resection of the apex of the heart in 1-day old mice, the cardiac muscle regenerates itself by boosting cardiomyocyte cell cycle re-entry [89]. Echocardiographic analysis, measuring systolic cardiac function of these regenerated hearts showed to be normal up to 2 months after surgery. Nevertheless, the regenerative capacity of the heart muscle seems to be inexorably lost by 7 days of age.

Interestingly, it has been suggested by Porrello et al. that upregulation of the miR-15 family during the postnatal period may be a possible regulatory mechanism directing

cardiomyocyte cell cycle withdrawal and binucleation [90]. In line, a microarray analysis revealed that miR-195, a miR-15 family member, was highly upregulated in mouse cardiac ventricles at postnatal day 10 versus postnatal day 1 [90]. Furthermore, knocking down the entire miR-15 family in neonatal mice showed a pro-proliferative boost of cardiomyocytes, associated with a higher expression of the cell cycle gene checkpoint kinase 1 (Check1). Check1 was identified as a direct downstream target of miR-195. Recently, it was reported that the expression of miR-195 can be modulated by the Long Non-coding RNA UC.283+A, which targets the lower stem region of pri-miR-195 transcript, preventing the cleavage by Drosha both *in vitro* and *in viv*o [91]. However, the exact role of UC.283+A in cardiomyocyte proliferation is unknown so far. Other studies also indicated that singular miR-15 knock down in a both a mouse and pig model for cardiac ischemia-reperfusion injury showed a reduction in infarct size and attenuation of cardiac remodeling, resulting in a better heart function [92].

In 2012, Eulalio et al. performed a high-throughput functional screening in neonatal rat cardiomyocytes, and reported that 204 miRNAs, of the 875 miRNAs tested, were able to boost cardiomyocyte proliferation *in vitro,* showing at least a 2-fold increase in nuclear EdU incorporation in stimulated cardiomyocytes compared to controls [93]. 40 of these miRNAs were confirmed to have pro-proliferative capacities in murine neonatal cardiomyocytes as well. In order to demonstrate true karyokinesis and cytokinesis occurred upon miRNA stimulation, histone H3 phosphorylation and Aurora B kinase localization were analysed and validated the screening results for the top 10 pro-proliferative miRNAs in both rodent models. Among these miRNAs, the top two candidates, namely miR-199a and miR-590, were validated in an *in vivo* model for mouse MI. Indeed, treatment with either miR-199a or miR-590 boosted post-natal cardiomyocyte proliferation and consequently preserved contractile function and decreased the levels of fibrosis after MI. The direct downstream targets identified for both microRNAs were Homer Scaffolding Protein 1 (Homer1), a regulator of the calcium signaling, and in HOP Homeobox (Hopx), a suppressor of the embryonic cardiomyocyte proliferation. Additionally, the chloride intracellular channel Clic5 showed to be a direct target of miR-590.

The past few years, more and more scientists reported the involvement of miRNAs in boosting cardiomyocyte proliferation, resulting in improved cardiac contractile function after injury. For example, the miR-17/92 cluster, consisting of miR-17, miR-18a, miR-19a/b, miR-20a and miR-92a, was also discovered to be a regulator of native cardiomyocyte proliferation [94]. *In vivo* knockout of this cluster specifically in the cardiomyocytes showed a reduction in number of cardiomyocyte, which was compensated by an increase in cell size. In line, overexpression of the entire cluster was able to boost cardiomyocyte proliferation *in vivo,* as well as in the embryonic phase, the postnatal period and in adult hearts*.* The tumor suppressor Phosphatase and tensin homolog (PTEN) showed to be altered both in the miR-17-92 transgenic and knockout mice. As a reported direct downstream target of miR19a/b, the PTEN overexpression abolished the pro-proliferative effect of miR19a/b completely [95].

Also the miR-302/367 cluster showed pro-proliferative effects in cardiomyocytes [96]. The miR-302/367 cluster decreases in expression while progressing from the embryonic phase towards the adult phase. However, upon overexpression of this cluster in the developing heart, cardiomyocyte proliferation and cardiomegaly is induced. Macrophage Stimulating 1 (Mst1), Large tumor suppressor 2 (Lats2), MOB Kinase Activator 1B (Mob1b) were identified to be putative targets of miR302/367, indicating a role of this microRNA cluster in regulation of the Hippo pathway, an important signaling cascade that regulates organ size by cell proliferation and death. Furthermore, transient overexpression of the miR-302/367 cluster, and in particular miR-302, promotes cardiac regeneration leading to improved cardiac contractile function after MI.

An interesting report on the role of miR-222 in cardiomyocytes has been published by Liu et al. [97]. The expression of miR-222 appears to be induced during physiological hypertrophy in two different mice model of exercise, while this was not observed during pathological cardiac remodeling. Furthermore, miR-222 inhibition completely blocked the physiological exercise-induced cardiomyocyte remodeling, and also reducing the expression of proliferation markers. Furthermore, by inducing ischemia-reperfusion in hearts of cardiac-specific miR-222 overexpression mice, the authors demonstrated improved cardiac contractile function and a 70% reduction on scar formation compared to wild-type mice. This protective effect, associated with the increase of cardiomyocyte proliferation and reduced apoptosis, was linked to the direct inhibitory effect of miR-222 on cyclin-dependent kinase inhibitor 1B (p27), homeodomain-interacting protein kinase 1 (HIPK1) and homeobox containing 1 (HMBOX1).

Delivery of therapeutics to heart failure patients

Stimulation of endogenous heart regeneration might lead to severe side effects, such as tumor formation in other organs. Therefore one must not oversee the importance of developing a strategy that lead to very specific targeting and thus directing the therapeutics need to turn their action. Concerning the essential role of microRNAs in recovering cardiac dysfunction, several efforts have been made in order to apply *in vivo* strategies to modulate miRNA expression [93, 98]. To inhibit microRNA expression, scientists developed antisense oligonucleotides (ASOs) and modified microRNA mimics, such as plasmid or lentiviral vectors, have been shown to carry microRNA sequences designed to deliver microRNAs to cells and tissues *in vivo.* The use of anti-microRNA oligonucleotides (AMOs), their modifications, perspectives and challenges has been extensively reviewed by Philippen et al. [99]. On the contrary, *in vivo* applications that overexpress and deliver miRNAs are still a challenge for the field. For example, The use of miRNA mimics is limited by their intolerance to extensive modifications [98]. Recombinant adeno-associated virus vectors and nanoparticles applications, with their limitations and difficulties, are nowadays two alternative and promising delivery systems that are finding their way in the present and future molecular medicine (Figure 2).

Recombinant Adeno-Associated Viral Vectors

The recombinant adeno-associated virus (rAAV) is a product of the adeno-associated virus (AAV), a nonpathogenic human virus that possesses a weak immunogenicity and does not induce inflammatory events (reviewed by Zacchigna et al. 2014 [100]). As a safe and efficient gene delivery vector, AAV has been used in a wide range of biotechnological applications during the last decades. In contrast to several other viral vectors, the rAAV are unable to integrate into the host-cell genome, and *in vivo,* rAAV is able to infect non-cycling cells, such as the majority of adult cardiomyocytes, with high efficiency.

The rAAV vector consist of a DNA transgene cassette of 4.5 kb, surrounded by two inverted terminal repeats essential for the viral packaging, which are the solely maintained elements of the original viral genome. The single-strand DNA genome is packaged in an icosahedral capsid built of 60 proteins [101]. Depending on the cluster of amino acid residues exposed on the surface, their topology and tridimensional structure, over more than 100 AAV variants have been isolated [102, 103]. However, only around 10 of these variants fit into the accepted definition of new serotypes. Their genomic simplicity allows their use as a carrier for the overexpression of both protein-coding and non-coding genes, such as miRNAs, or siRNAs against specific genes in the case a knockdown effect is desired. The interaction between the capsid and receptors/co-receptors exposed on the cell surface give them differential cell-tropism. However, also the route of delivery can affect both the efficiency of infection and the tissue-specificity. This modulation becomes even more complex when comparing the efficiency and specificity of the AAV vectors in different species. So far, AAV serotype 9 has been identified to show the best cardiotropic effect [104, 105]. As we mentioned before, miR-590 and miR-199a have been shown to be delivered to the mouse cardiac muscle via an rAAV9 vector, and show a functional effect on cardiac regeneration and heart function after MI [93]. Similarly, using rAAV9 transduction, miR-378 has been demonstrated to become overexpressed in the heart muscle, which attenuated hypertrophy, induced by thoracic aortic constriction [106]. Also, rAAV9-miR-669a treatment was reported to decrease cardiac dilatation in dystrophic mice [107]. Nevertheless, AAV serotype 1, 6 and 8 also report cardiomyocyte transduction, but with differential efficacy [108, 109]. In Rhesus Macaques and in pigs, delivery of AAV6 has been shown to result in highly efficient and global gene transfer [110, 111]. In human rAAV1 has been used to deliver Sarcoplasmic reticulum Ca^{2+}- ATPase (Serca2a), via intracoronary administration. SERCA is a calcium transporter critical to maintaining calcium homeostasis, which is downregulated in heart failure. Thus, these therapies are designed to restore impaired calcium signaling in the failing heart. AAV1-SERCA therapy has been proven to be safe and is already in use in the following clinical trials; the Calcium Up-Regulation by Percutaneous Administration of Gene Therapy in Cardiac Disease (CUPID), the AAV1-CMV-Serca2a Gene Therapy Trial in HF (AGENT-HF) and the SERCA2a Gene Therapy in LAVD [112]. Although for the CUPID trial, rAAV1 was used, in 60% out of 1552 heart failure patients the presence of high titers of neutralizing antibodies (Nab) against AAV2, which cross-reacted

with AAV1, caused a problem in this trial [113]. Second- or third-generation AAV vectors designed using mosaics and directed evolution will become very important.

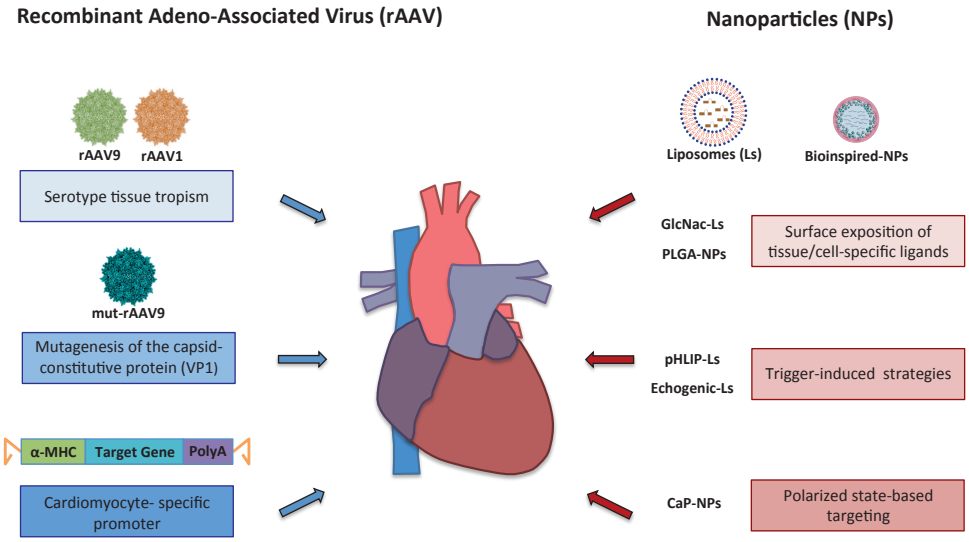

Figure 2. **Promising delivery strategies in cardiac molecular medicine**. **1)** Recombinant Adeno-Associated Viral vectors (rAAV): Among the different serotypes tested both rAAV9 and rAAV1 showed a high cardiotropic effect; this specificity can be further increased by mutagenesis of the capsid-constitutive protein VP1, which has been demonstrated for AAV9 (mut-rAAV9); further specificity can be obtained by using a cardiomyocyte-specific promoter, such as alpha-myosin heavy chain (α-MHC). **2)** Nanoparticles (NPs): which could be Liposomes (Ls) or Bioinspired-NPs. Their cardiac-specific targeting can be improved by a) surface exposition of tissue/cell-specific ligands, which has been shown for e.g. N-acetylglucosamine-conjugated liposomes (GlcNAc-Ls) and poly d,l-lactide-*co*-glycolide nanoparticles (PLGA-NPs); b) Instant activation by environmental or body-external factors, such as pH insertion peptide liposomes (pHLIP-Ls) and Echogenic liposomes (Echogenic-Ls); or c) via polarized state-based targeting as demonstrated with calcium phosphate nanoparticles (CaP-NPs).

To circumvent this problem, Pleger et al. showed that retrograde coronary venous delivery of rAAV9-mediated therapy, named AAV9-S100A1, at a concentration of 1.5 $x10^{13}$ viral particles is cardiotropic in a pig model for MI [114]. This was confirmed by Fish et al. by showing successful intracoronary gene transfer of I-1c to the heart using rAAV9 [115]. In meantime, uniQure's gene therapy platform to restore S100A1 levels was started-up. UniQure already successfully brought the AAV1-based gene therapy Glybera® to the market [116]. Glybera® is designed to restore the lipoprotein lipase (LPL) enzyme activity required to enable the processing and clearance of fat-carrying chylomicron particles formed in the intestine after a fat-containing meal [117]. After this success, they will now use retrograde delivery and include the cardiac-specific myosin light chain promoter into their vector, to

specifically deliver S100A1 to the heart muscle [114]. Indeed, alpha-myosin heavy chain (α-MHC) has already shown to be effective to deliver transgene expression solely in the heart [118]. Unfortunately, the use of a specific promoter causes a decrease in the transcription level, and therefore biotechnologists are still dealing with a dilemma between targeted delivery and system efficiency. Thus investigators have been working on manipulating these promoters. In rats, cardiac-selective expression of a therapeutic transgene has been achieved by using only a fragment of the mouse alpha-cardiac actin gene enhancer, which was ligated to the elongation factor 1alpha promoter [110]. Furthermore, the engineering of synthetic capsid variants gives further possibilities towards tissue specific targeting. By random mutagenesis of the mainly capsid-constitutive protein (VP1) of rAAV9 Pulicherla et al. provided several functional rAAV9 variants (mut-rAAV9) which seem to be more cardiac- and musculoskeletal- tropic, while the liver is effected less [119].

Given the progress scientists have been made during the latest years, the use of rAAV-based therapeutics for heart failure patients seems to become reality within a few years from now.

Nanoparticles (NP)

Another biotechnological development for drug delivery, which is worthwhile to mention in this context, is the use of nanotechnology. This technology, through controlling materials at nanoscale, has driven revolutionary developments in almost all fields. Nanoparticles (NPs) have been widely used for fast-diagnosis, molecule delivery, and tissue engineering. Nanoparticles are a class of nano-structures that can be composed and built by different kind of materials and motifs such as dendrimers, carbon nanotubes, polymers, micelle or liposomes [120].

A range of nanoparticle delivery systems have been investigated for the targeted delivery of miRNAs, in a variety of different disease models outside of the cardiovascular field, with varying degrees of success and translational potential, including Poly lactide-co-glycolide (PLGA) particles, dendrimers, lipid based systems and Polyethylenimine (PEI)-based delivery systems (reviewed by Zhang et al., Muthiah et al. and Christiakov et al. [121-123]). Due to their plasticity and the fact that nanoparticles are relatively easy to manipulate, the amount of research in this field to use nanoparticles as a possible drug delivery system in an *in vivo* context is increasing (reviewed by Ho et al. 2015 [124]). Moreover, their use has even paved a way for assisting stem cell therapy delivery to the ischemic heart (reviewed by Kai Zhu et al. [125]).

In the cancer field, nanoparticles are used to deliver therapeutics as well as to visualize within hours whether the treatment is effective or not [126, 127]. Obviously, among all existing molecules, non-coding RNAs seem to be good candidates to be delivered via nanoparticles in order to treat a variety of pathologies. However, one must overcome issues as low miRNA transfection efficiency and cytotoxicity [128]. In this context, polyethylene glycol-polyethylenimine nanocomplexes have been designed as carriers to deliver miR-150 to chronic myeloid leukemia cells with relatively high efficiency [129]. However, in the field

of heart disease, nanotechnology still has a long way to go. Lipids forming liposomes and bio-inspired nanoparticles are the most investigated nanoparticle varieties so far. In general, the main challenges are related to the loading efficacy, biodegradability, biocompatibility, retention of drug in the blood stream and specific release at the target site [130]. From this list, specific targeting as well as having a safe and optimized application is a fundamental need for heart regeneration therapeutics. Concerning the active delivery of the nanoparticles at a specific location, it has been described that after MI, an enhanced permeation and retention effect (EPR) takes place. This means that the vessels perfusing the left ventricles appear to be hyper-permeable, actually promoting the accumulation of lipidic particles in the border zone of the infarcted areas. Therefore, Tan et al. developed a particles-cell hybrid model to predict the nanoparticle dispersion related to blood dynamics [131]. They took in account the complexity of the blood composition (containing compounds such as deformable cells, proteins, platelets and plasma) and the blood stream in the capillaries, where the bigger compounds tend to flow in the core of the vessel. By this model the authors observed that the presence of a cell-free layer between the core and the wall of the vessel increases the dispersion of the nanoparticles toward the walls. Further studies demonstrate that the margination of the nanoparticles trough the wall appears significantly influenced by the size and shape of the nanoparticles. In fact, the smaller and oblate particles are, the more they are localized towards the vessel wall when compared with bigger-sized and sphere-shaped particles [132].

In case of a myocardial injury, the caliber of the arterioles is decreased, which is caused by occlusions or vessel spasms combined with enhanced extravasation. Therefore, it would be a merit to take into account the knowledge on the EPR effect for developing new therapeutics to target specifically the myocardium. This strategy could be even boosted by a local administration, for example during an angioplasty procedure.

Next, several researchers demonstrated the possibility to manipulate the surface of nanoparticles in order to expose different kinds of ligands that theoretically can give the nanoparticle a tissue-specific or cell-specific action [133-135]. Unfortunately, *in vivo* myocardial-specific targeting remains still an open challenge. In fact, the characterization of an exclusive surface marker for cardiomyocytes has not been discovered yet [136]. Nevertheless, the *in vitro* findings reported by Aso et al. combined with the *in vivo* work by Gray et al. already show interesting results in this context [137, 138]. These scientists demonstrated an interaction and uptake of N-acetylglucosamine-conjugated liposomes (GlcNAc-Ls) by cardiomyocytes. Moreover, as proof of concept, *in vivo* administration of this type of nanoparticles loaded with an inhibitor of p38 led to decreased apoptosis, a reduced infarct area and improved cardiac function. More recently also the peri-infarct injection of insulin-like growth factor (IGF)-1-complexed poly D,L-lactide-*co*-glycolide (PLGA) nanoparticles (PLGA-IGF-1 NPs) prevented cardiomyocytes apoptosis, improved left ventricle ejection fraction and reduced infarct size 21 days after MI in mice [139].

Another issue is the development of a smart drug delivery system in order to release the nanoparticle content only at the target location under specific conditions. This type of nanoparticles technology works via localized auto/induced destabilization or upon the intervention of an external effector, causing an indirect site-specific release. For the trigger-induced strategies, biotechnologists are considering heat, magnetics and light as different type of triggers to make the nanoparticles releasing their content when present at the target side [140, 141]. Unfortunately, no trustable application to target specifically the myocardium in this way has been found yet. However, knowing that the pH of the extracellular environment is lower in several pathological conditions, including myocardial ischemia [142, 143], a promising application of pH (low) insertion peptide (pHLIP) was demonstrated by Sosunova et al. [144]. The technology of pHLIP targets cells within an acid extracellular environment (low pH) [145]. In two different models of myocardial ischemia, it was reported that pHLIP–liposomes are able to target predominantly the ischemic but not the uninjured areas of the myocardium [144].

Another attractive strategy is based on the localized destruction of nanoparticles trough ultrasound high acoustic pressure. So far, this technique mainly has been applied to microbubbles in order to target the heart muscle. Microbubbles can image the heart via effectively reflecting sound waves when ultrasound pulses are present. Upon adjusting the acoustic setting of the ultrasound, they could burst and deliver their payload to a target region of the heart (reviewed by Dijkmans et al. 2004 [146]). However, microbubbles actually cannot be classified as nanoparticles because of their bigger size [147]. In the future, current available technology could be further optimized using echogenic liposomes (Els), which are more prone for extravessel targeting [148]. Interestingly, very recently Di Mauro et al. introduced a therapeutic system for the delivery of bioactive molecules to the heart, based on the polarized state of cardiomyocytes. By synthesizing negatively charged calcium phosphate bio-inspired nanoparticles (CaP-NPs), employing citrate as stabilizing agent, the authors could report an efficient delivery of synthetic microRNAs into cardiomyocytes both *in vitro* and *in vivo* [149]. In contrast to surface decoration or adsorption approaches, this approach seems to increase the stability and functionality of miRNAs. These findings will open up new avenues for the potential application of nanomedicine in the context of heart muscle regeneration.

Concluding remarks

Since microRNAs have been shown to be able to direct cell fate processes, many miRNA-based therapeutic strategies have been proposed in the context of heart regeneration. Taken into account the debate about the existence of CSCs and the difficulties of generating a mature and homogenous cardiomyocyte population from reprogrammed fibroblasts, stimulation of endogenous cardiomyocyte proliferation seems to give the most promising future perspective so far. In this context, AAV9 vectors have been used to successfully deliver miRNAs into the cardiac muscle, where this type of therapeutics has shown a clear regenerative effect in the mouse heart. Although usage of AAV vectors already showed to

be successful in pigs and humans as well, there is still a dire need for a more efficient, safe and cardiac-specific drug delivery system. Latest years, new biotechnological approaches have been developed e.g. by altering AAV vectors or by using bio-engineered nanoparticles. Further optimization of current technologies and obtaining better insight into molecular mechanisms underlying the successful therapeutics, would make a cardiac-specific drug delivery possible, efficient and safe for the future heart failure patient.

Conflict of interest diclosures

A.R.:none, E.D.: none

Acknowledgements

E.D. was supported by a Long Term Fellowship of the EMBO Organization (ALTF 848-2013), Marie Curie actions Intra-European fellowship (PIEF-GA-2013-627539) and VENI fellowship (016.156.016) from the Netherlands Organization for Health Research and Development (ZonMW).

References

1. Pagidipati, N.J. and T.A. Gaziano, *Estimating deaths from cardiovascular disease: a review of global methodologies of mortality measurement.* Circulation, 2013. **127**(6): p. 749-756.
2. Mozaffarian, D., et al., *Heart Disease and Stroke Statistics—2015 Update: a report from the American Heart Association.* Circulation, 2015. **131**: p. e29–e322.
3. Murry, C.E., H. Reinecke, and L.M. Pabon, *Regeneration gaps: observations on stem cells and cardiac repair.* J Am Coll Cardiol, 2006. **47**(9): p. 1777-1785.
4. Sutton, M.G.S.J. and N. Sharpe, *Left Ventricular Remodeling After Myocardial Infarction Pathophysiology and Therapy.* Circulation, 2000. **101**(25): p. 2981-2988.
5. Nelson, T.J., et al., *Repair of acute myocardial infarction by human stemness factors induced pluripotent stem cells.* Circulation, 2009. **120**(5): p. 408-416.
6. Min, J.Y., et al., *Long-term improvement of cardiac function in rats after infarction by transplantation of embryonic stem cells.* J Thorac Cardiovasc Surg, 2003. **125**(2): p. 361-369.
7. Meyer, G.P., et al., *Intracoronary bone marrow cell transfer after myocardial infarction: 5-year follow-up from the randomized-controlled BOOST trial.* European Heart Journal, 2009. **30**(24): p. 2978-2984.
8. Houtgraaf, J.H., et al., *First experience in humans using adipose tissue-derived regenerative cells in the treatment of patients with ST-segment elevation myocardial infarction.* J Am Coll Cardiol, 2012. **59**(5): p. 539-540.
9. Bolli, R., et al., *Cardiac stem cells in patients with ischaemic cardiomyopathy (SCIPIO): initial results of a randomised phase 1 trial.* The Lancet, 2011. **378**(9806): p. 1847-1857.
10. Hirt, M.N., A. Hansen, and T. Eschenhagen, *Cardiac tissue engineering: state of the art.* Circ Res, 2014. **114**(2): p. 354-367.
11. Bersell, K., et al., *Neuregulin1/ErbB4 signaling induces cardiomyocyte proliferation and repair of heart injury.* Cell, 2009. **138**(2): p. 257-270.
12. Rao, P.K., et al., *Loss of cardiac microRNA-mediated regulation leads to dilated cardiomyopathy and heart failure.* Circ Res, 2009. **105**(6): p. 585-94.
13. van Rooij, E., et al., *A family of microRNAs encoded by myosin genes governs myosin expression and muscle performance.* Dev Cell, 2009. **17**(5): p. 662-73.
14. Goldenberg, B., *Ueber Atrophie und Hypertrophie der Muskelfasern des Herzens.* Virchows Arch Pathol Anat Physiol Klin, 1886. **103**: p. 88-130.

15. Karsner, H.T., O. Saphir, and T.W. Todd, *The State of the Cardiac Muscle in Hypertrophy and Atrophy.* Am J Pathol, 1925. **1**(4): p. 351-372.
16. MacMahon, E.H., *Hyperplasia and Regeneration of the Myocardium in Infants and in Children.* Am J Pathol, 1937. **13**(5): p. 845-854.
17. Zak, R., *Development and proliferative capacity of cardiac muscle cells.* Circ Res 1974. **35**: p. Suppl II:17.
18. Grove, D., et al., *Biochemical Correlates of Cardiac Hypertrophy: IV. Observations On The Cellular Organization Of Growth During Myocardial Hypertrophy In The Rat.* Circ Res, 1969. **25**: p. 473-485.
19. Bergmann, O., et al., *Evidence for cardiomyocyte renewal in humans.* Science, 2009. **324**(5923): p. 98-102.
20. Sokol, N.S. and V. Ambros, *Mesodermally expressed Drosophila microRNA-1 is regulated by Twist and is required in muscles during larval growth.* Genes Dev, 2005. **19**(19): p. 2343-2354.
21. Ivey, K.N., et al., *MicroRNA Regulation of Cell Lineages in Mouse and Human Embryonic Stem Cells.* Cell stem cell, 2008. **2**(3): p. 219-229.
22. Zhang, Y., et al., *Targeted MicroRNA Interference Promotes Postnatal Cardiac Cell Cycle Re-Entry.* J Regen Med, 2013. **2**: p. 2.
23. Cao, X., et al., *MicroRNA profiling during rat ventricular maturation: A role for miR-29a in regulating cardiomyocyte cell cycle re-entry.* FEBS Lett, 2013. **587**(10): p. 1548-1555.
24. Liu, N., et al., *microRNA-133a regulates cardiomyocyte proliferation and suppresses smooth muscle gene expression in the heart.* Genes Dev, 2008. **22**(23): p. 3242-3254.
25. Jopling, C.L., et al., *Modulation of hepatitis C virus RNA abundance by a liver-specific MicroRNA.* Science, 2005. **309**(5740): p. 1577-81.
26. van der Ree, M.H., et al., *Miravirsen dosing in chronic hepatitis C patients results in decreased microRNA-122 levels without affecting other microRNAs in plasma.* Aliment Pharmacol Ther, 2016. **43**(1): p. 102-13.
27. Orlic , D., et al., *Bone marrow cells regenerate infarcted myocardium.* Nature, 2001. **410**: p. 701-705.
28. Wu, S.M., et al., *Developmental origin of a bipotential myocardial and smooth muscle cell precursor in the mammalian heart.* Cell, 2006. **127**(6): p. 1137-1150.
29. Tateishi, K., et al., *Clonally amplified cardiac stem cells are regulated by Sca-1 signaling for efficient cardiovascular regeneration.* J Cell Sci, 2007. **120**(Pt 10): p. 1791-1800.
30. Beltrami, A.P., et al., *Adult Cardiac Stem Cells Are Multipotent and Support Myocardial Regeneration.* Cell, 2003. **114**: p. 763-776.
31. Quaini, F., et al., *Chimerism of the transpanted heart.* The New England Journal of Medicine, 2002. **346**.
32. Bailey, B., et al., *Sca-1 knockout impairs myocardial and cardiac progenitor cell function.* Circ Res, 2012. **111**(6): p. 750-760.
33. Uchida, S., et al., *Sca1-derived cells are a source of myocardial renewal in the murine adult heart.* Stem Cell Reports, 2013. **1**(5): p. 397-410.
34. Urbanek, K., et al., *Myocardial regeneration by activation of multipotent cardiac stem cells in ischemic heart failure.* PNAS, 2005. **102**(24): p. 8692-8697.
35. Tallinia, Y.N., et al., *c-kit expression identifies cardiovascular precursors in the neonatal heart.* PNAS, 2009. **106**(6): p. 1808-1813.
36. Kubo, H., et al., *Increased cardiac myocyte progenitors in failing human hearts.* Circulation, 2008. **118**(6): p. 649-657.
37. Murry, C.E., et al., *Haematopoietic stem cells do not transdifferentiate into cardiac myocytes in myocardial infarcts.* Nature, 2004. **428**(6983): p. 664-668.
38. Balsam, L.B., et al., *Haematopoietic stem cells adopt mature haematopoietic fates in ischaemic myocardium.* Nature, 2008. **428**(6983): p. 668-673.

39. Patella, V., et al., *Stem Cell Factor in Mast Cells and Increased Mast Cell Density in Idiopathic and Ischemic Cardiomyopathy.* Circulation, 1998. **97**: p. 971-978.
40. Hsieh, P.C.H., et al., *Evidence from a genetic fate-mapping study that stem cells refresh adult mammalian cardiomyocytes after injury.* Nature Medicine, 2007. **13**: p. 970-974.
41. van Berlo, J.H., et al., *c-kit+ cells minimally contribute cardiomyocytes to the heart.* Nature, 2014. **509**(7500): p. 337-341.
42. Sultana, N., et al., *Resident c-kit(+) cells in the heart are not cardiac stem cells.* Nat Commun, 2015. **6**: p. 8701.
43. Liu, Q., et al., *Genetic lineage tracing identifies in situ Kit-expressing cardiomyocytes.* Cell Res, 2016. **26**(1): p. 119-130.
44. Yacoub, M.H. and J. Terrovitis, *CADUCEUS, SCIPIO, ALCADIA: Cell therapy trials using cardiac-derived cells for patients with post myocardial infarction LV dysfunction, still evolving.* Glob Cardiol Sci Pract, 2013. **2013**(1): p. 5-8.
45. Limana, F., et al., *Exogenous high-mobility group box 1 protein induces myocardial regeneration after infarction via enhanced cardiac C-kit+ cell proliferation and differentiation.* Circ Res, 2005. **97**(8): p. e73-e83.
46. Limana, F., et al., *HMGB1 attenuates cardiac remodelling in the failing heart via enhanced cardiac regeneration and miR-206-mediated inhibition of TIMP-3.* PLoS One, 2011. **6**(6): p. e19845.
47. Hosoda, T., et al., *Human cardiac stem cell differentiation is regulated by a mircrine mechanism.* Circulation, 2011. **123**(12): p. 1287-1296.
48. Cohen-Barak, O., *Sox6 regulation of cardiac myocyte development.* Nucleic Acids Research, 2003. **31**(20): p. 5941-5948.
49. Yamamoto, H., et al., *Isolation of a Mammalian Homologue of a Fission Yeast Differentiation Regulator.* Molecular and Cellular Biology, 1999: p. 3829–3841.
50. Sluijter, J.P., et al., *MicroRNA-1 and -499 regulate differentiation and proliferation in human-derived cardiomyocyte progenitor cells.* Arterioscler Thromb Vasc Biol, 2010. **30**(4): p. 859-68.
51. Liang, D., et al., *miR-10a regulates proliferation of human cardiomyocyte progenitor cells by targeting GATA6.* PLoS One, 2014. **9**(7): p. e103097.
52. Zhao, J., et al., *beta-arrestin2/miR-155/GSK3beta regulates transition of 5'-azacytizine-induced Sca-1-positive cells to cardiomyocytes.* J Cell Mol Med, 2014. **18**(8): p. 1562-1570.
53. Liu, J., et al., *MicroRNA-155 prevents necrotic cell death in human cardiomyocyte progenitor cells via targeting RIP1.* J Cell Mol Med, 2011. **15**(7): p. 1474-1482.
54. Sirish, P., et al., *MicroRNA profiling predicts a variance in the proliferative potential of cardiac progenitor cells derived from neonatal and adult murine hearts.* J Mol Cell Cardiol, 2012. **52**(1): p. 264-272.
55. Nag, A.C., *Study of non-muscle cells of the adult mammalian heart: a fine structural analysis and distribution.* Cytobios, 1980. **28**(109): p. 41-61.
56. Souders, C.A., S.L. Bowers, and T.A. Baudino, *Cardiac fibroblast: the renaissance cell.* Circ Res, 2009. **105**(12): p. 1164-1176.
57. Ieda, M., et al., *Direct reprogramming of fibroblasts into functional cardiomyocytes by defined factors.* Cell, 2010. **142**(3): p. 375-386.
58. Shechter, D., et al., *A distinct H2A.X isoform is enriched in Xenopus laevis eggs and early embryos and is phosphorylated in the absence of a checkpoint.* PNAS, 2009. **106**(3): p. 749-754.
59. Song, K., et al., *Heart repair by reprogramming non-myocytes with cardiac transcription factors.* Nature, 2012. **485**(7400): p. 599-604.
60. Qian, L., et al., *In vivo reprogramming of murine cardiac fibroblasts into induced cardiomyocytes.* Nature, 2012. **485**(7400): p. 593-598.

61. Efe, J.A., et al., *Conversion of mouse fibroblasts into cardiomyocytes using a direct reprogramming strategy.* Nat Cell Biol, 2011. **13**(3): p. 215-222.
62. Wang, H., et al., *Small molecules enable cardiac reprogramming of mouse fibroblasts with a single factor, Oct4.* Cell Rep, 2014. **6**(5): p. 951-960.
63. Traverse, J.H., et al., *Effect of the use and timing of bone marrow mononuclear cell delivery on left ventricular function after acute myocardial infarction: the TIME randomized trial.* JAMA, 2012. **308**(22): p. 2380-9.
64. Cordes, K.R., et al., *miR-145 and miR-143 regulate smooth muscle cell fate and plasticity.* Nature, 2009. **460**(7256): p. 705-710.
65. Judson, R.L., et al., *Embryonic stem cell-specific microRNAs promote induced pluripotency.* Nat Biotechnol, 2009. **27**(5): p. 459-461.
66. Anokye-Danso, F., et al., *Highly efficient miRNA-mediated reprogramming of mouse and human somatic cells to pluripotency.* Cell Stem Cell, 2011. **8**(4): p. 376-88.
67. Yoo, A.S., et al., *MicroRNA-mediated conversion of human fibroblasts to neurons.* Nature, 2011. **476**(7359): p. 228-231.
68. Jayawardena, T.M., et al., *MicroRNA-mediated in vitro and in vivo direct reprogramming of cardiac fibroblasts to cardiomyocytes.* Circ Res, 2012. **110**(11): p. 1465-1473.
69. Callis, T.E., et al., *MicroRNA-208a is a regulator of cardiac hypertrophy and conduction in mice.* J Clin Invest, 2009. **119**(9): p. 2772-2786.
70. Townley-Tilson, W.H., T.E. Callis, and D. Wang, *MicroRNAs 1, 133, and 206: critical factors of skeletal and cardiac muscle development, function, and disease.* Int J Biochem Cell Biol, 2010. **42**(8): p. 1252-1255.
71. Fish, J.E., et al., *miR-126 regulates angiogenic signaling and vascular integrity.* Dev Cell, 2008. **15**(2): p. 272-284.
72. Zhao, Y., et al., *Dysregulation of cardiogenesis, cardiac conduction, and cell cycle in mice lacking miRNA-1-2.* Cell, 2007. **129**(2): p. 303-317.
73. Jayawardena, T.M., et al., *MicroRNA induced cardiac reprogramming in vivo: evidence for mature cardiac myocytes and improved cardiac function.* Circ Res, 2015. **116**(3): p. 418-424.
74. Protze, S., et al., *A new approach to transcription factor screening for reprogramming of fibroblasts to cardiomyocyte-like cells.* J Mol Cell Cardiol, 2012. **53**(3): p. 323-32.
75. Nam, Y.J., et al., *Reprogramming of human fibroblasts toward a cardiac fate.* PNAS, 2012. **110**(4): p. 5588-5593.
76. Hou, P., et al., *Pluripotent stem cells induced from mouse somatic cells by small-molecule compounds.* Science, 2013. **341**(6146): p. 651-654.
77. Fu, Y., et al., *Direct reprogramming of mouse fibroblasts into cardiomyocytes with chemical cocktails.* Cell Res, 2015. **25**(9): p. 1013-1024.
78. Beltrami, A.P., et al., *Evidence That Human Cardiac Myocytes Divide After Myocardial Infarction.* The New England Journal of Medicine, 2001. **344**(23): p. 1750-1757.
79. Robledo, M., *Myocardial Regeneration in Young Rats.* Am J Pathol, 1956. **32**(6): p. 1215-1239.
80. Nag, A.C., T.R. Carey, and M. Cheng, *DNA synthesis in rat heart cells after injury and the regeneration of myocardia.* Tissue Cell, 1983. **15**(4): p. 597-613.
81. Kajstura, J., et al., *Myocyte cellular hyperplasia and myocyte cellular hypertrophy contribute to chronic ventricular remodeling in coronary artery narrowing-induced cardiomyopathy in rats.* Circ Res, 1994. **74**(3): p. 383-400.
82. Senyo, S.E., et al., *Mammalian heart renewal by pre-existing cardiomyocytes.* Nature, 2013. **493**(7432): p. 433-436.
83. Kimura, W., et al., *Hypoxia fate mapping identifies cycling cardiomyocytes in the adult heart.* Nature, 2015. **523**(7559): p. 226-230.
84. Jopling, C., et al., *Zebrafish heart regeneration occurs by cardiomyocyte dedifferentiation and proliferation.* Nature, 2010. **464**(7288): p. 606-609.

85. Kikuchi, K., et al., *Primary contribution to zebrafish heart regeneration by gata4(+) cardiomyocytes.* Nature, 2010. **464**(7288): p. 601-605.
86. Livet, J., et al., *Transgenic strategies for combinatorial expression of fluorescent proteins in the nervous system.* Nature, 2007. **450**(7166): p. 56-62.
87. Gupta, V. and K.D. Poss, *Clonally dominant cardiomyocytes direct heart morphogenesis.* Nature, 2012. **484**(7395): p. 479-484.
88. Drenckhahn, J.D., et al., *Compensatory growth of healthy cardiac cells in the presence of diseased cells restores tissue homeostasis during heart development.* Dev Cell, 2008. **15**(4): p. 521-533.
89. Porrello, E.R., et al., *Transient regenerative potential of the neonatal mouse heart.* Science, 2011. **331**(6020): p. 1078-1080.
90. Porrello, E.R., et al., *MiR-15 family regulates postnatal mitotic arrest of cardiomyocytes.* Circ Res, 2011. **109**(6): p. 670-679.
91. Liz, J., et al., *Regulation of pri-miRNA processing by a long noncoding RNA transcribed from an ultraconserved region.* Mol Cell, 2014. **55**(1): p. 138-147.
92. Hullinger, T.G., et al., *Inhibition of miR-15 protects against cardiac ischemic injury.* Circ Res, 2012. **110**(1): p. 71-81.
93. Eulalio, A., et al., *Functional screening identifies miRNAs inducing cardiac regeneration.* Nature, 2012. **492**(7429): p. 376-381.
94. Chen, J., et al., *mir-17-92 cluster is required for and sufficient to induce cardiomyocyte proliferation in postnatal and adult hearts.* Circ Res, 2013. **112**(12): p. 1557-66.
95. Olive, V., et al., *miR-19 is a key oncogenic component of mir-17-92.* Genes Dev, 2009. **23**(24): p. 2839-49.
96. Tian, Y., et al., *A microRNA-Hippo pathway that promotes cardiomyocyte proliferation and cardiac regeneration in mice.* ScienceTranslationalMedicine, 2015. **7**(279).
97. Liu, X., et al., *miR-222 is necessary for exercise-induced cardiac growth and protects against pathological cardiac remodeling.* Cell Metab, 2015. **21**(4): p. 584-595.
98. Olson, E.N., *MicroRNAs as therapeutic targets and biomarkers of cardiovascular disease.* Sci Transl Med, 2014. **6**(239): p. 239ps3.
99. Philippen, L.E., et al., *Antisense MicroRNA Therapeutics in Cardiovascular Disease: Quo Vadis?* Mol Ther, 2015. **23**(12): p. 1810-8.
100. Zacchigna, S., L. Zentilin, and M. Giacca, *Adeno-associated virus vectors as therapeutic and investigational tools in the cardiovascular system.* Circ Res, 2014. **114**(11): p. 1827-1846.
101. Xie, Q., et al., *The atomic structure of adeno-associated virus (AAV-2), a vector for human gene therapy.* PNAS, 2002. **99**(16): p. 10405-10410.
102. Atchison, R.W., B.C. Casto, and H. W.McD., *Adenovirus-Associated Defective Virus Particles.* Science, 1965. **149**(3685): p. 754-755.
103. Gao, G., et al., *Clades of Adeno-associated viruses are widely disseminated in human tissues.* J Virol, 2004. **78**(12): p. 6381-6388.
104. Pacak, C.A., et al., *Recombinant adeno-associated virus serotype 9 leads to preferential cardiac transduction in vivo.* Circ Res, 2006. **99**(4): p. e3-9.
105. Bish, L.T., et al., *Adeno-associated virus (AAV) serotype 9 provides global cardiac gene transfer superior to AAV1, AAV6, AAV7, and AAV8 in the mouse and rat.* Hum Gene Ther, 2008. **19**(12): p. 1359-1368.
106. Ganesan, J., et al., *MiR-378 controls cardiac hypertrophy by combined repression of mitogen-activated protein kinase pathway factors.* Circulation, 2013. **127**(21): p. 2097-2106.
107. Quattrocelli, M., et al., *Long-term miR-669a therapy alleviates chronic dilated cardiomyopathy in dystrophic mice.* J Am Heart Assoc, 2013. **2**(4): p. e000284.
108. Wang, Z., et al., *Adeno-associated virus serotype 8 efficiently delivers genes to muscle and heart.* Nat Biotechnol, 2005. **23**(3): p. 321-328.

109. Palomeque, J., et al., *Efficiency of eight different AAV serotypes in transducing rat myocardium in vivo.* Gene Therapy, 2007: p. 989-997.
110. Pleger, S.T., et al., *Stable myocardial-specific AAV6-S100A1 gene therapy results in chronic functional heart failure rescue.* Circulation, 2007. **115**(19): p. 2506-2515.
111. Gao, G., et al., *Transendocardial delivery of AAV6 results in highly efficient and global cardiac gene transfer in rhesus macaques.* Hum Gene Ther, 2011. **22**(8): p. 979-984.
112. Kawase, Y., D. Ladage, and R.J. Hajjar, *Rescuing the failing heart by targeted gene transfer.* J Am Coll Cardiol, 2011. **57**(10): p. 1169-1180.
113. Greenberg, B., et al., *Prevalence of AAV1 neutralizing antibodies and consequences for a clinical trial of gene transfer for advanced heart failure.* Gene Therapy, 2016. **23**: p. 313-319.
114. Pleger, S.T., et al., *Cardiac AAV9-S100A1 gene therapy rescues post-ischemic heart failure in a preclinical large animal model.* Sci Transl Med, 2011. **3**(92): p. 92ra64.
115. Fish, K.M., et al., *AAV9.I-1c delivered via direct coronary infusion in a porcine model of heart failure improves contractility and mitigates adverse remodeling.* Circ Heart Fail, 2013. **6**(2): p. 310-317.
116. http://www.uniqure.com/gene-therapy/glybera.php, *Glybera is the first gene therapy approved in the Western world.*
117. Carpentier, A.C., et al., *Effect of alipogene tiparvovec (AAV1-LPL(S447X)) on postprandial chylomicron metabolism in lipoprotein lipase-deficient patients.* J Clin Endocrinol Metab, 2012. **97**(5): p. 1635-44.
118. Pacak, C.A., et al., *Tissue specific promoters improve specificity of AAV9 mediated transgene expression following intra-vascular gene delivery in neonatal mice.* Genet Vaccines Ther, 2008. **6**.
119. Pulicherla, N., et al., *Engineering liver-detargeted AAV9 vectors for cardiac and musculoskeletal gene transfer.* Mol Ther, 2011. **19**(6): p. 1070-1078.
120. Matoba, T. and K. Egashira, *Nanoparticle-Mediated Drug Delivery System for Cardiovascular Disease.* Int Heart J, 2014. **55**(4): p. 281-286.
121. Zhang, Y., Z. Wang, and R.A. Gemeinhart, *Progress in microRNA delivery.* J Control Release, 2013. **172**(3): p. 962-974.
122. Muthiah, M., I.K. Park, and C.S. Cho, *Nanoparticle-mediated delivery of therapeutic genes: focus on miRNA therapeutics.* Expert Opin Drug Deliv, 2013. **10**(9): p. 1259-1273.
123. Chistiakov, D.A., I.A. Sobenin, and A.N. Orekhov, *Strategies to deliver microRNAs as potential therapeutics in the treatment of cardiovascular pathology.* Drug Deliv, 2012. **19**(8): p. 392-405.
124. Ho, Y.T., B. Poinard, and J.C.Y. Kah, *Nanoparticle drug delivery systems and their use in cardiac tissue therapy.* Nanomedice, 2015.
125. Zhu, K., et al., *Nanoparticles-Assisted Stem Cell Therapy for Ischemic Heart Disease.* Stem Cells Int, 2016. **2016**: p. 1384658.
126. Thakor, A.S. and S.S. Gambhir, *Nanooncology: The Future of Cancer Diagnosis and Therapy.* Ca Cancer J Clin, 2013: p. 395-418.
127. Kulkarni, A., et al., *Reporter nanoparticle that monitors its anticancer efficacy in real time.* Proc Natl Acad Sci U S A, 2016. **113**(15): p. E2104-E2113.
128. Shu, Y., et al., *Stable RNA nanoparticles as potential new generation drugs for cancer therapy.* Adv Drug Deliv Rev, 2014. **66**: p. 74-89.
129. Biray Avci, C., et al., *Design of polyethylene glycol-polyethylenimine nanocomplexes as non-viral carriers: mir-150 delivery to chronic myeloid leukemia cells.* Cell Biol Int, 2013. **37**(11): p. 1205-1214.
130. Eloy, J.O., et al., *Liposomes as carriers of hydrophilic small molecule drugs: strategies to enhance encapsulation and delivery.* Colloids Surf B Biointerfaces, 2014. **123**: p. 345-363.
131. Tan, J., A. Thomas, and Y. Liu, *Influence of Red Blood Cells on Nanoparticle Targeted Delivery in Microcirculation.* Soft Matter, 2011. **8**: p. 1934-1946.

132. Toy, R., et al., *Effect of Particle Size, Density and Shape on Margination of Nanoparticles in Microcirculation.* Nanotechnology, 2011.
133. Hsieh, P.C., et al., *Controlled delivery of PDGF-BB for myocardial protection using injectable self-assembling peptide nanofibers.* J Clin Invest, 2006. **116**(1): p. 237-248.
134. Sy, J.C., et al., *Surface functionalization of polyketal microparticles with nitrilotriacetic acid-nickel complexes for efficient protein capture and delivery.* Biomaterials, 2010. **31**(18): p. 4987-4994.
135. Kobayashi, K., et al., *Surface engineering of nanoparticles for therapeutic applications.* Polymer Journal, 2014. **46**(8): p. 460-468.
136. Skelton, R.J., et al., *SIRPA, VCAM1 and CD34 identify discrete lineages during early human cardiovascular development.* Stem Cell Res, 2014. **13**(1): p. 172-179.
137. Aso, S., et al., *Effective uptake of N-acetylglucosamine-conjugated liposomes by cardiomyocytes in vitro.* J Control Release, 2007. **122**(2): p. 189-198.
138. Gray, W.D., et al., *N-acetylglucosamine conjugated to nanoparticles enhances myocyte uptake and improves delivery of a small molecule p38 inhibitor for post-infarct healing.* J Cardiovasc Transl Res, 2011. **4**(5): p. 631-643.
139. Chang, M.Y., et al., *Functionalized nanoparticles provide early cardioprotection after acute myocardial infarction.* J Control Release, 2013. **170**(2): p. 287-294.
140. Chorny, M., et al., *Targeting stents with local delivery of paclitaxel-loaded magnetic nanoparticles using uniform fields.* Proc Natl Acad Sci U S A, 2010. **107**(18): p. 8346-51.
141. Kang, H., et al., *Near-Infrared Light-Responsive Core ShellNanogels for Targeted Drug Delivery.* AcsNano, 2011. **5**(6): p. 5094-5099.
142. Cobbe, S.M. and P.A. PooleWilson, *The Time of Onset and Severity of Acidosis in Myocardial Ischaemia* Journal pf Molecular and Cellular Cardiology 1980. **12**: p. 745-760.
143. Yan, G. and A.G. Kleber, *Changes in Extracellular and Intracellular pH in Ischemic Rabbit Papillary Muscle.* Circ Res, 1992. **71**: p. 460-470.
144. Sosunova, E.A., et al., *pH (low) insertion peptide (pHLIP) targets ischemic myocardium.* PNAS, 2012. **110**(1): p. 82-89.
145. Andreev, O.A., D.M. Engelman, and Y.K. Reshetnyak, *pH-sensitive membrane peptides (pHLIPs) as a novel class of delivery agents.* Mol Membr Biol, 2010. **27**(7): p. 341-52.
146. Dijkmans, P.A., et al., *Microbubbles and ultrasound: from diagnosis to therapy.* Eur J Echocardiogr, 2004. **5**(4): p. 245-256.
147. Chen, G., et al., *Delivery of Hydrogen Sulfide by Ultrasound Targeted Microbubble Destruction Attenuates Myocardial Ischemia-reperfusion Injury.* Sci Rep, 2016. **6**: p. 30643.
148. Huang, S.L. and R.C. MacDonald, *Acoustically active liposomes for drug encapsulation and ultrasound-triggered release.* Biochim Biophys Acta, 2004. **1665**(1-2): p. 134-141.
149. Di Mauro, V., et al., *Bioinspired negatively charged calcium phosphate nanocarriers for cardiac delivery of MicroRNAs.* Nanomedicine, 2016. **11**(8): p. 891-906.

CHAPTER 3

A microRNA program controls the transition of cardiomyocyte hyperplasia to hypertrophy and stimulates mammalian cardiac regeneration

[1]Ellen Dirkx*; [1]**Andrea Raso***; [1,2]Hamid el Azzouzi; [3,4]Ryan J. Cubero; [1]Servé Olieslagers; [5]Manon M. Huibers; [5]Roel de Weger; [6]Sailay Siddiqi; [7]Silvia Moimas; [7]Consuelo Torrini; [7]Lorena Zentillin; [7]Luca Braga; [1,8]Paula A. da Costa Martins; [7]Serena Zacchigna; [7]Mauro Giacca and [1]Leon J. De Windt

*These authors contributed equally to this work;

[1]Department of Cardiology, CARIM School for Cardiovascular Diseases, Maastricht University, 6229 ER Maastricht, The Netherlands;

[2]Department of Cardiology, University Medical Center Utrecht, 3584 CX Utrecht, The Netherlands;

[3] The Abdus Salam International Centre for Theoretical Physics, 34151 Trieste, Italy;

[4]Centre for Neural Computation, Kavli Institute for Systems Neuroscience, Norwegian University of Science and Technology, 7030 Trondheim, Norway

[5]Department of Pathology, University Medical Center Utrecht, 3584 CX Utrecht, The Netherlands;

[6]Department of Cardiothoracic Surgery, Radboud University Medical Center, Nijmegen, the Netherlands;

[7]International Centre for Genetic Engineering and Biotechnology (ICGEB), Trieste, Italy;

[8]Department of Physiology and Cardiothoracic Surgery, Faculty of Medicine, University of Porto, Porto, Portugal.

[In revision]

Abstract

Myocardial regeneration is restricted to early postnatal life, when mammalian cardiomyocytes still retain the ability to proliferate. The molecular cues that induce cell cycle arrest of neonatal cardiomyocytes towards terminally differentiated adult heart muscle cells remain obscure. Here we report that the miR-106b~25 cluster is highly expressed in the early postnatal myocardium and decreases in expression towards adulthood, especially under conditions of overload, and orchestrates the transition of cardiomyocyte hyperplasia towards cell cycle arrest and hypertrophy by virtue of its targetome. In line, gene delivery of miR-106b~25 to the mouse heart provokes cardiomyocyte proliferation by targeting a network of negative cell cycle regulators including E2f5, Cdkn1c, Ccne1 and Wee1. Conversely, gene-targeted miR-106b~25 null mice display spontaneous hypertrophic remodeling and exaggerated remodeling to overload by derepression of the prohypertrophic transcription factors Hand2 and Mef2d. Taking advantage of the regulatory function of miR-106b~25 on cardiomyocyte hyperplasia and hypertrophy, viral gene delivery of miR-106b~25 provokes nearly complete regeneration of the adult myocardium after ischemic injury. Our data demonstrate that exploitation of conserved molecular programs can enhance the regenerative capacity of the injured heart.

Introduction

Proliferation of cardiogenic precursor cells and division of immature cardiomyocytes is key to mammalian cardiac morphogenesis during embryonic and fetal development [1,2]. The neonatal mammalian heart still retains considerable proliferative capacity reminiscent of lower vertebrates [3-7], and is sustained by hypoxic conditions [8], activation of Hippo signaling [9], various transcriptional regulators [10-12], and endogenous microRNA mechanisms [13,14]. Complete regeneration of the injured myocardium, including the human neonatal heart [15], exclusively takes place in a short time window during fetal and early postnatal life, when cardiomyocytes still possess the ability to proliferate [7]. Shortly after birth, however, the majority of cardiomyocytes loses their proliferative capacity, and shift towards a terminally differentiated phenotype, with restricted ability to re-activate mitosis [16]. Limited myocyte turnover does occur in the adult mammalian heart, but insufficient to restore contractile function following injury [17]. The default growth response of the adult heart to overload or injury consists primarily of cardiomyocyte hypertrophy, a form of cellular growth without cell division that often precipitates in heart failure [18], a serious clinical disorder that represents a primary cause of morbidity and hospitalization. In humans, despite remarkable progresses made by device-based therapies and drug interventions [19], the only way to replace lost cardiomyocytes is heart transplantation. Identification of the developmental molecular mechanisms that stimulate a proliferative phenotype in early postnatal life, control cell cycle arrest and produce a hypertrophic response of the terminally differentiated heart muscle, may hold the key to unlock the regenerative potential of the adult mammalian heart.

RESULTS

Suppression of the miR-106b~25 cluster facilitates cardiac remodeling

We recently demonstrated that mature miR-25 transcripts are downregulated in two mouse models of heart failure, and results in the derepression of the bHLH transcription factor Hand2 in the postnatal mammalian myocardium [20]. miR-25 is embedded in the miR-106b~25 cluster, located on mouse chromosome 5 (chromosome 7 in humans) in an intronic region of the DNA-replication gene Mcm7 and consists of three miRNAs: miR-106b, miR-93 and miR-25 (Fig.1a). Here we show that each miR-106b~25 cluster member displayed decreased expression in human cardiac biopsies of end-stage heart failure obtained upon heart transplantation compared to healthy controls (Fig.1b) and decreased expression in two mouse models of heart failure (Suppl.Fig.1a).

To more directly address the ramifications of reduced expression of miR-106b~25 for the postnatal heart, we subjected cohorts of miR-106b~25 -/- mice [21] to sham surgery or pressure overload by transverse aortic constriction (TAC) surgery and serially assessed

cardiac geometry and function at four weeks (Fig.1c; Suppl.Fig.1b). Remarkably, miR-106b~25 -/- mice already suffered from a mild form of eccentric hypertrophy at baseline as evidenced in sham-operated mice by an increased cardiac geometry, reduced wall thickness, reduced ejection fraction (EF), and increased cardiomyocyte size at four weeks after sham surgery (Fig.1d-k; Table1). Four weeks of TAC surgery in wild-type mice or miR-106b~25 -/- mice resulted in severe myocyte disarray, interstitial fibrosis, increased heart weight, left ventricular dilation, systolic and diastolic dysfunction as well as a transcript induction of Nppa, Nppb, Acta1 and Myh7 as hypertrophic "stress" markers with consistently more severe phenotypes in miR-106b~25 -/- mice (Fig.1d-k; Table1).

Mechanistically, we have previously shown miR-25-dependent regulation of the pro-hypertrophic embryonic transcription factor Hand2 in the adult heart and could repeat this finding (Suppl.Fig1c,d) [20]. To further understand the mechanistic role of miR-106b~25 in cardiac remodeling, we analyzed bioinformatics databases to search for miR-106b, miR-93 and miR-25 binding sites in cardiac expressed protein-coding transcripts. We identified a perfect match for a miR-25 heptametrical seed sequence in the transcription factor Myocyte enhancer factor 2d (Mef2d) that showed complete evolutionary conservation among vertebrates (Fig.1l), validated the target gene using luciferase reporters harboring either the wild-type or site-directed mutagenesis of key nucleotides in the miR-25 binding site (Fig.1m), and finally demonstrated derepression of Mef2d protein expression in hearts from miR-106b~25 -/- mice in vivo by Western blotting (Fig.1n). Taken together, these data demonstrate that the miR-106b~25 cluster is repressed in the failing heart and causes eccentric hypertrophic remodeling by simultaneous derepression of the prohypertrophic transcription factors Hand2 and Mef2d.

Activation of the miR-106b~25 cluster provokes cardiac enlargement

To further evaluate the function of the miR-106b~25 cluster in cardiac disease, we measured the expression of miR-106b, miR-93 and miR-25 in the postnatal mouse heart at postnatal day 0 (p0), p5, p10, p15, and p20, representing developmental stages towards adulthood (p56, week 8). The data demonstrate that miR-106b~25 cluster was on average 6-8 fold higher expressed early in the postnatal phase and slowly decreased in expression to adult expression levels after which expression remained stable (Fig.2a).

Next, we made use of the high cardiac tropism and prolonged expression of serotype 9 adeno-associated viral (AAV9) vectors following systemic delivery [22]. AAV9 vectors expressing mmu-miR- 106b, mmu-miR-93 and mmu-miR-25 precursor miRNAs (AAV9-miR-106b~25), or a control vector with an empty multiple cloning site (AAV9-MCS), were injected intraperitoneally in neonatal mice at postnatal day 1 (p1; Fig.2b) in a gain-of-function approach (Fig.2c). Anticipating a cardiac phenotype resistant to hypertrophic remodeling, much to our surprise, at 4 weeks, the hearts of mice injected with AAV9-miR-

106b~25 were histologically normal but significantly enlarged (Fig.2d). There was no sign of inflammatory cell infiltration or cardiac fibrosis content (Fig.2d,k). Echocardiographic analysis demonstrated that heart size and interventricular septum thickness in systole was significantly increased (Fig.2e-h, table 2), but cardiac morphometric dimensions and contractile function was normal as evidenced by the absence of ventricular dilation (Fig.2i) and ejection fraction (Fig.2j). Even more peculiar, individual myocyte size was unaltered and there was no evidence for reactivation of a "fetal" gene expression pattern characteristic for hypertrophic cardiomyocytes (Fig.2l,m). Conclusively, overexpression of the miR-106b~25 cluster to physiological levels as observed in the early postnatal developmental period produced cardiac enlargement in the adult heart without classical signs of pathological hypertrophic remodeling.

The miR-106b~25 cluster stimulates cardiomyocyte proliferation

To understand how the miR-106b~25 cluster can evoke cardiac growth, we resorted to cardiomyocyte cultures isolated from neonatal hearts, which retain both hypertrophic and proliferative properties [23]. We performed a fluorescence-microscopy-based analysis in neonatal rat cardiomyocytes transfected with either a control precursor miRNA, or precursors for miR-106b, miR-93 or miR-25. At 72 h, cells were stained for sarcomeric α-actinin to distinguish cardiomyocytes from non-myocytes, and we included the proliferation marker 5-ethynyl-2'-deoxyuridine (EdU), a thymidine analogue that is incorporated into newly synthesized DNA (Fig.3a,b). Automated image segmentation and analysis was performed to selectively quantify number of proliferating cardiomyocytes (α-actinin+, EdU+; Fig.3c) and total number of cardiomyocytes (α-actinin+; Fig.3d). The data demonstrate that miR-106b, miR-93 or miR-25 stimulated cardiomyocyte proliferation and cardiomyocyte numbers by a factor of 3 with no substantial differences between the miRNA cluster members.

Next, to evaluate whether the miR-106b~25 cluster would also enhance cardiomyocyte proliferation in vivo, we injected AAV9-miR-106b~25 intraperitoneally in neonatal mice at p1 to elevate cardiac miR-106b~25 cluster expression, administered Edu intraperitoneally at p10 and analyzed the hearts at p12 (Fig.3e). The hearts of p12 mice injected with AAV9-106b~25 were significantly enlarged compared to those from mice injected with the control AAV9 (Fig.3f), with no sign of inflammatory cell infiltration or increased cardiac fibrosis content, and no increase in cardiomyocyte size (Fig.3f,g). Confocal microscopy indicated that the number of both cardiomyocytes in S phase of the cell cycle (α-actinin+, EdU+; Fig.3h, I; Suppl.Fig.1e) and mitotic cardiomyocytes (α-actinin+, PH3+; Fig.3h,j) or (α-actinin+, Aurora B+; Suppl.Fig.1f) was significantly increased in hearts of animals injected with AAV9-miR-106b~25 compared to hearts of animals injected with the control AAV9-MCS.

Next, to ascertain if the individual cluster members showed differences in activating cardiomyocyte proliferation, we also generated AAV9 vectors expressing either miR-106b, miR-93 or miR-25 and administered the viral vectors intraperitoneally in neonatal mice at p1, administered EdU at p10 and analyzed the hearts at p12 (Fig.4a). In each case, mice with increased expression of either miR-106b, miR-93 or miR-25 were significantly enlarged (Fig.4b), showed no increase in cardiomyocyte cell size (Fig.4b,c), demonstrated an increased number of cardiomyocytes in S phase of the cell cycle (α-actinin+, EdU+; Fig.4d,e) and mitotic cardiomyocytes (α-actinin+, PH3+; Fig.4f,g; or α-actinin+, Aurora B+; Fig.4h). Taken together, these results show that elevated cardiac expression of the complete miR-106b~25 cluster or the individual cluster members significantly enhance proliferation of at least a subset of cardiomyocytes in vivo.

The miR-106b~25 cluster suppress cell cycle inhibitors

To elucidate the molecular mechanisms underlying the proliferative effects of this microRNA cluster, we performed RNA-seq to assess the transcriptome changes in total neonatal rat cardiomyocyte RNA after transfection with miR-106b, miR-93 or miR-25 mimics. This analysis identified 1,082 genes for miR-106b, 1,347 genes for miR-93, and 1,673 genes for miR-25 upregulated and 1,253 genes for miR-106b, 1,594 genes for miR-93, and 2,327 genes for miR-25 downregulated (at 1.0 reads per kilobase of exon model per million mapped reads (RPKM) cutoff and 1.30 fold-change cutoff; Fig. 5a, Suppl.TableS1). We then imposed bioinformatic predictions of miRNA seed sequence interactions with rat transcripts that were downregulated by the miRNAs upon transfection to cardiomyocytes according to the transcriptomic data, yielding 112, 217, and 420 miR-106b, miR-93 and miR-25 target genes respectively, with substantial overlap between the miR-106b and miR-93 targetome (Fig. 5b). Next, a bioinformatic protein-protein interaction network was derived that integrates and scores protein interactions across different evidence channels (conserved neighborhood, co-occurrence, fusion, co-expression, experiments, databases and text mining). For each miRNA in the miR106b~25 cluster, a subnetwork was extracted. Analysis of the networks showed a particularly dense and often overlapping enrichment for genes functioning in cell cycle regulation, and to a lesser extent networks of genes involved in actin cytoskeletal organization, oxidative stress, and components of the Hippo pathway (Fig. 5c).

miR-106b and miR-93 had overlapping targets among the cyclins and cyclin-dependent kinases including Ccnb1 (cyclin B), Ccna2 (cyclin A), Ccnd1 and Ccnd2 (cyclin Ds) as well as Ccne2 (cyclin E), suggesting that these two miRNAs affected the G2-phase of the cell cycle (Fig 5d). miR-25 showed an upregulation of Ccnd1 and Ccnd2 (cyclin Ds) accompanied by a downregulation of Ccne1 and Ccne2 (cyclin E), Ccna2 (cyclin A) and Ccnb1 (cyclin B), suggesting that this miRNA affected the S-phase of the cell cycle (Fig 5d). Apart from

regulation of specific Cyclin/Cdk complexes, common targets among all members of the miR-106b~25 cluster included various cell cycle inhibitors that act on various cell cycle phases, including Cdkn1a (cyclin-dependent kinase inhibitor 1a or $p21^{CIP1}$), Cdkn1c (cyclin-dependent kinase inhibitor 1c or $p57^{KIP2}$), the retinoblastoma transcriptional corepressor 1 (Rb1) inhibitor E2F5, and the G2 checkpoint kinase Wee1 (Fig 5c,d). Experimentally, we identified perfect matches for the heptametrical seed sequence for the miRNAs in the 3'UTRs of Cdkn1c and E2F5 that showed evolutionary conservation among vertebrates (Suppl. Fig.1g,i), validated the target genes using luciferase reporters harboring either the wild-type or site-directed mutagenesis of key nucleotides in the miRNA binding sites (Suppl. Fig.1h,j), and finally demonstrated derepression of E2F5, Cdkn1c, Wee1 and Ccne1 protein expression in cultured cardiomyocytes transfected with an antimiR for miR-106b, miR-25 (Fig. 5e,f) or in hearts from miR-106b~25 null mice by Western blotting (Fig. 5g).

Collectively, these data demonstrate that the miR-106b~25 cluster regulates densily overlapping networks of genes involved in cell cycle regulation and a number of key cell cycle inhibitors, explaining the proliferative effects of this miRNA cluster.

The miR-106b~25 cluster stimulates post-infarction cardiac regeneration

The adult heart is characterized by a very poor regenerative potential. Given that the miR-106b~25 cluster is higher expressed in the early postnatal phase and regulates cell cycle regulators and postnatal cardiomyocyte proliferation, we realized that viral delivery of the miRNA cluster could potentially enhance post-infarction regeneration in adult heart. To test this, adult CD1 mice underwent permanent ligation of left anterior descending (LAD) coronary artery to induce myocardial infarction (MI) and hearts were injected in the peri-infarcted area with AAV9-miR-106~25 of a control AAV9 vector (AAV-MCS) (Fig.6a). This approach resulted in efficient overexpression of each miRNA over control expression levels after MI (Fig.6b). At three weeks of MI, cross-sectioning hearts from ligation to base demonstrated that hearts injected with the control AAV9 vector displayed the typical large and thinned scarred infarct accompanied with severe biventricular dilation (Fig.6c,d). In sharp contrast, hearts injected with AAV9-miR-106~25 demonstrated significantly reduced infarct size and preservation of viable LV tissue and cardiac geometry (Fig.6c,d). Echocardiographic analysis demonstrated near complete normalization of LV mass (Fig.6e), LVPWd (Fig.6f), LVIDs (Fig.6g), LV EF (Fig.6h) and other functional parameters (Table 3), and a reduction in "stress" marker genes (Fig.6i). Confocal microscopy revealed that in mice receiving AAV9-miR-106b~25 injections, at three weeks a significant number of EdU-positive cardiomyocyte nuclei was detected in the infarct zone (Fig.6j) with well integrated cardiomyocytes within the myocardial structure indicative of active proliferation and regeneration following infarction.

Conclusively, the miR-106b~25 cluster, relatively high expressed in the early postnatal myocardium that still retains regenerative potential, directs networks of cell cycle regulators and stimulates proliferation of at least a subset of cardiomyocytes in vivo. In adulthood, the relative low cardiac expression of miR-106b~25 sustains derepression of prohypertrophic cardiomyocyte gene programs that facilitate adverse remodeling in response to overload (Fig.6k). Exploiting this endogenous regulator between cardiomyocyte hyperplasia and hypertrophy by viral gene delivery enhances the endogenous regenerative capacity of the mammalian myocardium.

DISCUSSION

Upon after birth, cardiomyocytes enter cell cycle arrest and become terminally differentiated accompanied by polyploidy and hypertrophy as the default growth response to overload or injury [7,24,25]. This terminally differentiated phenotype and reduced cellular plasticity makes the heart more vulnerable in situations when increased workload is required as it either triggers irreversible cell death or hypertrophy [26], which often precipitates in heart failure, a serious clinical disorder that represents the primary cause of morbidity and hospitalization in Western societies.

Here we report on the evolutionary conserved microRNA cluster that is highly expressed in the early postnatal myocardium and repressed in the adult heart in man and mouse in disease conditions. Remarkably, mice lacking miR-106b~25 display spontaneous cardiomyocyte hypertrophy and eccentric remodeling, mechanistically explained by the derepression of prohypertrophic downstream targets, most notably the bHLH transcription factor Hand2, which controls embryonic gene programs, cardiac growth and features of heart failure [20]. Another downstream miR-106b~25 target, myocyte enhancer factor-2 (MEF2) transcription factor Mef2d, serves as terminal branch of stress signaling pathways that drive pathological cardiac remodeling. In line, forced overexpression of Mef2d was sufficient to drive a fetal gene program and pathological remodeling of the heart [27]. Overexpression of miR-106b~25 by adeno-associated viral (AAV) vectors stimulated cardiomyocyte proliferation, at least in a subset of cardiomyocytes, by targeting a network of genes with cell cycle regulatory functions including the key cell cycle inhibitors E2f5, Cdkn1c, Ccne1 and Wee1. Our data are in line with earlier observations that positive cell cycle regulators including subtypes of cyclins, cyclin-dependent kinases and proto-oncogenes are abundantly expressed in the fetal and neonatal heart [28,29]. In the adult heart, cyclin-dependent kinase inhibitors, negative regulators of the cell cycle, are more prevalent [28,29]. In line, forced overexpression of cyclin D2, a positive regulator of the G1/S transition, induced DNA synthesis and proliferation in mammalian cardiomyocytes [28,29]. Additionally, overexpression of cyclin A2, which promotes the G1/S and G2/M transitions, results in cardiomyocyte proliferation [30], improved cardiac function after

ischemic injury in mice [31] and pigs [32]. The combined observations suggest a model whereby defined orchestration of cell cycle regulators underlies the developmental cell cycle arrest of postnatal cardiomyocytes. Moreover, the characteristics of miR-106b~25 expression in this developmental time frame and its targetome provides a mechanistic explanation for cell cycle exit towards the acquirement of the terminally differentiated phenotype. Hence, when miR-106b~25 expression is higher, as is the case in the early postnatal heart, cell cycle inhibitors including E2f5, Cdkn1c, Ccne1 and Wee1 are actively suppressed resulting in a proliferative state and cardiomyocyte hyperplasia, while differentiation programs elicited by Hand2 and Mef2d are suppressed. Vice versa, in the overloaded or injured adult heart when miR-106b~25 expression is lower, cell cycle re-entry is actively suppressed by the derepression of cell cycle inhibitors, and a prohypertrophic terminal differentiation program is promoted. Taking advantage of the regulatory function between cardiomyocyte hyperplasia and hypertrophy by viral gene delivery of miR-106b~25 produced regeneration of the adult myocardium in response to chronic ischemic injury. Our data demonstrate that exploitation of conserved epigenetic molecular programs can enhance the regenerative capacity of the injured myocardium.

METHODS

Human heart samples. Approval for studies on human tissue samples was obtained from the Medical Ethics Committee of the University Medical Center Utrecht, The Netherlands, and by the Ethical Committee of the University Hospital Hamburg, Germany (Az. 532/ 116/ 9.7.1991). All patients or their relatives gave written informed consent before operation. In this study, we included tissue from the left ventricular free wall of patients with end-stage heart failure secondary to ischemic heart disease. Control tissue was taken from the left ventricular free wall of refused donor hearts. Failing hearts were also obtained from patients undergoing heart transplantation because of terminal heart failure. Non-failing donor hearts that could not be transplanted for technical reasons were used for comparison. The donor patient histories did not reveal any signs of heart disease.

Mouse models. Mice homozygous null for the mirc3 cluster (*miR-106b~25*) located in intron 13 of the *Mcm7* (minichromosome maintenance complex component 7) gene were generated previously [21], obtained from the Jackson Laboratory (Mirc3tm1.1Tyj/J, Stock No: 008460) and maintained in a B6SV129F1 background. Both male and female *miR-106b~25* null mice of 3-6 months of age were used in this study. Other mice used in this study were 3-6 month old male calcineurin transgenic mice in a B6SV129F1 background expressing an activated mutant of calcineurin in the postnatal heart under control of the 5.5 kb murine *myh6* promoter (MHC-CnA) [33]; male and female CD1 wild-type mice ranging between postnatal (p) day 0 and p56; male and female B6SV129F1 wild-type mice of 3-6 months of age (Charles River Laboratories). All animal studies were performed in

accordance with local institutional guidelines and regulations.

Production of recombinant AAV vectors. The precursors of *mmu-miR-106b*, *mmu-miR-93* and *mmu-miR-25* plus upstream and downstream flanking region sequences (total approximately 200 base pairs) were amplified from mouse genomic DNA isolated from a wild-type CD1 mouse heart, using QIAamp DNA mini kit (Qiagen), according to the manufacturer's instructions. The primers used to amplify the precursor sequences were: foward primer: 5'-GTATCATAAGGATCCCTTTCCACTGCTCTGGTGAG-3' and reverse primer: 3'-GTATCATAAGTCGACCTCACCTAGCTGTCTGTCC-5'. The amplified sequences were cloned into the pZac2.1 vector (Gene Therapy Program, Penn Vector core, University of Pennsylvania, USA) using the restriction enzymes BamH I and Sal I. Recombinant AAV serotype 9 vectors were generated at the AAV Vector Unit of ICGEB, Trieste (Italy), as described previously [34]. CD1 mice at postnatal day 1 were intraperitoneally injected with an empty AAV9 vector (AAV9-MCS; multiple cloning site, negative control) or AAV9-miR-106b~25 at a dose of 1 x 10^{11} viral genome particles per animal, using an insulin syringe with 30-gauge needle. 12 days after injection, the hearts were collected for histological analysis.

Aortic banding, myocardial infarction, AAV9 delivery and transthoracic echocardiography. Transverse aortic constriction (TAC) or sham surgery was performed in 2-6 month-old B6SV129F1 mice by subjecting the aorta to a defined 27 gauge constriction between the first and second truncus of the aortic arch as described previously [35,36]. Myocardial infarction (MI) was produced in 2-6 month-old CD1 mice by permanent left anterior descending (LAD) coronary artery ligation [34]. Briefly, mice were anesthetized with an intraperitoneally injection of ketamine and xylazine, endotracheally intubated and placed on a rodent ventilator. Body temperature was maintained at 37 °C on a heating pad. The beating heart was accessed via a left thoracotomy. After removing the pericardium, a descending branch of the LAD coronary artery was visualized with a stereomicroscope (Leica) and occluded with a nylon suture. Ligation was confirmed by the whitening of a region of the left ventricle, immediately post-ligation. Immediately after MI surgery, adult mice received an intracardiac injection of AAV9 vectors (AAV9-MCS or AAV9-miR-106b~25) at a dose of 1 x 10^{11} viral genome particles per animal. 5-ethynyl-2'-deoxyuridine (EdU, Life Technologies) was administered intraperitoneally (500 µg per animal) every 2 days, for a period of ten days. For Doppler-echocardiography, mice were shaved and lightly anaesthetized with isoflurane (mean 3% in oxygen) and allowed to breathe spontaneously via a nasal cone. Non-invasive, echocardiographic parameters were measured using a RMV707B (15-45 MHz) scan-head interfaced with a Vevo-770 high frequency ultrasound system (VisualSonics). Long-axis ECG-triggered cine loops of the left ventricular (LV) contraction cycle were obtained in B-mode to assess end-diastolic/systolic volume. Short-axis recordings of the LV contraction cycle were taken in M-mode to assess wall thickness of the anterior/posterior wall at the mid-papillary level. Doppler was used to determine the ratio between early (E) and late (A) ventricular filling velocity (E/A ratio) and to calculate the

pressure gradient between the proximal and distal sites of the transverse aortic constriction and only mice with a pressure gradient > 50 mm Hg were included. From B-mode recordings, LV length from basis to apex, LV internal diameter in systole (LVIDs) and diastole (LVIDd) were determined. From M-mode recordings, LV posterior wall thickness in systole (LV PWs) and diastole (LV PWd) were determined. LV mass was calculated with the following formula: (0,8*(1.04*(((LVIDd + LV PWd + IVSd)^3)-((LVIDd)^3))+0,6); fractional shortening (FS) was calculated with the following formula: (LVIDd-LVIDs)/LVIDd*100). Ejection fraction (EF) was calculated as ((SV/Vd)*100) with Vs, systolic volume (3,1416*(LVIDs^3)/6), Vd, diastolic volume (3,1416*(LVIDd^3)/6), and SV, stroke volume (Vd-Vs).[36]

Fluorescent Fluorescence activated cell sorting (FACS). Neonatal CD1 mice at age p1 randomly received AAV9-MCS or AAV9-miR106b~25. After 10 days, all mice we administered a single EdU injection and 2 days later cardiomyocytes were isolated and fixed using 4% PFA. Next, cells were permeabilized using 0.1% Triton-X and incubated for 2 hours at room temperature with mouse monoclonal antibody against sarcomeric α-actinin (1:100; Abcam), followed by an incubation of 1 hour with the secondary antibody conjugated to Alexa Fluor-488 (Life Technologies). Next, cells were further processed using the Click-IT EdU 647 Imaging kit to reveal EdU incorporation, according to the manufacturer's instructions, and stained with Hoechst 33342 (Life Technologies). Acquisition and analysis was performed on a BD FACSCelesta cell analyser. Analysis was performed using FACSDiva Version 6.1.3.

Histological analysis and (immunofluorescence) microscopy. Hearts were arrested in diastole, perfusion fixed with 4% paraformaldehyde/PBS solution, embedded in paraffin and sectioned at 4 μm. Paraffin sections were stained with hematoxylin and eosine (H&E) for routine histological analysis; Sirius Red for the detection of fibrillar collagen; and FITC-labelled antibody against wheat-germ-agglutinin (WGA) to visualize and quantify the myocyte cross-sectional area (1:100 Sigma Aldrich). Cell surface areas and Fibrotic areas were determined using ImageJ imaging software (http://rsb.info.nih.gov/ij/). For immunofluorescence, paraffin sections were deparaffinized, rehydrated, and permeabilized with 0.5% Triton X-100/PBS, followed by overnight incubation at 4 °C in 1% BSA with primary antibodies: mouse monoclonal [EA-53] to sarcomeric alpha-actinin (Abcam ab9465), rabbit polyclonal anti-phospho-Histone H3 (Ser10) (Sigma-Millipore 06-570), rabbit polyclonal anti-Aurora B (Abcam ab2254). Next, sections were washed with PBS and incubated for with the respective secondary antibodies conjugated with Alexa Fluor-488, -555, or -647. For Edu staining sections were processed with the Click-IT EdU 555 Imaging kit to according the manufacturer's instructions. The nuclear counter-staining was performed with Hoechst 33342 (Life Technologies) and slides were then mounted in Vectashield (Vector Labs). Slides were visualized using a Zeiss Axioskop 2Plus with an AxioCamHRc.

Western blot analysis. Whole tissue or cell lysates were produced in 150 mM NaCl, 50 mM Tris-HCl, 5 mM EDTA, 50 mM NaF, 1% Igepal™, 0,05 % SDS, 40 mM β-glycerophosphate, 10

mM Na-pyrophosphate, PhosSTOP- and Protease inhibitor cocktail (Roche Applied Science). Samples were boiled in 4x Leammli buffer, including 2% β-mercaptoethanol, for 5 minutes at 95°C. SDS-PAGE and Western blotting were performed using the Mini-PROTEAN 3 system (Biorad). Blotted membranes were blocked in 5% BSA / TBS-Tween. Primary antibody labeling was performed overnight at 4°C at a concentration of 2 µg IgG per 7 mL blocking buffer. Antibodies used included were: rabbit polyclonal antibody anti-p57 (H-91) (SantaCruz sc-8298), rabbit polyclonal antibody anti-E2f5 (Abcam ab22855), rabbit polyclonal antibody anti-E2F5 (E-19) (SantaCruz sc-999), rabbit monoclonal antibody anti-Cyclin E1 (D7T3U) (Cell Signaling Technology #20808), rabbit polyclonal antibody anti-Wee1 (Cell Signaling Technology #4936), rabbit polyclonal antibody anti-Mef2d (Abcam ab104515), mouse monoclonal anti-GAPDH (Millipore, MAB374 clone 6C5), mouse monoclonal anti-alpha-Tubulin (Sigma-Aldrich T6074) rabbit polyclonal anti-Histone H3 (Cell Signaling Technology 9715S) and the secondary polyclonal swine anti-rabbit immunoglobulins/HRP (DAKO P0399) and polyclonal rabbit anti-mouse immunoglobulins/HRP (DAKO P0161). Secondary HRP conjugated antibodies were applied for 1 hour at room temperature. Following antibody incubation, blots were washed for 3x10 minutes in TBS-Tween. Images were generated using Supersignal West Dura Extended Duration ECL Substrate (Pierce) and the LAS-3000 documentation system (FujiFilm Life Science). Stripping was performed with Restore Western blot stripping buffer (Pierce). Output intensities were normalized for loading.

Quantitative PCR. Total RNA (1 µg) was was extracted using miRNeasy Mini Kit (Qiagen) and applied to either miR-based or mRNA based reverse transcription. For miR-based reverse transcription, total RNA was reverse transcribed using miRCURY LNA Universal cDNA synthesis kit (Exiqon) followed by Real-time PCR using predesigned miRCURY LNA PCR primer sets (Exiqon) and miRCURY LNA SYBR Green master mix, according to the manufacturer's instructions.[36] Expression was normalized to expression levels of 5S rRNA. For mRNA-based reverse transcription, total RNA was reverse transcribed using hexameric random primers. The housekeeping gene ribosomal protein L7 (RPL7) was used for normalization. Fold changes were determined using the $2^{-\Delta\Delta CT}$ method. Real-time PCR primer sequences used in the study are:
mouse Nppa, 5'-TCTTCCTCGTCTTGGCCTTT-3' and 3'-CCAGGTGGTCTAGCAGGTTC-5'; mouse Nppb, 5'-TGGGAGGTCACTCCTATCCT-3' and 3'-GGCCATTTCCTCCGACTTT-5'; mouse Acta1, 5'-CCGGGAGAAGATGACTCAAA-3' and 3'-GTAGTACGGCCGGAAGCATA-5'; mouse Myh7, 5'-CGGACCTTGGAAGACCAGAT-3' and 3'-GACAGCTCCCCATTCTCTGT-5'; mouse Rpl7, 5'-GAAGCTCATCTATGAGAAGGC-3' and 3'-AAGACGAAGGAGCTGCAGAAC-5'.

Primary cardiomyocyte cultures and transfections. Cardiomyocyte cultures were isolated by enzymatic dissociation of 1 day-old neonatal rat hearts and processed for immunofluorescence as described previously [37]. Neonatal cardiomyocytes were seeded on Primaria 384-well plates (for microscopy) or in Primaria 10 cm dishes (for western

blotting) and one day later, cells were transfected with mimics (Life Technologies) of *hsa-miR-106b-5p*, *hsa-miR-93-5p*, *hsa-miR-25-3p* or *cel-miR-67* as control (25mM) using (Lipofectamine RNAiMAX, Life Technologies). Twenty-four hours after transfection, culture medium was replaced by fresh medium; and 52h after plating 5 µM 5-ethynyl-2'-deoxyuridine (EdU, Life Technologies) was added for 20 h. Cells were fixed at 72 h after plating and processed for immunofluorescence.

Immunofluorescence and image acquisition of cardiomyocytes. Cells were fixed with 4% paraformaldehyde for 15 min, permeabilized with 0.5% Triton X-100 in phosphate buffered saline (PBS) solution for 10 min, followed by 30 min blocking in 1% BSA (Roche). Cells were stained overnight at 4 °C with mouse monoclonal antibody against sarcomeric α-actinin (1:100; Abcam), followed by a secondary antibody conjugated to Alexa Fluor-488 (Life Technologies). Next, cells were further processed using the Click-IT EdU 555 Imaging kit to reveal EdU incorporation, according to the manufacturer's instructions, and stained with Hoechst 33342 (Life Technologies). Image acquisition was performed using an ImageXpress Micro automated high-content screening fluorescence microscope at 10x magnification; a total of 16 images were acquired per wavelength, well and replicate, corresponding to approximately 2.500 cells analyzed per condition. Image analysis was performed using the 'Multi-Wavelenght Cell Scoring' application module implemented in MetaXpress software (Molecular Devices) [34]. Proliferating cardiomyocytes were identified by a positive signal for the proliferation marker EdU and a positive signal for sarcomeric α-actinin.

Luciferase-reporter assays. Constructs bearing 309 bp of murine E2f5 3'UTR (pMIR-E2f5), 591 bp of murine Cdkn1a 3'UTR (pMIR- Cdkn1a), 625 bp of murine Cdkn1c 3'UTR (pMIR-Cdkn1c) and 656 bp of murine Mef2d 3'UTR (pMIR- Mef2d) were subcloned into the pmirGLO Dual-Luciferase miRNA Target Expression Vector (Promega). Correspondent seed-sequence mutated Dual-pMIR-report plasmids were obtained using the QuikChange XL Site-Directed Mutagenesis Kit (Agilent Technologies). Low-passage COS7 cells were grown in DMEM (Invitrogen) supplemented with 10% FCS and seeded ($2{,}5 \times 10^4$) in 48-well plates and transfected at 50-60% confluence with a total of 100 ng Dual-pMIR-report plasmids using X-tremeGENE 9 DNA Transfection Reagent (Roche), followed by transfection with mimics (Life Technologies) of *hsa-miR-106b-5p*, *hsa-miR-93-5p*, *hsa-miR-25-3p* or *cel-miR-67* as control (25mM) using Oligofectamine (Invitrogen). Firefly and Renilla luciferase activities were measured using the Dual Luciferase Reporter Assay System (Promega), according to the manufacturer's instructions.

Transcriptomic analysis and clustering of fold change expression. Deep-sequencing of total RNA isolated from neonatal rat cardiomyocyte cultures was performed 72 hr after transfection of mimics (Life Technologies) of *hsa-miR-106b-5p*, *hsa-miR-93-5p*, *hsa-miR-25-3p* or *cel-miR-67* as control (25mM) by IGA Technology Services (Italy) [34]. RNA purity, integrity and concentration were determined using an Agilent 2100 Bioanalyzer (Agilent Technologies). Only RNAs with a RIN value >7 and an rRNA 28S/18S ratio >2 were

considered for sample preparation. Two µg of total RNA per sample was sequenced on an Illumina HiSeq2000. Two lanes in 7-plex were run obtaining 2 millions of single-reads per sample, 50-bp long. Real-time image analysis, base calling, de-multiplexing and production of FASTQ sequence files were performed on the HiSeq2000 instrument using the HiSeq Software. Raw sequence files were quality checked using FASTQC software (www.bioinformatics.babraham.ac.uk/projects/fastqc) and trimmed to remove Illumina adaptor using Cutadapt software. The raw sequencing reads were then mapped to Ensembl Rattus norvegicus reference genome (GCA_000001895.4 Rnor 6.0.89.6) [38] using STAR software. Rounded gene counts were normalized to RPKM (reads per kilobase of exon model per million mapped reads) using the rpkm function in the Bioconductor package edgeR [39]. Genes with RPKM values greater than 2.00 in both miRNA and cel-miR-67 transfected rat CMs were considered as expressed genes. Fold changes were taken with respect to the expression upon *cel-miR-67* transfection. Genes whose expression fold change were greater than 1.3 were considered as differentially expressed.

Bioinformatics analyses: clustering of fold change expression; pathway enrichment analysis; target predictions; network analyses. The Pearson correlation between the log2-fold changes for all pairs of miRNA were calculated. Clustering was performed hierarchically using the average linkage criterion with a Euclidean distance metric as implemented in SciPy v0.18.1 (http://www.scipy.org). A dendrogram was then generated using the SciPy clustering package to visualize the arrangement of the resulting cluster. Statistically enriched pathways from the set of differentially expressed genes were determined using a hypergeometric distribution-based statistical method as implemented in the Database for Annotation, Visualization and Integrated Discovery (DAVID) Bioinformatics Resources 6.8. The calculated *P*-values were then corrected according to Benjamini-Hochberg procedure to control the false discovery rates arising from multiple testing. KEGG pathways with $P<0.01$ and Benjamini-Hochberg FDR<0.05 are considered as statistically significant. Since bioinformatic predictions of seed sequence interactions with rat transcripts are not available, we compiled a list of rat miRNA-gene interactions from mouse predictions. Predicted mouse gene targets of the seed sequences (corresponding to miRNA families) of miRNAs which belong to the *miR-106b~25* cluster were collected from TargetScanMouse Release 7.1. The scores were calculated to be the most efficient interaction between a mouse gene and a human miRNA in a given miRNA family as determined by the seed sequence. The mouse genes were then translated to its corresponding rat genes through homology using the HomoloGene database. The list of miRNA-gene interactions was filtered to only include genes that were downregulated by the miRNA upon transfection to CMs according to the transcriptomic data (397 downregulated bioinformatic targets by *miR-106b*, 429 by *miR-93* and 358 by *miR-25*). A bioinformatic protein-protein interaction network was derived from STRING database v10.5, which integrates and scores protein interactions across different evidence channels (conserved neighborhood, co-occurrence,

fusion, co-expression, experiments, databases and text mining) and combines the scores from these channels. Only those interactions solely involving rat proteins were considered. To obtain a high confidence interaction network, a cut-off score of 700 (out of 1000) on the combined score was imposed. For each miRNA, a subnetwork was extracted containing only the differentially expressed genes upon imposing a 1.3 fold-change cut-off and the genes of interest in this study. These subnetworks were then merged into a single multi-network wherein the gene components can now be connected by three interactions, one for each miRNA. To further elucidate the multi-network, we catalogued the set of genes that are involved to biological processes of interest using the EMBL annotations of gene ontologies. These biological processes include cell division (*GO:0051301* and *GO:0000086*) with 212 annotated genes, actin cytoskeleton (*GO:0015629*, *GO:0030036*, *GO:0031532* and *GO:0008154*) with 345 annotated genes and oxidative stress response (*GO:0006979*) with 143 annotated genes. Furthermore, knowing the importance of the Hippo signaling pathway in cardiomyocyte proliferation, we also catalogued the set of genes involved in the canonical [40] (19 genes) and non-canonical [41] (21 genes) pathways in which Yap can be phosphorylated. These gene sets were then used to extract a compartmentalized network of genes that are differentially expressed after transfection of the *miR-106b~25* cluster whose interactions can lead to cytokinesis. Network analysis was done using the NetworkX v1.11 package in Python while graph visualization was done using Cytoscape v3.4.0.

Statistical analysis. The results are presented as mean ± standard error of the mean (SEM). Statistical approaches for bioinformatics analyses are described above. All other statistical analyses were performed using Prism software (GraphPad Software Inc.), and consisted of ANOVA followed by Newman-Keuls Multiple Comparison Test when group differences were detected at the 5% significance level, or Student's *t*-test when comparing two experimental groups. Differences were considered significant when $P<0.05$.

Acknowledgements: E.D. is supported by a VENI award 916-150-16 from the Netherlands Organization for Health Research and Development (ZonMW), an EMBO Long-term Fellowship (EMBO ALTF 848-2013) and a FP7 Marie Curie Intra-European Fellowship (Project number 627539). P.D.C.M. is an Established Investigator of the Dutch Heart Foundation. L.D.W. acknowledges support from the *Netherlands CardioVascular Research Initiative*: the Dutch Heart Foundation, Dutch Federation of University Medical Centers, ZonMW and the Royal Netherlands Academy of Sciences. L.D.W. was further supported by grant 311549 from the European Research Council (ERC) and a VICI award 918-156-47 from NWO.

Author Contributions: E.D., A.R., S.O. performed real time PCR experiments. A.R., H.A., S.O. performed Western blots. A.R. performed luciferase assays. E.D., C.T. and R.C. performed transcriptome analysis. H.A. and S.Z. performed surgical procedures in mouse models. E.D. performed echocardiography. E.D., A.R. performed histology in mouse models. E.D., A.R. analysed data. E.D. and S.M. performed FACS analyses. L.B. performed microscopic imaging. M.H., R.W., L.Z., and M.G. provided reagents and models. E.D., M.G. S.S., P.D.C.M. and L.D.W. designed the study. E.D., and L.D.W. wrote the manuscript. E.D, P.D.C.M. and L.D.W. acquired funding for the study. E.D. and A.R. contributed equally as joint first authors.

Competing financial interests: E.D., M.G. and L.D.W filed the data in the manuscript for patent protection. P.D.C.M. and L.D.W. are co-founders and stockholders of Mirabilis Therapeutics BV.

Author Information: Correspondence and requests for materials should be addressed to L.D.W. (l.dewindt@maastrichtuniversity.nl).

References

1. Sedmera, D. & Thompson, R. P. Myocyte proliferation in the developing heart. *Dev Dyn* **240**, 1322-1334, doi:10.1002/dvdy.22650 (2011).
2. Soufan, A. T. *et al.* Three-dimensional measurement and visualization of morphogenesis applied to cardiac embryology. *J Microsc* **225**, 269-274, doi:10.1111/j.1365-2818.2007.01742.x (2007).
3. Becker, R. O., Chapin, S. & Sherry, R. Regeneration of the ventricular myocardium in amphibians. *Nature* **248**, 145-147 (1974).
4. Flink, I. L. Cell cycle reentry of ventricular and atrial cardiomyocytes and cells within the epicardium following amputation of the ventricular apex in the axolotl, Amblystoma mexicanum: confocal microscopic immunofluorescent image analysis of bromodeoxyuridine-labeled nuclei. *Anat Embryol (Berl)* **205**, 235-244, doi:10.1007/s00429-002-0249-6 (2002).
5. Gonzalez-Rosa, J. M., Martin, V., Peralta, M., Torres, M. & Mercader, N. Extensive scar formation and regression during heart regeneration after cryoinjury in zebrafish. *Development* **138**, 1663-1674, doi:10.1242/dev.060897 (2011).
6. Oberpriller, J. O. & Oberpriller, J. C. Response of the adult newt ventricle to injury. *J Exp Zool* **187**, 249-253, doi:10.1002/jez.1401870208 (1974).
7. Porrello, E. R. *et al.* Transient regenerative potential of the neonatal mouse heart. *Science* **331**, 1078-1080, doi:10.1126/science.1200708 (2011).
8. Puente, B. N. *et al.* The oxygen-rich postnatal environment induces cardiomyocyte cell-cycle arrest through DNA damage response. *Cell* **157**, 565-579, doi:10.1016/j.cell.2014.03.032 (2014).

9. Heallen, T. *et al.* Hippo pathway inhibits Wnt signaling to restrain cardiomyocyte proliferation and heart size. *Science* **332**, 458-461, doi:10.1126/science.1199010 (2011).
10. D'Uva, G. *et al.* ERBB2 triggers mammalian heart regeneration by promoting cardiomyocyte dedifferentiation and proliferation. *Nat Cell Biol* **17**, 627-638, doi:10.1038/ncb3149 (2015).
11. Mahmoud, A. I. *et al.* Meis1 regulates postnatal cardiomyocyte cell cycle arrest. *Nature* **497**, 249-253, doi:10.1038/nature12054 (2013).
12. Malek Mohammadi, M. *et al.* The transcription factor GATA4 promotes myocardial regeneration in neonatal mice. *EMBO Mol Med* **9**, 265-279, doi:10.15252/emmm.201606602 (2017).
13. Aguirre, A. *et al.* In vivo activation of a conserved microRNA program induces mammalian heart regeneration. *Cell Stem Cell* **15**, 589-604, doi:10.1016/j.stem.2014.10.003 (2014).
14. Tian, Y. *et al.* A microRNA-Hippo pathway that promotes cardiomyocyte proliferation and cardiac regeneration in mice. *Sci Transl Med* **7**, 279ra238, doi:10.1126/scitranslmed.3010841 (2015).
15. Haubner, B. J., Schuetz, T. & Penninger, J. M. A reproducible protocol for neonatal ischemic injury and cardiac regeneration in neonatal mice. *Basic Res Cardiol* **111**, 64, doi:10.1007/s00395-016-0580-3 (2016).
16. Li, F., Wang, X., Capasso, J. M. & Gerdes, A. M. Rapid transition of cardiac myocytes from hyperplasia to hypertrophy during postnatal development. *J Mol Cell Cardiol* **28**, 1737-1746, doi:10.1006/jmcc.1996.0163 (1996).
17. Bergmann, O. *et al.* Evidence for cardiomyocyte renewal in humans. *Science* **324**, 98-102, doi:10.1126/science.1164680 (2009).
18. Maillet, M., van Berlo, J. H. & Molkentin, J. D. Molecular basis of physiological heart growth: fundamental concepts and new players. *Nat Rev Mol Cell Biol* **14**, 38-48, doi:10.1038/nrm3495 (2013).
19. Velazquez, E. J. *et al.* Coronary-Artery Bypass Surgery in Patients with Ischemic Cardiomyopathy. *N Engl J Med* **374**, 1511-1520, doi:10.1056/NEJMoa1602001 (2016).
20. Dirkx, E. *et al.* Nfat and miR-25 cooperate to reactivate the transcription factor Hand2 in heart failure. *Nat Cell Biol* **15**, 1282-1293, doi:10.1038/ncb2866 (2013).
21. Ventura, A. *et al.* Targeted deletion reveals essential and overlapping functions of the miR-17 through 92 family of miRNA clusters. *Cell* **132**, 875-886, doi:10.1016/j.cell.2008.02.019 (2008).
22. Inagaki, K. *et al.* Robust systemic transduction with AAV9 vectors in mice: efficient global cardiac gene transfer superior to that of AAV8. *Mol Ther* **14**, 45-53, doi:10.1016/j.ymthe.2006.03.014 (2006).
23. Buja, L. M. *et al.* Characterization of a potentially reversible increase in beta-adrenergic receptors in isolated, neonatal rat cardiac myocytes with impaired energy metabolism. *Circ Res* **57**, 640-645 (1985).
24. Senyo, S. E. *et al.* Mammalian heart renewal by pre-existing cardiomyocytes. *Nature* **493**, 433-436, doi:10.1038/nature11682 (2013).
25. Brodsky, V., Sarkisov, D. S., Arefyeva, A. M., Panova, N. W. & Gvasava, I. G. Polyploidy in cardiac myocytes of normal and hypertrophic human hearts; range of values. *Virchows Arch* **424**, 429-435 (1994).
26. Olson, E. N. & Schneider, M. D. Sizing up the heart: development redux in disease. *Genes Dev* **17**, 1937-1956, doi:10.1101/gad.1110103 (2003).
27. Kim, Y. *et al.* The MEF2D transcription factor mediates stress-dependent cardiac remodeling in mice. *J Clin Invest* **118**, 124-132, doi:10.1172/JCI33255 (2008).
28. Busk, P. K. *et al.* Involvement of cyclin D activity in left ventricle hypertrophy in vivo and in vitro. *Cardiovasc Res* **56**, 64-75 (2002).

29. Pasumarthi, K. B., Nakajima, H., Nakajima, H. O., Soonpaa, M. H. & Field, L. J. Targeted expression of cyclin D2 results in cardiomyocyte DNA synthesis and infarct regression in transgenic mice. *Circ Res* **96**, 110-118, doi:10.1161/01.RES.0000152326.91223.4F (2005).
30. Chaudhry, H. W. *et al.* Cyclin A2 mediates cardiomyocyte mitosis in the postmitotic myocardium. *J Biol Chem* **279**, 35858-35866, doi:10.1074/jbc.M404975200 (2004).
31. Cheng, R. K. *et al.* Cyclin A2 induces cardiac regeneration after myocardial infarction and prevents heart failure. *Circ Res* **100**, 1741-1748, doi:10.1161/CIRCRESAHA.107.153544 (2007).
32. Shapiro, S. D. *et al.* Cyclin A2 induces cardiac regeneration after myocardial infarction through cytokinesis of adult cardiomyocytes. *Sci Transl Med* **6**, 224ra227, doi:10.1126/scitranslmed.3007668 (2014).
33. Molkentin, J. D. *et al.* A calcineurin-dependent transcriptional pathway for cardiac hypertrophy. *Cell* **93**, 215-228 (1998).
34. Eulalio, A. *et al.* Functional screening identifies miRNAs inducing cardiac regeneration. *Nature* **492**, 376-381, doi:10.1038/nature11739 (2012).
35. Armand, A. S. *et al.* Cooperative synergy between NFAT and MyoD regulates myogenin expression and myogenesis. *J Biol Chem* **283**, 29004-29010, doi:10.1074/jbc.M801297200 (2008).
36. da Costa Martins, P. A. *et al.* MicroRNA-199b targets the nuclear kinase Dyrk1a in an auto-amplification loop promoting calcineurin/NFAT signalling. *Nat Cell Biol* **12**, 1220-1227, doi:10.1038/ncb2126 (2010).
37. De Windt, L. J., Lim, H. W., Haq, S., Force, T. & Molkentin, J. D. Calcineurin promotes protein kinase C and c-Jun NH2-terminal kinase activation in the heart. Cross-talk between cardiac hypertrophic signaling pathways. *J Biol Chem* **275**, 13571-13579 (2000).
38. Yates, A. *et al.* Ensembl 2016. *Nucleic Acids Res* **44**, D710-716, doi:10.1093/nar/gkv1157 (2016).
39. McCarthy, D. J., Chen, Y. & Smyth, G. K. Differential expression analysis of multifactor RNA-Seq experiments with respect to biological variation. *Nucleic Acids Res* **40**, 4288-4297, doi:10.1093/nar/gks042 (2012).
40. Yu, F. X. & Guan, K. L. The Hippo pathway: regulators and regulations. *Genes Dev* **27**, 355-371, doi:10.1101/gad.210773.112 (2013).
41. Mohseni, M. *et al.* A genetic screen identifies an LKB1-MARK signalling axis controlling the Hippo-YAP pathway. *Nat Cell Biol* **16**, 108-117, doi:10.1038/ncb2884 (2014).

FiGURE LEGENDS

Figure 1. *miR-106b~25* gene deletion induces hypertrophic cardiac remodeling. (a) A schematic representation of the mouse *Mcm7* gene harboring the *miR-106b~25* cluster in intron 13. **(b)** Real-time PCR analysis of *miR-106b*, *miR-93* and *miR-25* abundance in human non-failing or failing myocardium, *n* refers to number of hearts. **(c)** Design of the study. Transverse aortic constriction (TAC) or sham surgery was performed in 2 month-old mice. Cardiac geometry and function were determined by Doppler/echocardiography at 4 weeks after surgery. **(d)** Representative images of whole hearts (top panels), haematoxylin & eosin (H&E)-stained sections of four-chamber view (second panel), high magnification sections (third panel), Sirius Red stained sections (fourth panel) and wheat germ agglutinin (WGA)-stained (fifth panel) histological sections. Quantification of **(e)** left ventricular mass/body weight (BW) ratio, **(f)** left ventricular posterior wall thickness in systole (LVPWs), **(g)** left ventricular internal diameter in systole (LVIDs), **(h)** ejection fraction (EF). *n* refers to the number of animals. **(i)** Quantification of the fibrotic area by Sirius Red staining and **(j)** cell surface areas by wheat germ agglutinin (WGA) staining, *n* refers to number of animals. **(k)** Real-time PCR analysis of *Nppa*, *Nppb, Acta1* and *Myh7*, *n* refers to number of hearts. **(l)** Location and evolutionary conservation of *hsa-miR-25* seed region on Mef2d. **(m)** Activity assay of luciferase reporter constructs in COS7 cells shows the binding of *hsa-miR-25* to the 3'UTR of Mef2d, *n* refers to number of transfection experiments. **(n)** Western blot analysis of endogenous Mef2d and GAPDH as a loading control in hearts from wild type (WT) versus miR-106b~25 knock-out (KO) mice, *n* refers to number of hearts. **P < 0.05* vs corresponding control group; #*P < 0.05* vs corresponding age group (error bars are s.e.m.).

Figure 2. Overexpression of the *miR-106b~25* cluster induces cardiac growth with sustained function. (a) Real-time PCR analysis of *miR-106b*, *miR-93* and *miR-25* abundance in mouse hearts at postnatal day 0 (p0), p5, p10, p15, p20 and p56 (2 months) of age, *n* refers to number of hearts. **(b)** Design of the study. Mice at age p1 were injected intraperitoneally (i.p.) with AAV9-MCS (empty control vector) or AAV9- miR-106b~25 and cardiac geometry and function were determined by Doppler/echocardiography at 4 weeks after injection. **(c)** Real-time PCR analysis of *miR- 106b*, *miR-93* and *miR-25* abundance in AAV9-MCS versus AAV9-miR-106b~25 hearts, 4 weeks after injection, *n* refers to number of hearts. **(d)** Representative images of whole hearts (top panels), haematoxylin & eosin (H&E)-stained sections of four-chamber view (second panel), high magnification sections (third panel), Sirius Red stained sections (fourth panel) and wheat germ agglutinin (WGA)-stained (fifth panel) histological sections. Quantification of **(e)** left ventricular mass/body weight (BW) ratio, **(f)** left ventricular posterior wall thickness in systole (LVPWd), **(g)** interventricular septum thickness in systole (IVSs), **(h)** interventricular septum thickness in diastole (IVSs), **(i)** left ventricular internal diameter in systole (LVIDs), and **(j)** ejection fraction (EF) of mice that received AAV9-MCS or AAV9-miR-106b~25, *n* refers to the number of animals. Quantification of **(k)** the fibrotic area by Sirius Red stainings and **(l)** the cell surface areas by wheat germ agglutinin (WGA)-staining, *n* refers to number of animals. **(m)** Real-time PCR analysis of *Nppa*, *Nppb*, *Acta1,* and *Myh7* in heart tissue from mice that received AAV9-MCS or AAV9-miR-106b~25; or WT or calcineurin transgenic (Myh6-CnA) mice, a mouse model for heart failure, *n* refers to number of hearts. **P < 0.05* vs corresponding control group; #*P < 0.05* vs corresponding age group (error bars are s.e.m.).

Figure 3. Overexpression of the *miR-106b~25* cluster induces cardiomyocyte proliferation. (a) Schematic overview of the experiment. **(b)** Representative fluorescent microscopic images of rat neonatal cardiomyocytes transfected with a control precursor miRNA, or precursors for *miR-106b*,

miR-93 or *miR-25* and stained for α-actinin, 5- ethynyl-2'-deoxyuridine (EdU), and Hoechst. Quantification of **(c)** the number of proliferating cardiomyocytes (α-actinin+, EdU+) and **(d)** total number of cardiomyocytes (α-actinin+) after transfection with a control precursor miRNA, or precursors for *miR- 106b*, *miR-93* or *miR-25*, *n* refers to the number of transfection experiments. **(e)** Design of the study. Mice at postnatal day (p)1 were injected intraperitoneally (i.p.) with AAV9- MCS (empty control vector) or AAV9-miR-106b~25, injected i.p. with EdU at p10 and hearts were analyzed at p12. **(f)** Representative images of whole hearts (top panels), haematoxylin & eosin (H&E)-stained sections of four-chamber view (second panel), Sirius Red stained sections (third panel) and wheat germ agglutinin (WGA)-stained (fourth panel) histological sections. **(g)** Quantification of the cell surface areas from WGA-stained sections, *n* refers to number of animals. **(h)** Confocal microscopy images of heart sections of mice treated with AAV9-MCS or AAV9-miR-106b~25 and stained for α-actinin, EdU and Hoechst or α-actinin, pH3 and Hoechst. Quantification of **(i)** the number of proliferating cardiomyocytes (α-actinin+, EdU+) and **(j)** the number of phospho-histone 3 (pH3) positive cardiomyocytes (α-actinin+, pH3+), *n* refers to number of hearts. **P < 0.05* vs corresponding control group; #*P < 0.05* vs corresponding age group (error bars are s.e.m.).

Figure 4. Overexpression of *miR-106b*, *miR-93* or *miR-25* induces cardiac enlargement by stimulating cardiomyocyte proliferation. (a) Design of the study. Mice at postnatal day (p)1 were injected intraperitoneally (i.p.) with AAV9-MCS (empty control vector), AAV9-miR-106b, AAV9-miR-93 or AAV9-miR-25, injected i.p. with EdU at p10 and hearts were analyzed at p12. **(b)** Representative images of whole hearts (top panels), haematoxylin & eosin (H&E)-stained histological sections of four-chamber view (second panel) and wheat germ agglutinin (WGA)-stained (third panel) histological sections. **(c)** Quantification of the cell surface areas, *n* refers to number of animals. **(d)** Representative confocal microscopy images and **(e)** quantification of proliferating cardiomyocytes (α-actinin+, EdU+) in heart sections of mice receiving AAV9-MCS, AAV9-miR-106b, AAV9-miR-93 or AAV9-miR-25 and stained for α-actinin, EdU and Hoechst, *n* refers to number of hearts. **(f)** Representative confocal microscopy images and **(g)** quantification of the number of pH3 positive cardiomyocytes (α-actinin+, pH3+) in heart sections of mice receiving AAV9-MCS, AAV9-miR-106b, AAV9-miR-93 or AAV9- miR-25 and stained for α-actinin, pH3 and Hoechst, *n* refers to number of hearts. **(h)** Representative confocal microscopy images of heart sections of mice receiving AAV9-MCS, AAV9-miR-106b, AAV9-miR-93 or AAV9-miR-25 and stained for α-actinin, Aurora B and Hoechst. **P < 0.05* vs corresponding control group; #*P < 0.05* vs corresponding age group (error bars are s.e.m.).

Figure 5 . **The *miR-106b~25* cluster suppressss cell cycle inhibitors. (a)** Schematic overview of the experiment. **(b)** Venn diagram showing the relationship between the sets of downregulated genes with *miR-106b*, *miR-93* or *miR-25* seed regions and a 1.3-fold change cut-off with respect to *cel-miR-67*. **(c)** A compartmentalized network of differentially expressed genes involved in cell cycle regulation. Each connection is color- coded according to the miRNA that regulates the differentially expressed gene (magenta for *miR-106b*, cyan for *miR-93* and dark yellow for *miR-25*). Genes indicated by blue circles are downregulated by at least one miRNA while downregulated genes shown in blue squares are found to be bioinformatic targets by at least 1 miRNA. Genes represented by yellow circles are upregulated genes by all three miRNAs. **(d)** Heatmap represention of cell cycle regulators differentially expressed by *miR-106b~25* relative to *cel-miR-67*. **(e)** Western blot analysis

of endogenous E2f5 and Cdkn1c and histone 3 (H3) as a loading control in cardiomyocytes transfected with a control antimiR, or antimiRs for *miR-106b* or *miR-25*, *n* refers to number of transfection experiments. **(f)** Western blot analysis of endogenous Wee1, Ccne1 and Tubulin-a (Tuba1a) as a loading control in cardiomyocytes transfected with a control antimiR, or an antimiR for *miR-106b*, *n* refers to number of transfection experiments. **(g)** Western blot analysis of endogenous E2f5, Cdkn1c, Ccne1 and Gapdh as a loading control in hearts from WT versus *miR- 106b~25* KO mice, *n* refers to the number of animals. **P < 0.05* vs corresponding control group; #*P < 0.05* vs corresponding age group (error bars are s.e.m.).

Figure 6 . **The *miR-106b~25* cluster evokes post-infarction myocardial regeneration. (a)** Design of the study. Adult mice were subjected to sham or myocardial infarction (MI) surgery and received AAV9-MCS or AAV9-miR-106b~25 by intracardiac injections. Cardiac geometry and function were determined by Doppler/echocardiography at 3 weeks after surgery. **(b)** Real-time PCR analysis of *miR- 106b*, *miR-93* and *miR-25* abundance in infarcted hearts receiving AAV9-MCS or AAV9- miR-106b~25, *n* refers to the number of hearts. **(c)** Representative images of Sirius Red- stained ventricular cross-sections from the point of ligation towards the apex of hearts post-MI, treated with AAV9-MCS or AAV9-miR-106b~25. **(d)** Quantification of the infarct area of the post-infarcted left ventricles from mice receiving AAV9-MCS or AAV9-miR- 106b~25, *n* refers to the number of hearts. Quantification of **(e)** left ventricular mass/body weight (BW) ratio, **(f)** left ventricular posterior wall thickness in diastole (LVPWd), **(g)** left ventricular internal diameter in systole (LVIDs) and **(h)** ejection fraction (EF) of mice that received AAV9-MCS or AAV9-miR-106b~25 after sham or MI surgery, *n* refers to the number of animals. **(i)** Real-time PCR analysis of *Nppa*, *Acta1* and *Myh7*, *n* refers to number of hearts. **(j)** Representative images of the infarct border zone of mice treated with AAV9-MCS or AAV9-miR-106b~25 after MI surgery, and stained for α- actinin and EdU. **(k)** Schematic representation of the model depicted. **P < 0.05* vs corresponding control group; #*P < 0.05* vs corresponding age group (error bars are s.e.m.).

Supplemental Figure 1. The *miR-106b~25* cluster expression, target genes and proliferative effects. **(a)** Real-time PCR analysis of *miR-106b*, *miR-93* and *miR-25* abundance in hearts from calcineurin transgenic mice (Myh6-CnA) or mice subjected to transverse aortic constriction (TAC), *n* refers to number of hearts. **(b)** Real-time PCR analysis of *miR-106b*, *miR-93* and *miR-25* abundance in hearts of wild-type (WT) or miR- 106b~25 null mice, *n* refers to the number of hearts. **(c)** Location and evolutionary conservation of *hsa-miR-25* seed region on Hand2. **(d)** Activity assay of luciferase reporter constructs in COS7 cells shows the binding of *hsa-miR-25* to the 3'UTR of Hand2, *n* refers to number of transfection experiments. **P < 0.05* vs corresponding control group; #*P < 0.05* vs corresponding age group (error bars are s.e.m.). **(e)** FACS analysis showing the percentage of α-actinin+, EdU+ cardiomyocytes isolated from p12- old mice that received AAV9-MCS or AAV9-miR-106b~25. **(f)** Representative confocal microscopy images of heart sections of mice treated with AAV9-MCS or AAV9-miR- 106b~25 and stained for α-actinin, Aurora B and Hoechst. **(g)** Location and evolutionary conservation of the *hsa-miR-106b* seed region on E2f5. **(h)** Activity assay of luciferase reporter constructs in COS7 cells shows the binding of *hsa-miR-106b* to the 3'UTR of E2f5, *n* refers to number of transfection experiments. **(i)** Location and evolutionary conservation of the *hsa-miR-25* seed region on Cdkn1c. **(j)** Activity assay of luciferase reporter constructs in COS7 cells shows the binding of *hsa-miR-25* to the 3'UTR of Cdkn1c, *n* refers to number of transfection experiments.

Figure 1

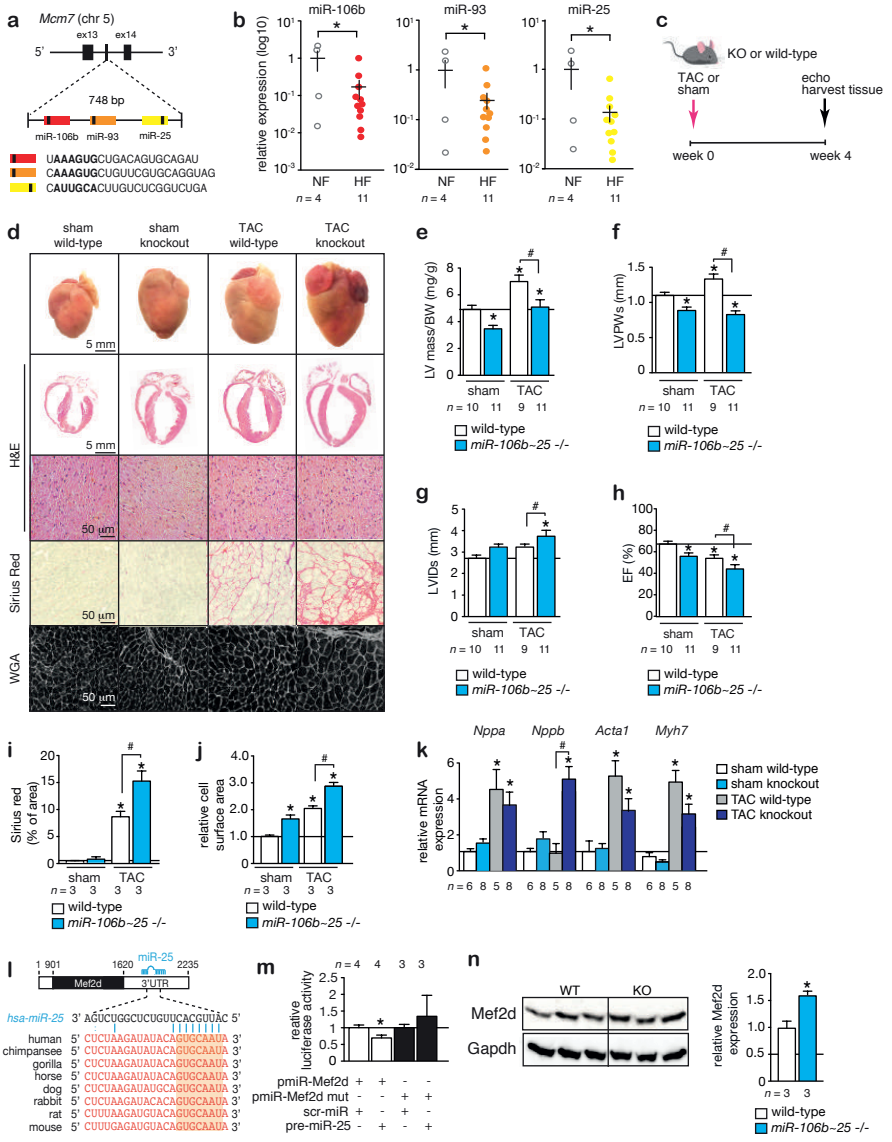
a
Mcm7 (chr 5)
ex13
ex14
748 bp
miR-106b
miR-93
miR-25
UAAAGUGCUGACAGUGCAGAU
CAAAGUGCUGUUCGUGCAGGUAG
CAUUGCACUUGUCUCGGUCUGA
b
miR-106b
miR-93
miR-25
relative expression (log10)
NF
HF
n = 4
11
c
KO or wild-type
TAC or sham
echo harvest tissue
week 0
week 4
d
sham wild-type
sham knockout
TAC wild-type
TAC knockout
5 mm
H&E
Sirius Red
WGA
50 µm
e
LV mass/BW (mg/g)
f
LVPWs (mm)
g
LVIDs (mm)
h
EF (%)
sham
TAC
wild-type
miR-106b~25 -/-
i
Sirius red (% of area)
j
relative cell surface area
k
Nppa
Nppb
Acta1
Myh7
relative mRNA expression
sham wild-type
sham knockout
TAC wild-type
TAC knockout
l
miR-25
Mef2d
3'UTR
hsa-miR-25
human
chimpansee
gorilla
horse
dog
rabbit
rat
mouse
m
relative luciferase activity
pmiR-Mef2d
pmiR-Mef2d mut
scr-miR
pre-miR-25
n
WT
KO
Mef2d
Gapdh
relative Mef2d expression

Figure 2

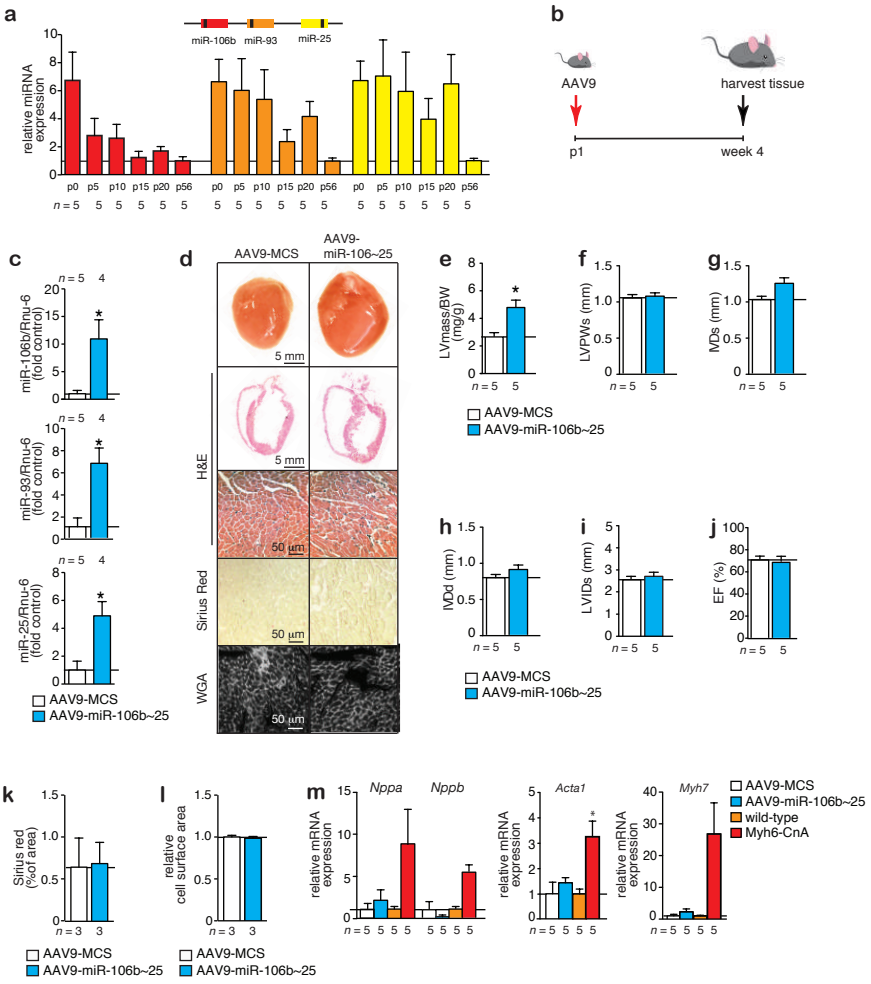
a
relative miRNA expression
miR-106b
miR-93
miR-25
p0 p5 p10 p15 p20 p56
b
AAV9
harvest tissue
p1
week 4
c
miR-106b/Rnu-6 (fold control)
miR-93/Rnu-6 (fold control)
miR-25/Rnu-6 (fold control)
AAV9-MCS
AAV9-miR-106b~25
d
AAV9-MCS
AAV9-miR-106~25
H&E
Sirius Red
WGA
5 mm
50 µm
e
LVmass/BW (mg/g)
f
LVPWs (mm)
g
IVDs (mm)
h
IVDd (mm)
i
LVIDs (mm)
j
EF (%)
k
Sirius red (%of area)
l
relative cell surface area
m
Nppa
Nppb
Acta1
Myh7
relative mRNA expression
AAV9-MCS
AAV9-miR-106b~25
wild-type
Myh6-CnA

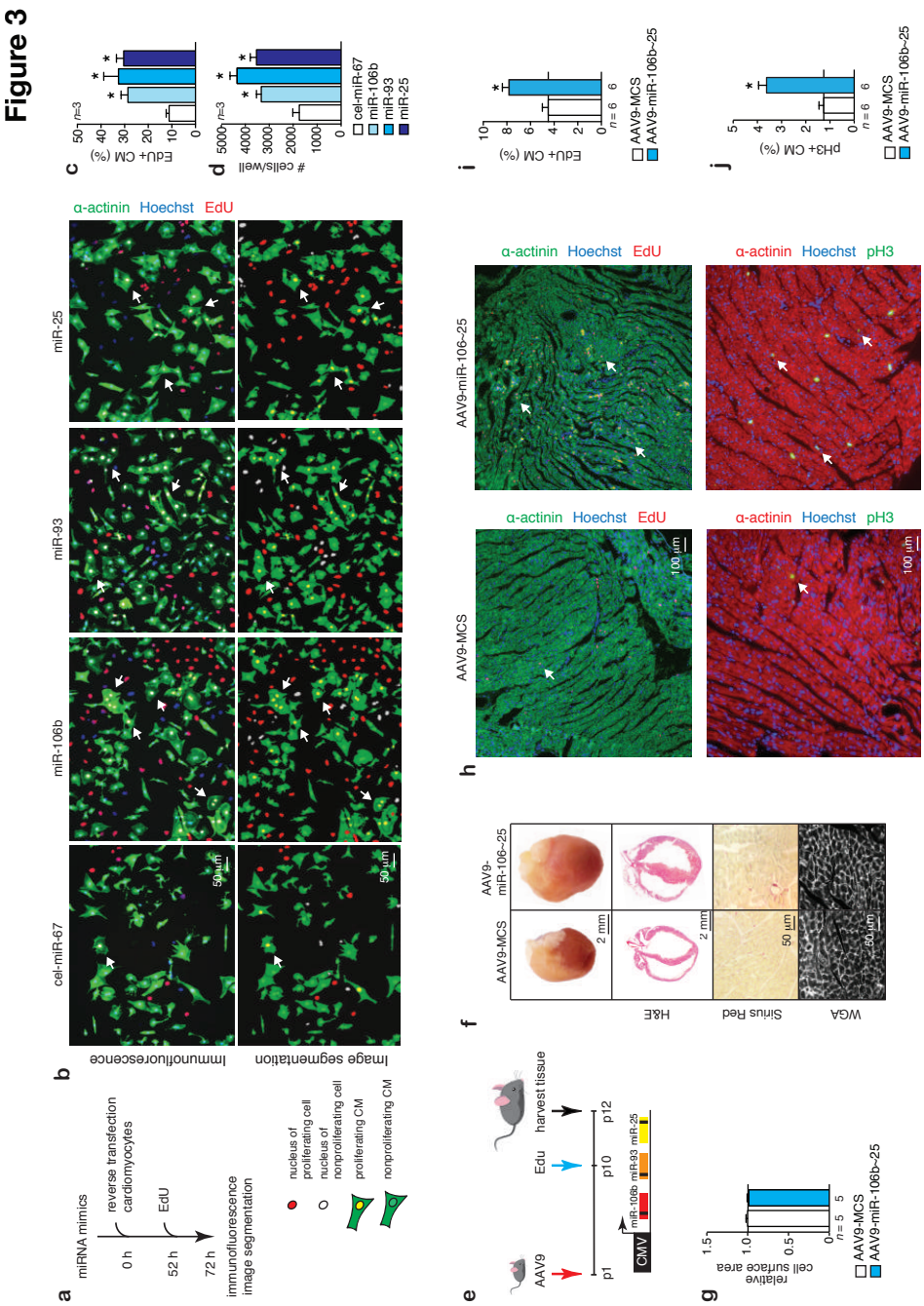
Figure 3
a
miRNA mimics
reverse transfection cardiomyocytes
0 h
EdU
52 h
72 h
immunofluorescence
image segmentation
b
cel-miR-67
miR-106b
miR-93
miR-25
α-actinin Hoechst EdU
50 μm
immunofluorescence
image segmentation
nucleus of proliferating cell
nucleus of nonproliferating cell
proliferating CM
nonproliferating CM
c
EdU+ CM (%)
n=3
d
# cells/well
n=3
cel-miR-67
miR-106b
miR-93
miR-25
e
AAV9
Edu
harvest tissue
p1
p10
p12
CMV
miR-106b
miR-93
miR-25
f
AAV9-MCS
AAV9-miR-106~25
2 mm
H&E
Sirius Red
WGA
50 μm
g
relative cell surface area
n= 5 5
AAV9-MCS
AAV9-miR-106b~25
h
AAV9-MCS
AAV9-miR-106~25
α-actinin Hoechst EdU
α-actinin Hoechst pH3
100 μm
i
EdU+ CM (%)
n= 6 6
AAV9-MCS
AAV9-miR-106b~25
j
pH3+ CM (%)
n= 6 6
AAV9-MCS
AAV9-miR-106b~25

Figure 4

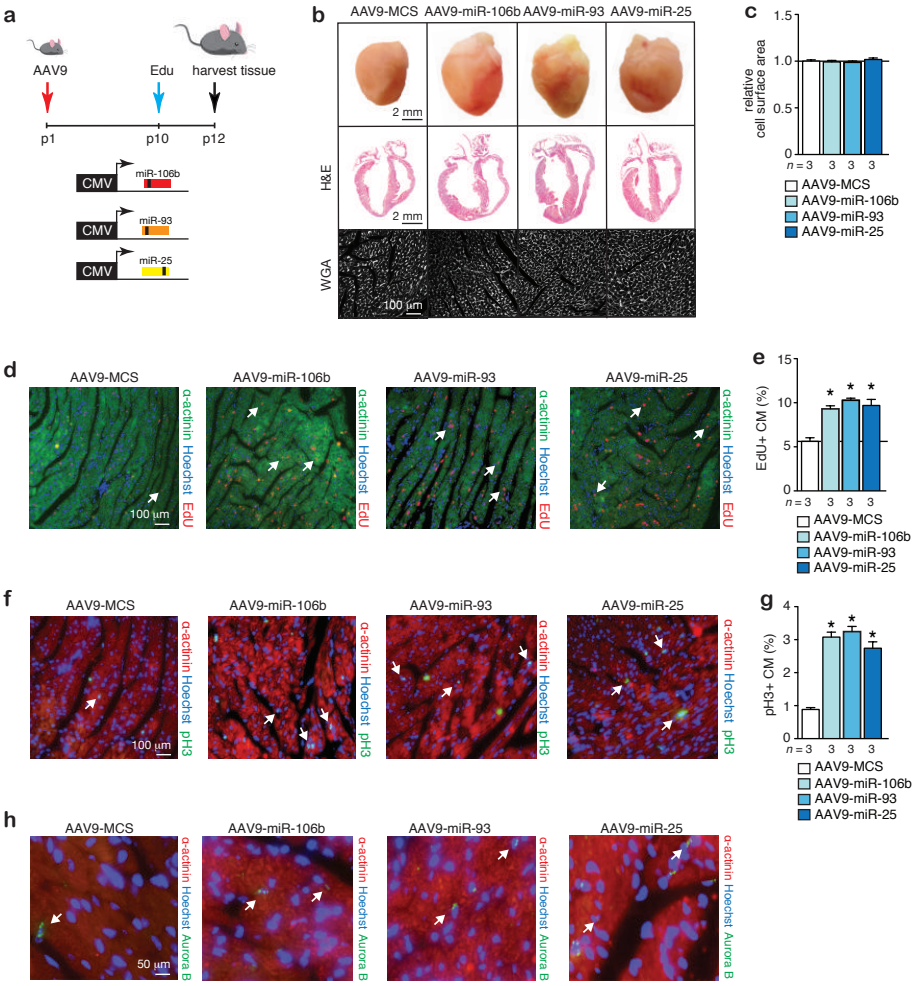
a
AAV9
Edu
harvest tissue
p1
p10
p12
CMV
miR-106b
CMV
miR-93
CMV
miR-25
b
AAV9-MCS
AAV9-miR-106b
AAV9-miR-93
AAV9-miR-25
H&E
WGA
2 mm
2 mm
100 μm
c
relative cell surface area
1.5
1.0
0.5
0
n = 3 3 3 3
AAV9-MCS
AAV9-miR-106b
AAV9-miR-93
AAV9-miR-25
d
AAV9-MCS
AAV9-miR-106b
AAV9-miR-93
AAV9-miR-25
α-actinin Hoechst EdU
100 μm
e
EdU+ CM (%)
15
10
5
0
n = 3 3 3 3
AAV9-MCS
AAV9-miR-106b
AAV9-miR-93
AAV9-miR-25
f
AAV9-MCS
AAV9-miR-106b
AAV9-miR-93
AAV9-miR-25
α-actinin Hoechst pH3
100 μm
g
pH3+ CM (%)
4
3
2
1
0
n = 3 3 3 3
AAV9-MCS
AAV9-miR-106b
AAV9-miR-93
AAV9-miR-25
h
AAV9-MCS
AAV9-miR-106b
AAV9-miR-93
AAV9-miR-25
α-actinin Hoechst Aurora B
50 μm

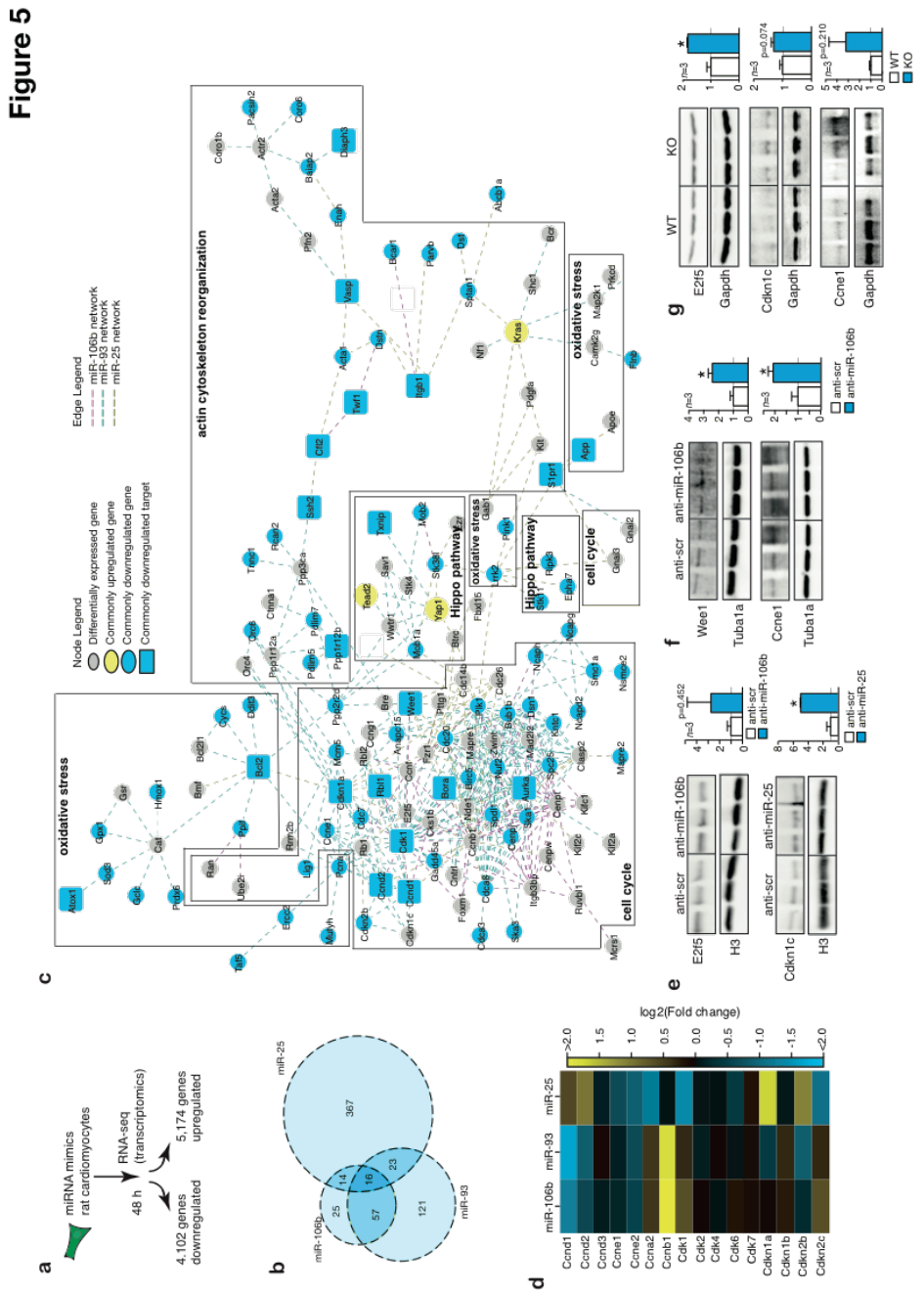
Figure 5
a
miRNA mimics
rat cardiomyocytes
48 h
RNA-seq
(transcriptomics)
4.102 genes
downregulated
5,174 genes
upregulated
b
miR-25
miR-106b
miR-93
367
25
14
16
23
57
121
c
Node Legend
Differentially expressed gene
Commonly upregulated gene
Commonly downregulated gene
Commonly downregulated target
Edge Legend
miR-106b network
miR-93 network
miR-25 network
oxidative stress
actin cytoskeleton reorganization
Hippo pathway
cell cycle
d
log2(Fold change)
>2.0
1.5
1.0
0.5
0.0
-0.5
-1.0
-1.5
<2.0
miR-106b
miR-93
miR-25
Ccnd1
Ccnd2
Ccnd3
Ccne1
Ccne2
Ccna2
Ccnb1
Cdk1
Cdk2
Cdk4
Cdk6
Cdk7
Cdkn1a
Cdkn1b
Cdkn2b
Cdkn2c
e
anti-scr
anti-miR-106b
E2f5
H3
p=0.452
anti-scr
anti-miR-25
Cdkn1c
H3
f
anti-scr
anti-miR-106b
Wee1
Tuba1a
anti-scr
anti-miR-106b
Ccne1
Tuba1a
anti-scr
anti-miR-106b
g
WT
KO
E2f5
Gapdh
Cdkn1c
Gapdh
p=0.074
Ccne1
Gapdh
p=0.210
WT
KO

Figure 6

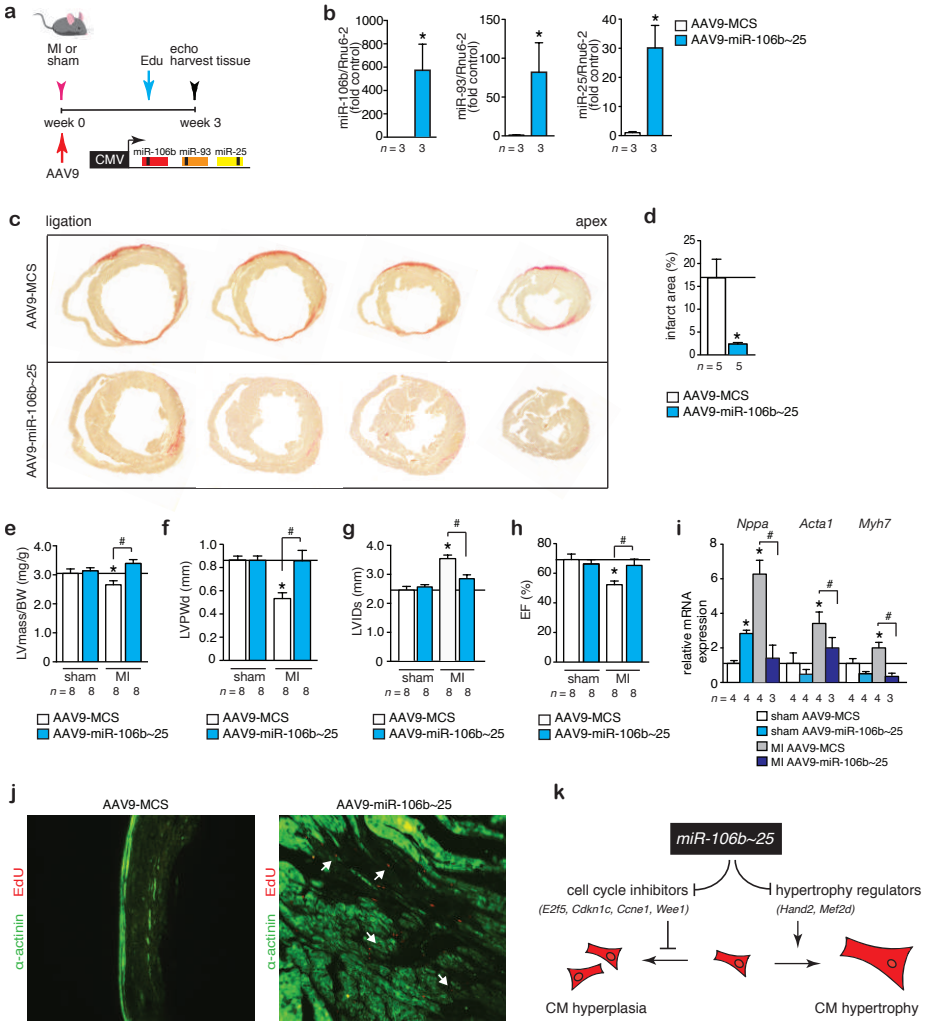
a
MI or sham
Edu
echo harvest tissue
week 0
week 3
AAV9
CMV
miR-106b miR-93 miR-25
b
miR-106b/Rnu6-2 (fold control)
miR-93/Rnu6-2 (fold control)
miR-25/Rnu6-2 (fold control)
AAV9-MCS
AAV9-miR-106b~25
c
ligation
apex
AAV9-MCS
AAV9-miR-106b~25
d
infarct area (%)
AAV9-MCS
AAV9-miR-106b~25
e
LVmass/BW (mg/g)
f
LVPWd (mm)
g
LVIDs (mm)
h
EF (%)
sham
MI
AAV9-MCS
AAV9-miR-106b~25
i
Nppa
Acta1
Myh7
relative mRNA expression
sham AAV9-MCS
sham AAV9-miR-106b~25
MI AAV9-MCS
MI AAV9-miR-106b~25
j
AAV9-MCS
AAV9-miR-106b~25
EdU
α-actinin
k
miR-106b~25
cell cycle inhibitors
(E2f5, Cdkn1c, Ccne1, Wee1)
hypertrophy regulators
(Hand2, Mef2d)
CM hyperplasia
CM hypertrophy

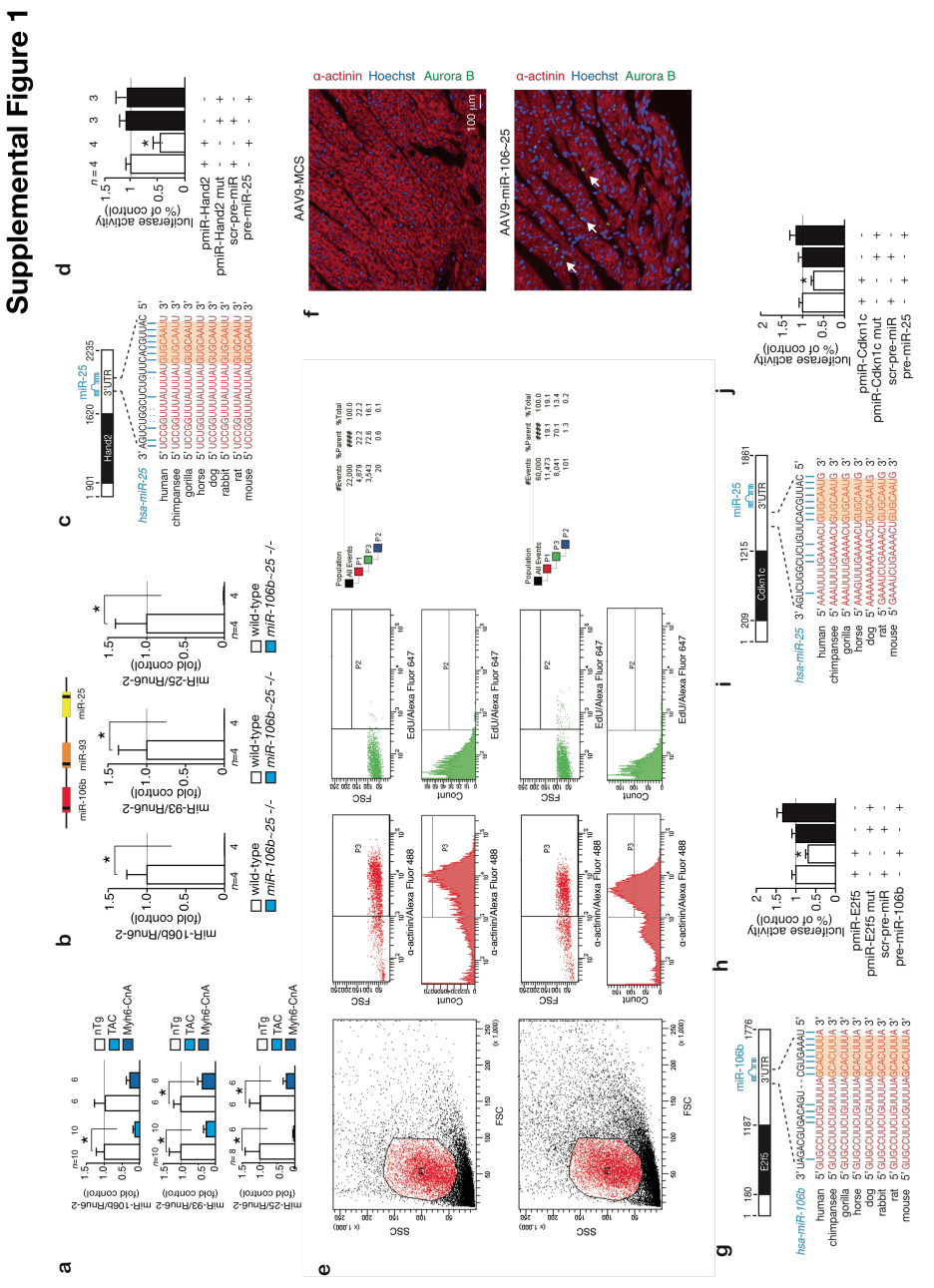
Supplemental Figure 1
a
b
c
d
e
f
g
h
i
j
nTg
TAC
Myh6-CnA
wild-type
miR-106b~25 -/-
miR-106b-25 -/-
miR-106b~25 -/-
miR-106b
miR-93
miR-25
Hand2
3'UTR
hsa-miR-25
human
chimpanzee
gorilla
horse
dog
rabbit
rat
mouse
pmiR-Hand2
pmiR-Hand2 mut
scr-pre-miR
pre-miR-25
luciferase activity
(% of control)
α-actinin Hoechst Aurora B
AAV9-MCS
AAV9-miR-106~25
100 μm
Cdkn1c
hsa-miR-106b
E2f5
pmiR-E2f5
pmiR-E2f5 mut
pmiR-Cdkn1c
pmiR-Cdkn1c mut
pre-miR-106b

Table 1. Morphometric and echocardiographic characteristics of WT versus miR-106b~25 KO mice subjected to sham or TAC surgery for 4 weeks.

	Sham		TAC	
	WT	**KO**	**WT**	**KO**
n	10	11	9	10
BW (g)	21.2±0.2	21.3±0.4	21.0±0.5	21.0±0.4
LV mass (mg)	107±5	80±5*	145±12*	110±8#
LV mass/BW (mg/g)	5.1±0.3	3.8±0.4*	7.1±0.7*	5.3±0.5#
IVSd (mm)	0.83±0.05	0.68±0.03*	1.04±0.06*	0.89±0.04#
IVSs (mm)	1.16±0.06	1.04±0.03	1.40±0.07*	1.16±0.05#
LVIDd (mm)	4.09±0.08	4.15±0.09	4.10±0.14	4.41±0.11
LVIDs (mm)	2.87±0.08	3.14±0.08	3.14±0.07	3.61±0.15*#
LVPWd (mm)	0.89±0.04	0.65±0.04*	1.04±0.06*	0.70±0.05*#
LVPWs (mm)	1.11±0.05	0.83±0.03*	1.30±0.08*	0.88±0.05*#
EF (%)	64±1	57±1*	54±2*	45±3*#
FS (%)	29±1	25±1*	23±1*	18±1*#
E/A (mm/s)	1.73±0.11	1.53±0.10	1.62±0.10	1.57±0.24*

Data are expressed as means ± SEM. BW, body weight; LV, left ventricular; IVSd, interventricular septal thickness at end-diastole; IVSs, interventricular septal thickness at end-systole; LVIDd, left ventricular internal dimension at end-diastole; LVIDs, left ventricular internal dimension at end-systole; LVPwd, left ventricular posterior wall thickness at end-diastole; LVPws, left ventricular posterior wall thickness at end-systole; EF, ejection fraction; FS, fractional shortening; E/A, Doppler E/A ratio. *, indicates $P<0.05$ vs sham group subjected to treatment with a control antagomir; #, indicates $P<0.05$ vs experimental group.

Table 2. Morphometric and echocardiographic characteristics of mice treated for 4 weeks with AAV9-MCS or AAV9-miR-106b~25.

	AAV9-MCS	AAV9-miR-106b~25
n	5	5
BW (g)	29.4±0.5	24.3±1.7
LV mass (mg)	79±7	121±26*
LV mass/BW (mg/g)	2.7±0.2	4.8±0.6*
IVSd (mm)	0.68±0.03	0.91±0.08*
IVSs (mm)	1.05±0.04	1.28±0.09
LVIDd (mm)	3.75±0.12	4.08±0.08*
LVIDs (mm)	2.50±0.14	2.78±0.19
LVPWd (mm)	0.84±0.09	0.85±0.08
LVPWs (mm)	1.07±0.06	1.09±0.07
EF (%)	70±3	66±5
FS (%)	33±2	31±3

Data are expressed as means ± SEM. BW, body weight; LV, left ventricular; IVSd, interventricular septal thickness at end-diastole; IVSs, interventricular septal thickness at end-systole; LVIDd, left ventricular internal dimension at end-diastole; LVIDs, left ventricular internal dimension at end-systole; LVPwd, left ventricular posterior wall thickness at end-diastole; LVPws, left ventricular posterior wall thickness at end-systole; EF, ejection fraction; FS, fractional shortening; E/A, Doppler E/A ratio. *, indicates $P<0.05$ vs sham group subjected to treatment with a control antagomir; #, indicates $P<0.05$ vs experimental group.

Table 3. Morphometric and echocardiographic characteristics of mice subjected to sham or MI surgery and treated for 3 weeks with AAV9-MCS or AAV9-miR-106b~25.

	Sham		MI	
	AAV9-MCS	**AAV9-miR-106~25**	**AAV9-MCS**	**AAV9-miR-106~25**
n	8	8	8	8
BW (g)	22.8±2.1	25.3±2.0	23.8±1.5	24.3±1.7
LV mass (mg)	84±3	90±2	88±5	107±4*#
LV mass/BW (mg/g)	3.2±0.2	3.8±0.4	5.2±0.4*	6.4±1.0*
IVSd (mm)	0.79±0.03	0.81±0.02	0.75±0.03	0.90±0.03*#
IVSs (mm)	1.18±0.05	1.23±0.07	1.10±0.04	1.40±0.06*#
LVIDd (mm)	3.62±0.07	3.78±0.10	4.53±0.19*	4,00±0.02#
LVIDs (mm)	2.42±0.13	2.56±0.14	3.55±0.20*	2.79±0.26#
LVPWd (mm)	0.88±0.03	0.86±0.05	0.55±0.05*	0.87±0.10#
LVPWs (mm)	1.16±0.05	1.21±0.06	0.69±0.07*	1.05±0.13#
EF (%)	69±4	67±3	52±2*	65±4*#
FS (%)	33±3	31±2	22±1*	31±3*#

Data are expressed as means ± SEM. BW, body weight; LV, left ventricular; IVSd, interventricular septal thickness at end-diastole; IVSs, interventricular septal thickness at end-systole; LVIDd, left ventricular internal dimension at end-diastole; LVIDs, left ventricular internal dimension at end-systole; LVPwd, left ventricular posterior wall thickness at end-diastole; LVPws, left ventricular posterior wall thickness at end-systole; EF, ejection fraction; FS, fractional shortening; E/A, Doppler E/A ratio. *, indicates $P<0.05$ vs sham group subjected to treatment with a control antagomir; #, indicates $P<0.05$ vs experimental grou

CHAPTER 4

Therapeutic delivery of miR-148a suppresses ventricular dilation in heart failure

[1]***Andrea Raso****; [1,2]*Ellen Dirkx**; [1,3]*Leonne E. Philippen**, [4]*Amaya Fernandez-Celis*; [1]*Federica De Majo*; [1]*Vasco Sampaio-Pinto*; [1]*Marida Sansonetti*; [1]*Rio Juni*; [1,5]*Hamid el Azzouzi*; [1]*Martina Calore*; [1]*Nicole Bitsch*; [1]*Servé Olieslagers*; [5]*Martinus I.F.J. Oerlemans*; [6]*Manon M. Huibers*; [6]*Roel A. de Weger*; [7]*Yolan J. Reckman*; [7]*Yigal M. Pinto*; [2]*Lorena Zentilin*; [2,8]*Serena Zacchigna*; [2,8]*Mauro Giacca*; [1,9]*Paula A. da Costa Martins*; [4]*Natalia López-Andrés*; [1]*Leon J. De Windt Ph.D*

*These authors contributed equally to this work;

[1]*Department of Cardiology, CARIM School for Cardiovascular Diseases, Maastricht University, Maastricht, The Netherlands;*

[2]*International Centre for Genetic Engineering and Biotechnology (ICGEB), Trieste, Italy;*

[3]*Cardiovascular Research Institute, Baylor College of Medicine, Houston, Texas, USA;*

[4]*Cardiovascular Translational Research, Navarrabiomed, Instituto de Investigación Sanitaria de Navarra (IdiSNA), Pamplona, Spain;*

[5,6]*Departments of Cardiology and Pathology, University Medical Center Utrecht, Utrecht, The Netherlands;*

[7]*Department of Experimental Cardiology, Academic Medical Center, Amsterdam, the Netherlands;*

[8]*Department of Medicine, Surgery and Health Sciences, University of Trieste, Italy;*

[9]*Department of Physiology and Cardiothoracic Surgery, Faculty of Medicine, University of Porto, Porto, Portugal.*

[Mol Ther. 2019 Mar 6;27(3):584-599. doi: 10.1016/j.ymthe.2018.11.011. Epub 2018 Nov 17]

Abstract

Heart failure is preceded by ventricular remodeling, changes in left ventricular mass and myocardial volume after alterations in loading conditions. Concentric hypertrophy arises after pressure overload, involves wall thickening and forms a substrate for diastolic dysfunction. Eccentric hypertrophy develops in volume overload conditions and leads wall thinning, chamber dilation, and reduced ejection fraction. The molecular events underlying these distinct forms of cardiac remodeling are poorly understood. Here, we demonstrate that *miR-148a* expression changes dynamically in distinct subtypes of heart failure: while it is elevated in concentric hypertrophy, it decreased in dilated cardiomyopathy. In line, antagomir-mediated silencing of *miR-148a* caused wall thinning, chamber dilation, increased left ventricle volume and reduced ejection fraction. Additionally, adeno-associated viral delivery of *miR-148a* protected the mouse heart from pressure overload-induced systolic dysfunction by preventing the transition of concentric hypertrophic remodeling towards dilation. Mechanistically, *miR-148a* targets the cytokine co-receptor glycoprotein 130 (gp130) and connects cardiomyocytes responsiveness to extracellular cytokines by modulating the Stat3 signaling. These findings show the ability of *miR-148a* to prevent the transition of pressure-overload induced concentric hypertrophic remodeling towards eccentric hypertrophy and dilated cardiomyopathy and provide evidence for the existence of separate molecular programs inducing distinct forms of myocardial remodeling.

Introduction

Heart failure is a major cause of morbidity and death with little recent progress to reduce its high mortality. This disease is preceded by ventricular remodeling, changes in left ventricular mass and volume of the myocardium in response to alterations in loading conditions, with two distinct outcomes. Concentric hypertrophy results from cardiac growth and wall thickening which arises from pressure overload situations on the heart, as observed in patients with chronic hypertension, aortic valve stenosis or inherited forms of hypertrophic cardiomyopathy, and often yields a substrate for left ventricular diastolic dysfunction [1, 2]. Contrary, eccentric hypertrophy often develops under conditions of volume overload of the myocardium, with mitral- and aortic regurgitation or familial dilated cardiomyopathy as clinical correlates, resulting in pronounced systolic dysfunction and a concomitant decrease in ejection fraction [2]. Pathological forms of concentric hypertrophy in certain hypertensive or aortic stenosis patients in time may gradually lead to eccentric remodeling of the heart and worsening prognosis [3]. Despite this spectrum of clinically relevant cardiac remodeling phenotypes, the molecular events that underlie these distinct forms of cardiac hypertrophy still remain poorly understood [4]. Accordingly, the stimulatory circulatory agonists, membrane-bound receptors and intracellular signaling cascades that connect biomechanical forces and the activation of myocardial stress pathways are central to understanding the initiation and progression to concentric *versus* eccentric hypertrophy.

Cardiotrophin-1 (CT-1), a member of the interleukin-6 cytokine superfamily, exerts its pleiotropic functions using a gp130 homodimer or gp130/leukemia inhibitory factor receptor-β (LIFRβ) heterodimer, induces eccentric hypertrophy in cultured primary cardiomyocytes *in vitro* [5-7] and exerts cardioprotective proliferative and survival effects in cultured embryonic, neonatal or adult cardiomyocytes [8-11]. *In vivo*, CT-1 treatment induces left ventricular dilation in rats [12]. In humans, increased CT-1 serum levels are observed in patients with unstable angina [13], acute myocardial infarction [14], hypertension, valvular diseases or heart failure [15], correlated with the degree of left ventricular systolic dysfunction [16, 17] and left ventricular mass index in patients with dilated cardiomyopathy [18, 19].

Cytokines of the interleukin-6 superfamily couple to gp130 receptors and confer a level of cellular protection against cell death mechanisms in a variety of cardiac stress conditions, and genetic deletion strategies of gp130 or downstream signaling components render widespread cell death in the myocardium in response to biomechanical stress [20-22]. On the other hand, unrestrained activation of cytokine/gp130 signaling transmits prohypertrophic cues that facilitate the transition to eccentric hypertrophy and systolic dysfunction,[23] suggesting that the expression of gp130 is determinant in the balance between cellular survival pathways *versus* maladaptive hypertrophic remodeling in the myocardium.

Here, we demonstrate that cardiac expression of *miR-148a* alters dynamically in distinct subtypes of human and mouse forms of heart failure. In human and mouse forms of concentric hypertrophy *miR-148a* expression is elevated, while forms of dilated cardiomyopathy are accompanied by profoundly decreased *miR-148a* myocardial expression. In the heart, *miR-148a* targets gp130 and determines the extracellular cytokines responsiveness and cardiac signaling strength of canonical STAT3 hypertrophic signaling by altering the abundance of gp130. These findings provide evidence that myocardial *miR-148a* functions to prevent the transition of pressure-overload induced concentric hypertrophic remodeling towards eccentric hypertrophy and are proof of the existence of separable molecular cues that provoke distinct forms of hypertrophy in the early steps toward end-stage heart failure.

RESULTS

miR-148a is dynamically expressed in heart failure subtypes

From previous microRNA profiling studies in human cardiac biopsies and mouse cardiac disease models, we observed that *miR-148a-3p* displayed opposite expression patterns depending on the type of heart disease studied [24]. *miR-148a* is an intergenic microRNA, located on chromosome 6 or 7 in the murine and human genome, respectively, and distantly flanked by lncRNA genes (Figure 1a). The major mature *miR-148a* form in the heart is *miR-148a-3p*, which is fully conserved from the mouse to human genome, indicating an evolutionary pressure to resist variations in this microRNA gene (Figure 1a). Northern blotting revealed that *miR-148a* is broadly expressed in various tissues, with a relatively high expression in kidney, spleen and lung, to a lesser extent in liver and heart, and with traces of expression in brain, muscle and fat tissue (Figure 1b). In the heart, *miR-148a* is most abundantly expressed in cardiomyocytes and fibroblasts (Figure 1d). Most remarkable, *miR-148a* displayed an opposite direction of differential expression in human cardiac biopsies of end-stage heart failure obtained upon heart transplantation, with a pronounced decrease of *miR-148a* in left ventricular biopsies of dilated cardiomyopathy compared to healthy controls (Figure 1e), compared to an increased expression of *miR-148a* in the left ventricular myocardium of patients with hypertrophic cardiomyopathy compared to the respective healthy controls (Figure 1e). Next, we compared cardiac *miR-148a* expression differences in mouse models of dilated or hypertrophic cardiac remodeling. Cysteine and glycine-rich protein 3 (*Csrp3*), also known as Muscle LIM Protein, is a Z disc protein involved in cardiac mechanical stretch sensing and required for proper cardiac geometry, energy metabolism and function. Mice homozygous null for *Csrp3* develop early onset dilated cardiomyopathy and have been extensively used to study the pathophysiology of this subtype of heart failure. *Csrp3* null mice displayed a very strong reduction of *miR-148a* in left ventricular tissue (Figure 1f). In contrast, mice harboring a constitutively activated mutant of Calcineurin A (CnA) under control of the myosin heavy chain promoter (Myh6-CnA) develop

severe hypertrophic concentric remodeling soon after birth. Hearts from young Myh6-CnA mice revealed an increase in *miR-148a* expression (Figure 1g). Taken together, cardiac *miR-148a* expression is increased in human and mouse forms of concentric hypertrophic cardiac remodeling and decreased in human and mouse forms of eccentric remodeling or dilated cardiomyopathy.

miR-148a targets cardiac glycoprotein 130 (gp130)

MicroRNAs exert their action by regulating gene expression at the post-transcriptional level by imperfect base pairing with protein-coding transcripts. Hence, to understand the mechanistic role of *miR-148a* in cardiac remodeling, we first performed a bioinformatic analysis aimed at identifying *miR-148a* binding sites in cardiac expressed protein-coding transcripts. We identified an enrichment of three putative *miR-148a* seed regions in interleukin 6 signal transducer (*Il6st*), better known as glycoprotein 130 (gp130), and among them, the more proximal *miR-148a* binding site in the ~2.5 kb gp130 3'UTR demonstrated a perfect match for the *miR-148a* heptametrical seed sequence and showed complete evolutionary conservation (Fig.2a, Suppl. Figure 2a,b). The gp130 co-receptor couples the responsiveness of the heart to cytokines from the interleukin-6 (IL-6) family, including IL-6, leukemia inhibitory factor (LIF), oncostatin M or cardiotrophin-1 (CT-1), and intracellular MAPK, PI3K or JAK/STAT signaling by homodimerisation or heterodimerisation with LIF receptors at the cell surface [25].

To more directly establish the regulation of gp130 by *miR-148a* in the myocardium, we generated series of luciferase reporters harboring either the complete or truncated forms of the gp130 3'UTR, including a reporter with site-directed mutagenesis of key nucleotides in the *miR-148a* binding site (Figure 2b). Transient transfection of synthetic precursor *miR-148a* in cultured Cos7 cells decreased gp130 3'UTR reporter activity when either the intact ~2.5 kb 3'UTR or a distal truncation was coupled to luciferase compared to co-transfection with scrambled precursor molecules (Figure 2c). In contrast, a proximal truncation of the gp130 3'UTR, harboring two putative miR-148a binding sites, as well as a site-directed mutant of the complete gp130 3'UTR, remained unresponsive to synthetic precursor *miR-148a* molecules (Figure 2c). In line, endogenous gp130 protein expression in primary cardiomyocytes was derepressed by transfection of *miR-148a* antimir molecules, while pretreatment with *miR-148a* precursor molecules provoked significant downregulation of endogenous gp130 at the protein level (Figure 2d).

miR-148a dynamically influences gp130 downstream signaling

miR-148a expression was found increased in forms of concentric hypertrophic cardiac remodeling, while its expression was downregulated in forms of eccentric cardiac remodeling (Figure 1e-g). To mimic this dynamic expression pattern *in vivo* and study the

effects of differential *miR-148a* expression on gp130 expression levels and downstream signaling events in the intact heart, we subjected cohorts of mice to pressure overload by transverse aortic constriction (TAC) surgery, serially assessed cardiac geometry and function and sacrificed mice at 0 weeks (sham) or 2, 4, 6 or 8 weeks after TAC to measure cardiac *miR-148a* expression and evaluate the activation status of signaling cascades (Figure 2e-l). In line with our previous observations [24, 26, 27], concentric hypertrophic remodeling with sustained systolic function was evident in mice in the first four weeks following TAC surgery, which gradually transitioned to eccentric remodeling and loss of systolic contractile performance. First, *miR-148a* expression gradually increased up to ten fold in pressure-overloaded hearts following 2 or 4 weeks of TAC compared to hearts from sham-operated mice (Figure 2f). In this time period, pressure-overloaded hearts increased in heart mass but still displayed sustained systolic function and showed no signs of left ventricular dilation, consistent with concentric hypertrophic remodeling (Figure 2g-i). More prolonged periods of pressure overload induced a subsequent steep reduction of cardiac *miR-148a* expression, resulting in a significantly lower *miR-148a* expression at 8 weeks of pressure overload compared to sham-operated mice (Figure 2f). Interestingly, at 6 and 8 weeks following TAC, when miR-148a expression steeply reduced, left ventricular mass was clearly increased compared to 2 and 4 weeks after TAC. Additionally, at 6 and 8 weeks following TAC surgery systolic function was drastically reduced and hearts displayed substantial left ventricular dilation concordant with further eccentric cardiac remodeling compared to 2 and 4 weeks after TAC (Figure 2g-i). Conclusively, in sustained pressure overload, concentric cardiac remodeling in early phases correlated with high *miR-148a* expression, while eccentric cardiac remodeling in later phases correlated with low expression of *miR-148a*.

Using this model of transient elevation and reduction of *miR-148a* accompanied with a phenotypic switch from concentric to eccentric cardiac remodeling, we assessed expression and activation status of the CT-1/gp130 co-receptor axis. This CT-1/gp130 co-receptor axis has been reported to result in ERK1/2 or ERK5 MAPK, PI3K/Akt or JAK/STAT3 downstream signaling activation in the heart.[11] Our data show that cardiac CT-1 levels gradually increase in time with the pressure overload stimulus until 6 weeks after TAC, after which this increase ceased (Figure 2j). Interestingly, the expression of the direct *miR-148a* target gene gp130 was reduced by ~50% at week 4 after TAC, a time point that coincides with the highest induction of cardiac *miR-148a* expression (Figure 2k). We also determined the expression of leukemia inhibitory factor (LIF), the LIF receptor itself, IL-6, ciliary neurotrophic factor (CNTF) and oncostatin M (OSM) as possible ligands that could all signal through the gp130 co-receptor. No changes in LIF receptor expression were evident during this time period, the expression changes in LIF or OSM remained unchanged or only demonstrated a transient increase at 2 weeks of TAC surgery as was the case for CNTF or IL-6 (Suppl.Fig.1a, e-h). These observations lend support to a specificity of the interaction between *miR-148a* and CT-1/gp130 co-receptor axis. A reduction in gp130 expression would be expected to result in ramifications in the activation status of downstream ERK1/2 or ER5

MAPK, PI3K/Akt or JAK/STAT3 signaling. Indeed, in this model of sustained pressure overloading, a reduction in both phosphorylated STAT3 (Figure 2l) and phosphorylated Akt **(**Figure S1b), but not total STAT3 or Akt expression, was evident at early time points after TAC, which coincided with the highest induction of cardiac *miR-148a* expression and lowest expression of gp130 (Figure 2f,k). No changes in ERK5 or ERK1/2 activation were evident at the time points analyzed (Figure S1c,d).

CT-1-mediated gp130 activation and signaling is well known to induce eccentric hypertrophic remodeling and chamber dilatation. Despite clinical and experimental evidence that CT-1 levels are elevated in plasma and myocardium of patients with heart failure, direct evidence that CT-1 is sufficient to promote aspects of cardiac disease *in vivo* is conspicuously lacking in literature. To address whether *miR-148a* expression reduces eccentric cardiac remodeling by attenuating gp130 responsiveness to CT-1, we compared cardiac phenotypes of mice that were either left untreated, infused with 20 µg/kg/day of CT-1 [12], or infused with 60 mg/kg/day isoproteronol [28] for two weeks (Figure S2c). Our data demonstrate that isoproterenol exposure produced a classical cardiac hypertrophic response accompanied by increased cardiac mass and wall thickening, interstitial fibrosis, and reduced ejection fraction (Figure S2d-g). Remarkably, sustained CT-1 exposure produced typical features of eccentric remodeling with mild cardiac enlargement, wall thinning and severe systolic dysfunction (Figure S2d-g). Having established that CT-1 is a direct stimulator of eccentric cardiac remodeling *in vivo*, we observed that primary cardiomyocytes responded to CT-1 with a mild hypertrophic response *in vitro*, which was clearly attenuated by transfection of synthetic precursor *miR-148a* molecules (Figure S2h,i). Taken together, these data provide evidence for miR-148a-based regulation of gp130 expression in the adult heart, influencing the responsiveness of the heart to the pro-hypertrophic agonist CT-1.

miR-148a silencing provokes dilated cardiac remodeling

To further address the involvement of *miR-148a* in cardiac remodeling, we made use of an antagomir to specifically silence endogenous *miR-148a* expression *in vivo*, a situation that mimics cardiac *miR-148a* reduction as observed in hearts from human and mouse models of dilated cardiomyopathy (Figure 1e,f). To this end, we designed chemically modified antisense oligonucleotides to target either *Caenorhabditis elegans miR-39-5p* as control antagomir (antagomir-ctrl or antagomir-*Cel*-39) or *mmu-miR-148a-3p* (antagomir-148a). Antagomirs (80 mg/kg/day) were delivered by IP injection on three consecutive days to wild-type mice randomized to receive sham or TAC surgery for six weeks (Figure 3a). Cardiac *miR-148a* expression was efficiently silenced (Figure 3b).

Remarkably, antagomir-148a treatment sufficed to provoke a mild form of eccentric remodeling with systolic dysfunction in sham-operated mice at six weeks after sham operation (Figure 3c). As expected, upon TAC surgery the left ventricular weight (LV)-to-

body weight (BW) ratio increased (Figure 3d). As expected, TAC surgery in mice treated with a control antagomir provoked transient hypertrophic remodeling with relatively well-preserved cardiac function at three weeks (Table 1). Six weeks of TAC surgery in mice treated with a control antagomir or antagomir-148a resulted in severe myocyte disarray, interstitial fibrosis, systolic and diastolic dysfunction, left ventricular dilation, increased heart weight as well as an induction of a "fetal" gene program with a tendency of more severe phenotypes in antagomir-148a treated mice (Figure 3c-j; Table 2). Next, we analyzed protein levels of gp130 and p-STAT3 by Western blotting. The data demonstrate that silencing *miR-148a* in sham-operated mice substantially derepressed (induced) its downstream target gp130 (Figure 3k). As a result, the phosphorylated (activated) form of STAT3 was increased when gp130 was increased in expression (Figure 3k). Total expression levels of STAT3 remained unchanged, indicating activation of STAT3 downstream of gp130 signaling in the heart (Figure 3l,m). This result further supports our conclusion that endogenous *miR-148a* expression levels directly target gp130, subsequently resulting in activation of STAT3 signaling in the heart. Taken together, these data demonstrate that *miR-148a* silencing *in vivo* evokes mild cardiac dilation with derepression of gp130 under baseline conditions and mildly exacerbated pressure overload-induced cardiac remodeling and dysfunction.

miR-148a overexpression suppresses pressure overload-induced cardiac dilation

Next, we mimicked the increased expression of *miR-148a* as observed in conditions of concentric cardiac remodeling in human and mouse hypertrophic cardiomyopathy (Figure 1d,f). To this end, we made use of the high cardiac tropism and prolonged expression of viral vectors based on adeno-associated virus serotype 9 (AAV9) upon systemic delivery. AAV9 vectors expressing either *mmu-miR-148a* (AAV9-148a) or an empty control vector (AAV9-MCS) were administered intravenously (i.v.) by injection into the internal jugular vein of adult mice (Figure 4a). The hearts of AAV9-148a injected animals displayed an induction of *miR-148a* of about two-fold over control (Figure 4b) and appeared morphologically normal with no signs of cardiomyocyte hypertrophy, changes in collagen content, or induction of a fetal gene program apart from a mild induction of *Nppa* (Figure 4c-j), indicating that increased *miR-148a* expression alone is not an active driver of cardiac hypertrophy or remodeling *in vivo* in the absence of additional stimuli.

To analyze *miR-148a* cardiac function under pressure overload conditions, AAV9-148a and AAV9-MCS treated animals were randomized to receive sham or TAC surgery. Six weeks of TAC surgery in AAV9-MCS mice resulted in increased left ventricular weight, severe myocyte disarray, interstitial fibrosis, increased cardiomyocyte size, systolic and diastolic dysfunction, left ventricular dilation, as well as an induction of the classical "fetal" gene program (Figure 4c-j; Tables 3,4). In addition, cardiomyocyte apoptosis was increased in TAC samples

compared to both sham groups (Figure S4). Strikingly, cardiac histopathology, cardiomyocyte hypertrophy and systolic function were clearly attenuated in AAV9-148a injected mice after 6 weeks of TAC surgery (Figure 4c-j; Table 4). A more pronounced induction of transcripts encoding *Nppa, Acta1* and *Myh7* as part of the "fetal" gene program was observed in hearts from AAV9-148a injected mice receiving TAC surgery compared to AAV9-MCS injected mice that received TAC surgery (Figure 4j). Importantly, the extent of cardiomyocyte apoptosis was similar between the two groups receiving TAC surgery (Figure S4).

We also performed Western blotting in hearts from the four experimental groups. We probed the membranes with antibodies specific for gp130 or its immediate downstream signal transducer STAT3 to assess phospho-STAT3 and total STAT3 levels. The data demonstrate that overexpression of *miR-148a* substantially reduced the expression of its downstream target gp130 (Figure 4k-m). As a result, the phosphorylated (activated) form of STAT3 was decreased when gp130 was reduced in expression. Total expression levels of STAT3 remained unchanged, indicating reduced activation status of STAT3 downstream of gp130 signaling in the heart. This result further supports our conclusion that endogenous *miR-148a* controls gp130 expression levels, subsequently resulting in differential activation status of STAT3 in the heart. Conclusively, these data demonstrate that elevation of cardiac *miR-148a* expression *in vivo* protects the myocardium from dilation and cardiac dysfunction following pressure overload and this suppression was accompanied by the reduction of gp130 signaling.

miR-148a overexpression attenuates the transition of pressure-overload induced concentric towards eccentric remodeling

Our data indicate a correlation between the dynamic *miR-148a* expression and the distinct phases of cardiac remodeling under sustained pressure overload conditions, starting from concentric hypertrophy in early phases towards eccentric remodeling in later phases of overload. To more firmly demonstrate the functional significance of lowered *miR-148a* expression in the transition towards eccentric cardiac hypertrophy, we designed a gene therapeutic approach with AAV9-148a, where mice were first randomized to receive sham or TAC surgery for 4 weeks. Next, AAV9 vectors expressing either *mmu-miR-148a* (AAV9-148a) or an empty control vector (AAV9-MCS) were then administered intravenously (i.v.) by injection into the internal jugular vein of adult mice (Figure 5a) to prevent the observed decrease in *miR-148a* in later phases of pressure overload as an approach to maintain high expression of *miR-148a* for another 3 weeks. We confirmed that this approach resulted in higher cardiac *miR-148a* expression in sham-operated AAV9-148a injected mice (Figure 5b), and these hearts appeared morphologically normal with no signs of altered cardiac contractile function, cardiomyocyte hypertrophy, changes in collagen content, except for a relatively mild induction of *Nppb* and *Myh7* (Figure 5c-j).

As expected, at seven weeks of sustained pressure overload, AAV9-MCS injected mice displayed reduced LV wall thickness and increased LV dilation accompanied with interstitial fibrosis, increased cardiomyocyte size, systolic dysfunction, as well as an induction of the classical "fetal" gene program (Figure 5c-j; Table 5-7). In contrast, LV wall thickness was maintained, the extent of LV dilation was attenuated and systolic contractility was clearly improved in AAV9-148a injected mice at seven weeks of TAC surgery compared to AAV9-MCS mice receiving TAC surgery (Figure 5c-g, Table7). *miR-148a* overexpression also resulted in less fibrotic remodeling (Figure 5h) and a more pronounced induction of "fetal" gene transcripts encoding *Nppb* and *Myh7* (Figure 5j).

Combined, our data reveal that *miR-148a* expression dynamically regulates cardiac gp130 expression and alters the responsiveness of the heart to CT-1 stimulation and downstream STAT3 signaling strength, where relatively high *miR-148a* expression produces forms of concentric hypertrophic remodeling and dampens CT-1 overstimulation that drives deleterious eccentric cardiac remodeling (Figure 5k).

DISCUSSION

Here, we demonstrate that cardiac expression of *miR-148a* alters dynamically in distinct subtypes of human and mouse forms of heart failure, with high *miR-148a* expression in human and mouse forms of concentric hypertrophy and decreased *miR-148a* expression in forms of dilated cardiomyopathy. Mechanistically, *miR-148a* modulates the coupling between extracellular cardiotrophin-1 and cardiac signaling strength of the canonical STAT3, Akt, Erk5 and Erk1/2 hypertrophic cascades by targeting gp130, a pivotal co-receptor for cytokines of the interleukin 6 superfamily.

Using complimentary gain- and loss-of-function studies for *miR-148a* in mouse models for cardiac pressure overload, we demonstrate that the abundance of *miR-148a*, and consequently the reduction of gp130 levels, connects sustained biomechanical forces to diverse forms myocardial remodeling, with an overall conclusion that *miR-148a* expression acts as a protective molecular driver that promotes wall thickening and concentric remodeling. Here, we used adeno-associated vectors (AAV) as genetic tool to accomplish overexpression of miR-148a. Naturally occurring viruses have evolved to efficiently transduce their genetic information into host cells. Recombinant viral vectors are engineered by replacing non-essential viral genes with foreign genes of therapeutic interest, and used as vehicles for efficient infecting a wide variety of cell types. AAV vectors are increasingly recognized as reliable tool for research purposes due to their low immunogenicity, tissue tropism, and relative safety due to their low rate of genomic integration [29, 30]. Specifically, AAV vectors of serotype 1/6/9 (AAV1/6/9) that display varying ranges of cardiac tropism, are used to deliver a variety of therapeutic genes, including small functional non-coding RNAs such as microRNAs. Future improvement of AAV vectors should address their limited capacity to carry transgenes of larger sizes. Likewise,

the existence of pre-existing neutralizing antibodies against AAV in the general population hampers immediate translation of AAV cardiac gene therapy to clinical stages. Notwithstanding these drawbacks, AAV vectors can be considered as safe, efficient and reliable tools for preclinical cardiac gene therapy applications with high potential as vectors in clinical trials. *Vice versa*, lowering of cardiac *miR-148a* expression results in increased gp130 expression leading to enhanced gp130-coupled intracellular signaling, and incites wall thinning and chamber dilation with the associated increase in stress on the ventricular wall, representing the first irreversible steps towards overt heart failure in dilated cardiomyopathy. Our findings are proof of the existence of separable molecular programs primary to concentric hypertrophy *versus* eccentric hypertrophy, chamber narrowing *versus* chamber dilation and wall thickening *versus* wall thinning, all occurring within the venue of biomechanical driven pathways of cardiac growth and failure.

Cardiac remodeling in patients with heart disease encompass all quantifiable changes in left ventricular mass and volume, with a wide variety in the ratio of left ventricular wall thickness to chamber radius, often referred to as relative wall thickness (RWT), and diagnosed by echocardiographic or cardiac magnetic resonance imaging (MRI) data [3]. A normal left ventricular chamber size refers to normal geometry, while differences in RWT distinguish concentric from normal and from eccentric remodeling. Concentric hypertrophy tends to arise from pressure overload situations in the heart, as observed in patients with aortic valve stenosis or hypertensive heart diseases, often yielding a substrate for left ventricular diastolic dysfunction. In contrast, eccentric hypertrophy develops secondary to conditions of volume overload of the myocardium, clinically observed in mitral and aortic regurgitation, precipitating in a strong reduction of ejection fraction [3]. Despite the existence of a relatively detailed clinical diagnosis and physiological underpinnings of this spectrum of clinically relevant remodeling phenotypes, the molecular events that underlie distinct forms of cardiac hypertrophy still remain poorly charted [31]. Accordingly, the stimulatory circulatory agonists, membrane-bound receptors and intracellular signaling cascades that connect biomechanical forces and the activation of myocardial stress pathways are central to understanding the initiation and progression to concentric hypertrophy as clinically observed in hypertrophic cardiomyopathies versus eccentric hypertrophy as it occurs in forms of dilated cardiomyopathy.

In cultured cardiomyocytes, cardiotrophin-1 signals through a gp130 homodimer or gp130/leukemia inhibitory factor receptor-β (LIFRβ) heterodimer. Moreover, it was reported to induce a peculiar form of hypertrophy with increased cardiomyocyte size, consisting on an increase in cell length but no significant change in cell width, due to the assembly of sarcomeric units in series, as is more commonly observed upon stimulation with the canonical pro-hypertrophic adrenergic agonists or endothelin-1 [6, 7]. The involvement of ERK5 and STAT3 in cardiotrophin-1-induced longitudinal elongation has been reported in adult cardiomyocytes [7] and it is further supported by the molecular observation that overexpression of activated ERK5 induces serial insertion of sarcomeres in

neonatal cardiomyocytes *in vitro* [32]. Interestingly, STAT3 upregulates ERK5 in other cell types. Thus, the possibility that STAT3 mediates the longitudinal elongation through the downstream activation of ERK5, which determines cardiomyocyte elongation, requires further investigations.

These morphological differences find a basis in the activation of distinct signaling cascades and proteomic outcomes between cytokines from the interleukin-6 superfamily or endothelin-1 [33]. Elongated cardiomyocytes, myocardial dilation and decreased ejection fraction were also evident following 6 weeks of cardiotrophin-1 treatment in rats.[7] In line, in the current study we developed and characterized a mouse model with continuous cardiotrophin-1 infusion at a clinically relevant concentration of 20 µg/kg/day, which displayed the hallmarks of eccentric hypertrophy after two weeks: wall thinning, severe chamber dilation and a stark reduction in ejection fraction. The cardiotrophin-1 infusion rodent models may proof useful for future studies examining the biochemical, geometric or functional ramifications of distinct hypertrophic agonists on the myocardium.

Genetic studies on the involvement of gp130 in cardiac remodeling reveal a requirement of gp130-dependent signaling for myocyte survival pathways, on the one hand, as well as transmitting prohypertrophic signals, on the other. Indeed, myocyte-restricted deletion of gp130 yielded massive apoptotic cell death and rapid onset of dilated cardiomyopathy following biomechanical stress [20]. Heart-restricted overexpression of a dominant negative form of gp130 suppressed many molecular and morphological features of pressure overload-induced concentric hypertrophic remodeling [21]. The molecular decision between survival and hypertrophy is regulated by the interplay between gp130-mediated JAK/STAT activation and suppression of cytokine signaling 1/3 (SOCS1/3), intrinsic JAK inhibitors and negative feedback regulators for gp130 signaling. AAV transfer of SOCS1 dampened JAK/STAT activation and the transition of hypertrophy to failure in a pressure overload model *in vivo* [34]. Moreover, adenovirus-mediated gene transfer of SOCS3 to ventricular cardiomyocytes completely suppressed both hypertrophic and antiapoptotic phenotypes in cultured cardiomyocytes induced by leukemia inhibitory factor (LIF) [35]. In another study, cardiac-specific SOCS3 knockout mice showed enhanced activation of the signaling targets STAT3, Akt, ERK1/2 - and p38 MAPK and spontaneous cardiac eccentric remodeling, occurrence of arrhythmias and signs of heart failure, all in dependence on the presence of gp130, since SOCS3/gp130 double knockout mice displayed suppression of the cardiomyopathic phenotype [36]. Further downstream of gp130, a variety of signaling branches are differentially activated by IL-6 cytokines, including the ERK1/2, p38 and ERK5 MAPK terminal branches, JAK/STAT3, PI3K/Akt, Gab1/SHP2 and RhoA [11, 37, 38]. In line, Mek5 transgenic mice displayed a severe form of eccentric remodeling with wall thinning, chamber dilation and severe fibrosis [32] a phenotype that was largely recapitulated by silencing endogenous *miR-148a* using an antagomir strategy in the current study. In contrast, STAT3-deficient mice spontaneously develop signs of injury, inflammation and cardiac dysfunction with advancing age and in response to cardiac stress.

Accordingly, the prevailing message supports a model where IL-6 cytokine/gp130 confers a level of protective signaling in a variety of cardiac stress conditions, and that complete deletion of gp130 signaling components causes widespread cell death. On the other hand, unrestrained activation of cytokine/gp130 signaling also confers prohypertrophic cues that facilitate the transition to eccentric hypertrophy and systolic dysfunction in situations of biomechanical stress. This model of cytokine/gp130 signaling is in line with a regulatory function of cardiac *miR-148a,* where higher *miR-148a* expression, and concomitant reduction of gp130 expression, sustains the protective cell survival effects while dampens over-activation of downstream signaling cascades, yielding concentric forms of hypertrophy. With sustained periods of biomechanical stress, decreased *miR-148a* expression, and concomitant derepression of gp130, promotes over-activation of a variety of hypertrophic intracellular signals, yielding eccentric hypertrophic remodeling, dilated cardiomyopathy and systolic dysfunction. As such, the biphasic regulation of *miR-148a* provides a mechanistic explanation for the clinically observed transition from early phase "compensatory" forms of hypertrophy to later phase decompensation and overt heart failure in the setting of sustained biomechanical stress.

METHODS

Human heart samples. Approval for studies on human tissue samples was obtained from the Medical Ethics Committee of the University Medical Center Utrecht, The Netherlands. All patients or their relatives gave written informed consent before operation and procedures were compliant with the WMA Declaration of Helsinki and the Department of Health and Human Services Belmont Report. In this study, we included tissue from the left ventricular free wall of patients undergoing heart transplantation with end-stage heart failure and dilated cardiomyopathy (DCM) or hypertrophic cardiomyopathy (HCM). Control tissue was taken from the left ventricular free wall of refused donor hearts that could not be transplanted for technical reasons and where neither donor patient histories nor autopsy revealed signs of heart disease.

Mouse models. Mice used in this study were male and female B6CBAF1 wild-type mice (Charles River Laboratories) of 2–6 months of age. Other mice used in this study were male calcineurin transgenic mice in a B6CBAF1 background expressing an activated mutant of calcineurin in the postnatal heart under control of the 5.5 kb murine *Myh6* promoter (Myh6-CnA; [39]). Sample size was determined by a power calculation based on an echocardiographic effect size. Randomization of subjects to experimental groups was based on a single sequence of random assignments. Animal caretakers and investigators were blinded to group allocation during the experiment and/or when assessing the outcome. All protocols were performed according to institutional guidelines and approved by local Animal Care and Use Committees. All mice were housed on a 12hr:12hr light:dark cycle in a temperature-controlled environment with *ad libitum* access to water and chow at Innoser

Netherlands BV, a commercial mouse breeding company with a quarterly animal health monitoring system that complies with FELASA guidelines and recommendations.

Aortic banding, CT-1 infusion and transthoracic echocardiography. Transverse aortic constriction (TAC) or sham surgery was performed in 2-month-old wildtype B6CBAF1 female and male mice by subjecting the aorta to a defined 27-gauge constriction between the first and second truncus of the aortic arch, as described previously [26, 40] For Doppler-echocardiography, mice were shaved, lightly anaesthetized with isoflurane (mean 1% in oxygen) and allowed to breathe spontaneously through a nasal cone. Non-invasive, echocardiography was performed as describes previously in detail [24]. Doppler was used to calculate the pressure gradient between the proximal and distal sites of the transverse aortic constriction and only mice with a pressure gradient >50 mm Hg were included. Chronic cardiotrophin 1 (20 µg/kg/day dissolved in phosphate-buffered saline), isoproterenol (60 mg/kg/day dissolved in phosphate-buffered saline) or saline administration was performed using Alzet miniosmotic pumps (no. 2002; Alza) surgically inserted dorsally and s.c. in 2-month-old wild-type B6CBAF1 female and male mice under isoflurane anesthesia and left for an additional 2 weeks. All protocols were performed according to institutional guidelines and approved by local Animal Care and Use Committees.

Antagomir studies. Chemically modified antisense oligonucleotides designed to target *mmu-miR-148a-3p* (5′-ACAAAGUUCUGUAGUGCAC-3′/3CholTEG-3′ or *C.elegans miR-39-5p* (5′-AAGGCAAGCUGACCCUGAAGUU-3′/3CholTEG-3′) with a 3′ cholesterol conjugation and 2 phosphorothioate bonds at the very first 5′ end and 4 phosphorothioate bonds between the last 3′ bases [41] were synthesized at Integrated DNA Technologies (IDT). All antagomirs were HPLC purified and desalted before use. Female and male wild-type B6CBAF1 mice (8–10 weeks of age) were subjected to sham or TAC surgery. Following 3 days, mice were injected (intraperitoneally) with antagomir-148a (80 mg kg^{-1} body weight) or control antagomir (80 mg kg^{-1} body weight) for 3 consecutive days. Echo analysis was performed at 3 weeks and 6 weeks after surgery.

AAV Vectors. All of the AAV vectors used in this study were generated by the International Centre for Genetic Engineering and Biotechnology (ICGEB) AAV Vector Unit (AVU) (www.icgeb.org/avu-core-facility.html) using a dual/triple plasmid co-transfection procedure followed by PEG precipitation and purification through CsCl2 gradient centrifugations as described previously [42]. Adult mice were intravenously injected with AAV9-MCS and AAV9-miR-148a via the jugular vein at a dose of $1x10^{12}$ viral genome particles per animal.

Primary cardiomyocyte cultures and immunocytochemistry. Cardiomyocytes were isolated by enzymatic dissociation of 1–2-day-old neonatal rat hearts and processed for immunofluorescence microscopy as described previously.[43] Primary fibroblasts and endothelial cells were obtained from neonatal rat hearts using endothelial and fibroblast

isolation kits (Miltenyi Biotec). Neonatal cardiomyocytes were transfected with precursors (Ambion) and inhibitors (Exiqon) of microRNAs (10 nM) using Oligofectamine (Invitrogen). For visualization of cardiomyocyte size and sarcomeric organization, the cells were stained for α2-actinin with mouse monoclonal anti-sarcomeric α-actinin antibody (Sigma-Aldrich, A7811 clone EA-53, 1:500) followed by rat anti-mouse phenylephrine–Texas red-conjugated monoclonal antibody (Life Technologies, RM2817 clone M1/70.15, 1:800). Nuclear staining was performed with VECTASHIELD Mounting Medium (Vector Laboratories) containing 4′,6-diamidino-2-phenylindole (DAPI). Myocyte hypertrophy was induced by stimulation for 24 h with phenylephrine (10 μM) as described previously [43] or with Cardiotrophin-1 (CT-1, 2nM).

Isolation of adult mouse cardiomyocytes, fibroblasts and endothelial cells. Cardiomyocytes, fibroblasts and endothelial cells were isolated from hearts of B6CBAF1 wild-type mice (2–6 months old) following the procedure and the buffer preparations of the Langherdorff-free method previously described [*10.1161/CIRCRESAHA.116.309202*]. Briefly, mice were sacrificed via cervical dislocation; the still beating heart was fully exposed, isolated from systemic circulation and perfused ones with EDTA buffer through left ventricular injection. Following, the heart was transferred into a 60mm dish and perfused again with new EDTA buffer. Moved in a new dish, treated with Perfusion buffer and then serially perfused with Collagenase buffer. The tissue was then pulled gently into~1mm^3 pieces using forceps and dissociated by pipetting. Stop buffer was added, cells suspension was passed through a strainer and cardiomyocytes were left to settle for 20min. Fibroblasts and endothelial cells were separated from the supernatant through Magnetic-activated cell sorting method.

pMIR-reporter assays. Cos7 cells were purchased at the American Type Culture Collection (ATCC; CRL-1651) and cultured in DMEM supplemented with 10% FBS, 100 units/ml penicillin/streptomycin and 2 mmol/liter L-glutamine (Thermo Fischer). Cos7 cells were screened for mycoplasma with the MycoAlert PLUS Mycoplasma Detection kit (Lonza) upon receipt from ATCC and subsequently checked on a yearly basis. Cos7 cells were transfected with pMIR reporter plasmids harboring the entire 3′ UTR of mouse gp130, or with pMIR reporter plasmids harboring the first part of the 3′ UTR of mouse gp130, or with pMIR reporter plasmids harboring the latter section of the gp130 3′ UTR using X-tremeGENE 9 (Roche) transfection reagent, followed by transfection with *miR-148a* or scrambled miR precursor molecules using Oligofectamine reagent (Invitrogen). Luciferase activity was measured 24 h after transfection with a dual luciferase assay kit (Promega) using Renilla luciferase as internal control to correct for transfection efficiency.

Northern blot analysis. Northern blotting was performed as described previously [24] using 3′-digoxigenin-labelled locked nucleic acid oligonucleotides for *miR-148a* and U6 small nuclear RNA (*Rnu6-2*). Detection was achieved with Fab fragments from polyclonal anti-digoxigenin antibodies, conjugated to alkaline phosphatase (Roche).

Western blot analysis. SDS PAGE electrophoresis and blotting were performed as described previously.[7] Primary antibodies that were used included anti-gp130 (Cell Signaling Technology; rabbit pAb cat. no. 3732), anti-LIFR (Santa Cruz Biotechnology; mouse mAb cat sc-515337), anti-CT-1 (Santa Cruz Biotechnology; mouse mAb cline AN-B3 cat. no. sc-9991), anti-GAPDH (Millipore; mouse mAb clone 6C5, cat. no. MAB374), anti-STAT3 (Cell Signaling Technology; mouse mAb clone 124H6, cat. no. 9139), anti-phospho-STAT3 (p-Tyr705) (Cell Signaling Technology; mouse mAb clone M9C6 cat. no. 4113), anti-Akt (Cell Signaling Technology; mouse mAb clone 2H10 cat. no. 2967), anti-phospho-Akt (pSer473) (Cell Signaling Technology; rabbit mAb clone D7F10 cat. no. 9018), anti-p44/42 MAPK (ERK1/2) (Cell Signaling Technology; rabbit mAb clone 137F5 cat. no. 4695), anti-phopsho-p44/42 MAPK (p-Thr202-204-Erk1/2) (Cell Signaling Technology; rabbit mAb clone D13.14.4E cat. no. 4370), anti-ERK5 (Cell Signaling Technology' rabbit mAb clone D3I5V cat. no. 12950), anti-phospho-ERK5 (p-Thr218/Tyr220) (Cell Signaling Technology; rabbit pAb cat. no. 3371) followed by corresponding horseradish peroxidase (HRP)-conjugated secondary antibodies and enhanced chemiluminescence ECL detection. Western Blots were performed with Stain Free gels for loading control or probed with secondary antibodies: anti-beta-actin (Sigma-Aldrich; mouse mAb cat. No. A1978-100UL) or anti-tubulin (Sigma-Aldrich mouse mAb cat. no. T6199-100UL). Signals were detected using the ECL system (Amersham Pharmacia Biotech). Results are expressed as an n-fold increase over the values of the control group in densitometric arbitrary units.

Quantitative real-time PCR. Total RNA (1 μg) was used in either miR-based or mRNA-based reverse transcription. Real-time PCR was performed on a BioRad iCycler (Biorad) using SYBR Green. Transcript quantities were compared using the relative Ct method, where the amount of target normalized to the amount of endogenous control (L7) and relative to the control sample is given by $2^{-\Delta\Delta Ct}$. For microRNA real-time PCR, miRNAs were isolated with TRIzol reagent (Invitrogen) and cDNA was generated with the miScript Reverse Transcription Kit (Qiagen). For real-time PCR detection of miRNAs, miScript Primer Assays and the miScript SYBR Green PCR Kit (Qiagen) were used. Regarding the viral genome copy number assay, total DNA was extracted and used as substrate of the real-time PCR against the Cytomegalovirus (CMV) promoter cloned into the AAV vector genome (primer pair 5'-GGACTTTCCTACTTGGCAGT-3' and 5'-GTGAGTCAAACCGCTATCCA-3'). A standard curve was obtained by serial dilutions of the AAV plasmid with known concentration. The data were quantified by interpolation with the standard curve, solving the equation for the linear regression Ct = m (log quantity) + b .

microRNA target prediction. Putative microRNA-148a target genes were identified using the microRNA databases and target prediction tools miRWalk 2.0 (http://zmf.umm.uni-heidelberg.de/apps/zmf/mirwalk2/index.html), miRBase (http://microrna.sanger.ac.uk/), PicTar (http://pictar.mdc-berlin.de/) and TargetScan (http://targetscan.org/index.html).

Histological analysis and (immunofluorescence) microscopy. Hearts were arrested in diastole, perfusion fixed with 4% paraformaldehyde/PBS solution, embedded in paraffin and sectioned at 4 µm. Paraffin sections were stained with haematoxylin and eosine for routine histological analysis; Sirius red for the detection of fibrillar collagen; and FITC-labelled wheat-germ-agglutinin (Sigma-Aldrich, 1:100) to visualize and quantify myocyte cross-sectional area. Slides were visualized using a Zeiss Axioskop 2Plus with an AxioCamHRc. Cell surface areas were determined using ImageJ imaging software (http://rsb.info.nih.gov/ij/). Immune cell stainings were performed using rat monoclonal anti-CD45 antibody (Abcam ab23910 IBL-3/16, 1:50) followed by goat anti-rat Alexa Fluor 568 conjugated polyclonal antibody (ThermoFisher, A11077, 1:1000), rabbit polyclonal anti-sarcomeric α-actinin antibody (Abcam, ab137346, 1:100) followed by goat anti-rabbit Alexa Fluor 488 conjugated polyclonal antibody (ThermoFisher, A11008, 1:1000) and Hoechst 34580 (ThermoFisher, H21486, 1:1000). TUNEL stainings were performed on 10 µm paraffin sections as described previously in detail [44, 45] using a TMR red TUNEL kit (Roche). Double staining was performed with anti-phalloidin-FITC (Sigma,1:500) and/or DAPI (Molecular Probes, 1:500). The samples were examined with a confocal scanning laser microscope Leica TCSNT equipped with argon/krypton and helium/neon lasers.

Statistical analysis. The results are presented as mean ± standard error of the mean. Statistical analyses were performed using Prism software (GraphPad Software Inc.), and consisted of ANOVA followed by Bonferroni's multiple comparison test when group differences were detected at the 5% significance level, or Student's *t*-test when comparing two experimental groups. Differences were considered significant when $P<0.05$. For Western blots analysis, normality of distributions was verified by means of the Kolmogorov–Smirnov test. Data were analyzed using ANOVA followed by a Newman-Keuls multiple comparison test when group differences were detected at the 5% significance level. Differences were considered significant when $P<0.05$.

Acknowledgements: E.D. is supported by a VENI award 916-150-16 from the Netherlands Organization for Health Research and Development (ZonMW), P.D.C.M. is supported by a MEERVOUD grant from The Netherlands Organisation for Scientific Research (NWO) and is an Established Investigator of the Dutch Heart Foundation. N.L.A. is supported by Miguel Servet contract CP13/00221 from the "Instituto de Salud Carlos III-FEDER". L.D.W. acknowledges support from the *Netherlands CardioVascular Research Initiative*: the Dutch Heart Foundation, Dutch Federation of University Medical Centers, ZonMW and the Royal Netherlands Academy of Sciences. L.D.W. was further supported by grant 311549 from the European Research Council (ERC) and a VICI award 918-156-47 from NWO. P.D.C.M. and L.D.W. are co-founders and stockholders of Mirabilis Therapeutics BV.

Author Contributions: A.R., E.D., L.E.P., A.F.C., F.D.M., V.S.P., M.S., R.J., H.E.A., N.B., S.O., L.Z. and S.Z. performed experiments. A.R. L.E.P., E.D., M.O. P.D.C.M., N.L.A. and L.D.W. analyzed data. E.D., L.E.P., P.D.C.M. and L.D.W. designed the study. M.M.H., R.D.W, Y.J.R., Y.M.P., M.G. and N.L.A. provided reagents, models or data. A.R., E.D., L.E.P., P.D.C.M., N.L.A., M.C. and L.D.W. wrote the manuscript.

References

1. Opie LH, Commerford PJ, Gersh BJ and Pfeffer MA. Controversies in ventricular remodelling. *Lancet*. 2006;367:356-67.
2. Dorn GW, 2nd, Robbins J and Sugden PH. Phenotyping hypertrophy: eschew obfuscation. *Circulation research*. 2003;92:1171-5.
3. Gaasch WH and Zile MR. Left ventricular structural remodeling in health and disease: with special emphasis on volume, mass, and geometry. *Journal of the American College of Cardiology*. 2011;58:1733-40.
4. Heineke J and Molkentin JD. Regulation of cardiac hypertrophy by intracellular signalling pathways. *Nature reviews Molecular cell biology*. 2006;7:589-600.
5. Pennica D, King KL, Shaw KJ, Luis E, Rullamas J, Luoh SM, Darbonne WC, Knutzon DS, Yen R, Chien KR and et al. Expression cloning of cardiotrophin 1, a cytokine that induces cardiac myocyte hypertrophy. *Proceedings of the National Academy of Sciences of the United States of America*. 1995;92:1142-6.
6. Wollert KC, Taga T, Saito M, Narazaki M, Kishimoto T, Glembotski CC, Vernallis AB, Heath JK, Pennica D, Wood WI and Chien KR. Cardiotrophin-1 activates a distinct form of cardiac muscle cell hypertrophy. Assembly of sarcomeric units in series VIA gp130/leukemia inhibitory factor receptor-dependent pathways. *The Journal of biological chemistry*. 1996;271:9535-45.
7. Lopez N, Diez J and Fortuno MA. Differential hypertrophic effects of cardiotrophin-1 on adult cardiomyocytes from normotensive and spontaneously hypertensive rats. *Journal of molecular and cellular cardiology*. 2006;41:902-13.
8. Sheng Z, Pennica D, Wood WI and Chien KR. Cardiotrophin-1 displays early expression in the murine heart tube and promotes cardiac myocyte survival. *Development*. 1996;122:419-28.
9. Brar BK, Stephanou A, Liao Z, O'Leary RM, Pennica D, Yellon DM and Latchman DS. Cardiotrophin-1 can protect cardiac myocytes from injury when added both prior to simulated ischaemia and at reoxygenation. *Cardiovascular research*. 2001;51:265-74.
10. Liao Z, Brar BK, Cai Q, Stephanou A, O'Leary RM, Pennica D, Yellon DM and Latchman DS. Cardiotrophin-1 (CT-1) can protect the adult heart from injury when added both prior to ischaemia and at reperfusion. *Cardiovascular research*. 2002;53:902-10.
11. Lopez N, Diez J and Fortuno MA. Characterization of the protective effects of cardiotrophin-1 against non-ischemic death stimuli in adult cardiomyocytes. *Cytokine*. 2005;30:282-92.
12. Lopez-Andres N, Rousseau A, Akhtar R, Calvier L, Inigo C, Labat C, Zhao X, Cruickshank K, Diez J, Zannad F, Lacolley P and Rossignol P. Cardiotrophin 1 is involved in cardiac, vascular, and renal fibrosis and dysfunction. *Hypertension*. 2012;60:563-73.
13. Talwar S, Squire IB, Downie PF, Davies JE and Ng LL. Plasma N terminal pro-brain natriuretic peptide and cardiotrophin 1 are raised in unstable angina. *Heart*. 2000;84:421-4.
14. Talwar S, Squire IB, O'Brien R J, Downie PF, Davies JE and Ng LL. Plasma cardiotrophin-1 following acute myocardial infarction: relationship with left ventricular systolic dysfunction. *Clinical science*. 2002;102:9-14.
15. Talwar S, Squire IB, Downie PF, O'Brien RJ, Davies JE and Ng LL. Elevated circulating cardiotrophin-1 in heart failure: relationship with parameters of left ventricular systolic dysfunction. *Clinical science*. 2000;99:83-8.
16. Pemberton CJ, Raudsepp SD, Yandle TG, Cameron VA and Richards AM. Plasma cardiotrophin-1 is elevated in human hypertension and stimulated by ventricular stretch. *Cardiovascular research*. 2005;68:109-17.
17. Lopez B, Gonzalez A, Lasarte JJ, Sarobe P, Borras F, Diaz A, Barba J, Tomas L, Lozano E, Serrano M, Varo N, Beloqui O, Fortuno MA and Diez J. Is plasma cardiotrophin-1 a marker of hypertensive heart disease? *Journal of hypertension*. 2005;23:625-32.

18. Zolk O, Ng LL, O'Brien RJ, Weyand M and Eschenhagen T. Augmented expression of cardiotrophin-1 in failing human hearts is accompanied by diminished glycoprotein 130 receptor protein abundance. *Circulation*. 2002;106:1442-6.
19. Tsutamoto T, Wada A, Maeda K, Mabuchi N, Hayashi M, Tsutsui T, Ohnishi M, Fujii M, Matsumoto T, Yamamoto T, Wang X, Asai S, Tsuji T, Tanaka H, Saito Y, Kuwahara K, Nakao K and Kinoshita M. Relationship between plasma level of cardiotrophin-1 and left ventricular mass index in patients with dilated cardiomyopathy. *Journal of the American College of Cardiology*. 2001;38:1485-90.
20. Hirota H, Chen J, Betz UA, Rajewsky K, Gu Y, Ross J, Jr., Muller W and Chien KR. Loss of a gp130 cardiac muscle cell survival pathway is a critical event in the onset of heart failure during biomechanical stress. *Cell*. 1999;97:189-98.
21. Uozumi H, Hiroi Y, Zou Y, Takimoto E, Toko H, Niu P, Shimoyama M, Yazaki Y, Nagai R and Komuro I. gp130 plays a critical role in pressure overload-induced cardiac hypertrophy. *The Journal of biological chemistry*. 2001;276:23115-9.
22. Yoshida K, Taga T, Saito M, Suematsu S, Kumanogoh A, Tanaka T, Fujiwara H, Hirata M, Yamagami T, Nakahata T, Hirabayashi T, Yoneda Y, Tanaka K, Wang WZ, Mori C, Shiota K, Yoshida N and Kishimoto T. Targeted disruption of gp130, a common signal transducer for the interleukin 6 family of cytokines, leads to myocardial and hematological disorders. *Proceedings of the National Academy of Sciences of the United States of America*. 1996;93:407-11.
23. Kunisada K, Tone E, Fujio Y, Matsui H, Yamauchi-Takihara K and Kishimoto T. Activation of gp130 transduces hypertrophic signals via STAT3 in cardiac myocytes. *Circulation*. 1998;98:346-52.
24. da Costa Martins PA, Salic K, Gladka MM, Armand AS, Leptidis S, el Azzouzi H, Hansen A, Coenen-de Roo CJ, Bierhuizen MF, van der Nagel R, van Kuik J, de Weger R, de Bruin A, Condorelli G, Arbones ML, Eschenhagen T and De Windt LJ. MicroRNA-199b targets the nuclear kinase Dyrk1a in an auto-amplification loop promoting calcineurin/NFAT signalling. *Nature cell biology*. 2010;12:1220-7.
25. Taga T and Kishimoto T. Gp130 and the interleukin-6 family of cytokines. *Annu Rev Immunol*. 1997;15:797-819.
26. Bourajjaj M, Armand AS, da Costa Martins PA, Weijts B, van der Nagel R, Heeneman S, Wehrens XH and De Windt LJ. NFATc2 is a necessary mediator of calcineurin-dependent cardiac hypertrophy and heart failure. *The Journal of biological chemistry*. 2008;283:22295-303.
27. Dirkx E, Gladka MM, Philippen LE, Armand AS, Kinet V, Leptidis S, El Azzouzi H, Salic K, Bourajjaj M, da Silva GJ, Olieslagers S, van der Nagel R, de Weger R, Bitsch N, Kisters N, Seyen S, Morikawa Y, Chanoine C, Heymans S, Volders PG, Thum T, Dimmeler S, Cserjesi P, Eschenhagen T, da Costa Martins PA and De Windt LJ. Nfat and miR-25 cooperate to reactivate the transcription factor Hand2 in heart failure. *Nature cell biology*. 2013;15:1282-93.
28. De Windt LJ, Lim HW, Bueno OF, Liang Q, Delling U, Braz JC, Glascock BJ, Kimball TF, del Monte F, Hajjar RJ and Molkentin JD. Targeted inhibition of calcineurin attenuates cardiac hypertrophy in vivo. *Proceedings of the National Academy of Sciences of the United States of America*. 2001;98:3322-7.
29. Zacchigna S, Zentilin L and Giacca M. Adeno-associated virus vectors as therapeutic and investigational tools in the cardiovascular system. *Circulation research*. 2014;114:1827-46.
30. Raso A and Dirkx E. Cardiac regenerative medicine: At the crossroad of microRNA function and biotechnology. *Noncoding RNA Res*. 2017;2:27-37.
31. Torrado M, Iglesias R, Nespereira B and Mikhailov AT. Identification of candidate genes potentially relevant to chamber-specific remodeling in postnatal ventricular myocardium. *J Biomed Biotechnol*. 2010;2010:603159.

32. Nicol RL, Frey N, Pearson G, Cobb M, Richardson J and Olson EN. Activated MEK5 induces serial assembly of sarcomeres and eccentric cardiac hypertrophy. *The EMBO journal*. 2001;20:2757-67.
33. Kuwahara K, Saito Y, Ogawa Y, Tamura N, Ishikawa M, Harada M, Ogawa E, Miyamoto Y, Hamanaka I, Kamitani S, Kajiyama N, Takahashi N, Nakagawa O, Masuda I and Nakao K. Endothelin-1 and cardiotrophin-1 induce brain natriuretic peptide gene expression by distinct transcriptional mechanisms. *J Cardiovasc Pharmacol*. 1998;31 Suppl 1:S354-6.
34. Cittadini A, Monti MG, Iaccarino G, Castiello MC, Baldi A, Bossone E, Longobardi S, Marra AM, Petrillo V, Saldamarco L, During MJ, Sacca L and Condorelli G. SOCS1 gene transfer accelerates the transition to heart failure through the inhibition of the gp130/JAK/STAT pathway. *Cardiovascular research*. 2012;96:381-90.
35. Yasukawa H, Hoshijima M, Gu Y, Nakamura T, Pradervand S, Hanada T, Hanakawa Y, Yoshimura A, Ross J, Jr. and Chien KR. Suppressor of cytokine signaling-3 is a biomechanical stress-inducible gene that suppresses gp130-mediated cardiac myocyte hypertrophy and survival pathways. *The Journal of clinical investigation*. 2001;108:1459-67.
36. Yajima T, Murofushi Y, Zhou H, Park S, Housman J, Zhong ZH, Nakamura M, Machida M, Hwang KK, Gu Y, Dalton ND, Yajima T, Yasukawa H, Peterson KL and Knowlton KU. Absence of SOCS3 in the cardiomyocyte increases mortality in a gp130-dependent manner accompanied by contractile dysfunction and ventricular arrhythmias. *Circulation*. 2011;124:2690-701.
37. Takahashi N, Saito Y, Kuwahara K, Harada M, Tanimoto K, Nakagawa Y, Kawakami R, Nakanishi M, Yasuno S, Usami S, Yoshimura A and Nakao K. Hypertrophic responses to cardiotrophin-1 are not mediated by STAT3, but via a MEK5-ERK5 pathway in cultured cardiomyocytes. *Journal of molecular and cellular cardiology*. 2005;38:185-92.
38. Fahmi A, Smart N, Punn A, Jabr R, Marber M and Heads R. p42/p44-MAPK and PI3K are sufficient for IL-6 family cytokines/gp130 to signal to hypertrophy and survival in cardiomyocytes in the absence of JAK/STAT activation. *Cell Signal*. 2013;25:898-909.
39. Molkentin JD, Lu JR, Antos CL, Markham B, Richardson J, Robbins J, Grant SR and Olson EN. A calcineurin-dependent transcriptional pathway for cardiac hypertrophy. *Cell*. 1998;93:215-28.
40. Rockman HA, Ross RS, Harris AN, Knowlton KU, Steinhelper ME, Field LJ, Ross J, Jr. and Chien KR. Segregation of atrial-specific and inducible expression of an atrial natriuretic factor transgene in an in vivo murine model of cardiac hypertrophy. *Proceedings of the National Academy of Sciences of the United States of America*. 1991;88:8277-81.
41. Krutzfeldt J, Rajewsky N, Braich R, Rajeev KG, Tuschl T, Manoharan M and Stoffel M. Silencing of microRNAs in vivo with 'antagomirs'. *Nature*. 2005;438:685-9.
42. Arsic N, Zentilin L, Zacchigna S, Santoro D, Stanta G, Salvi A, Sinagra G and Giacca M. Induction of functional neovascularization by combined VEGF and angiopoietin-1 gene transfer using AAV vectors. *Molecular therapy : the journal of the American Society of Gene Therapy*. 2003;7:450-9.
43. De Windt LJ, Lim HW, Haq S, Force T and Molkentin JD. Calcineurin promotes protein kinase C and c-Jun NH2-terminal kinase activation in the heart. Cross-talk between cardiac hypertrophic signaling pathways. *J Biol Chem*. 2000;275:13571-9.
44. Kostin S, Pool L, Elsasser A, Hein S, Drexler HC, Arnon E, Hayakawa Y, Zimmermann R, Bauer E, Klovekorn WP and Schaper J. Myocytes die by multiple mechanisms in failing human hearts. *Circ Res*. 2003;92:715-24.
45. van Empel VP, Bertrand AT, van der Nagel R, Kostin S, Doevendans PA, Crijns HJ, de Wit E, Sluiter W, Ackerman SL and De Windt LJ. Downregulation of apoptosis-inducing factor in harlequin mutant mice sensitizes the myocardium to oxidative stress-related cell death and pressure overload-induced decompensation. *Circ Res*. 2005;96:e92-e101.

FIGURE LEGENDS

Figure 1. *MicroRNA-148a* (*miR-148a*) shows dynamic expression patterns in distinct forms of heart failure. (a) Schematic representation of the genomic localization and precursor sequence of *mmu-miR-148a* located on the opposite strand on chromosome 6 in the mouse genome. The mature *miR-148a-3p* strand is conserved among several species. **(b)** Northern blot analysis of *miR-148a-3p* expression in diverse mouse organs. **(c)** RT-PCR analysis of *miR-148a-3p* expression in diverse mouse organs. **(d)** RT-PCR analysis of *miR-148a-3p* expression in isolated cardiomyocytes, fibroblasts and endothelial cells from adult mouse hearts. **(e)** RT-PCR analysis of *miR-148a-3p* expression in human non-failing (control) hearts, human left ventricular myocardium with hypertrophic cardiomyopathy or human left ventricular myocardium with dilated cardiomyopathy. **(f)** RT-PCR analysis of *miR-148a-3p* expression in hearts from wild-type and *Csrp3* knockout mice, the gene encoding muscle LIM protein (MLP). **(g)** RT-PCR analysis of *miR-148a-3p* expression in hearts from 3 week-old non-transgenic littermates and Myh6-CnA transgenic mice.
Data information: Data are means ± SEM. One-way ANOVA with Bonferroni's multiple comparison test or Student's paired 2-tailed *t*-test was used to compare groups. *n*, number of hearts; RT-PCR, real-time-polymerase chain reaction; NF, non failing; DCM, dilated cardiomyopathy; HCM, hypertrophic cardiomyopathy; *Csrp3*, cysteine and glycine-rich protein 3; Myh6, alpha myosin heavy chain; CnA, calcineurin. *$P < 0.05$ vs corresponding control group.

Figure 2. *miR-148a* targets glycoprotein 130 (gp130) and differentially regulates gp130 downstream signaling in concentric and eccentric cardiac remodeling. (a) Location and evolutionary conservation of the *mmu-miR-148a* seed region on gp130 3'UTR [ENSMUST00000183663.7]. **(b)** Schematic representation of luciferase reporter constructs. **(c)** Activity assay of luciferase reporter constructs in Cos7 cells. **(d)** Western blot for endogenous gp130 in neonatal rat cardiomyocytes when transfected with scrambled control antimir (scr.anti-miR), antimir-148a (anti-miR-148a), or precursor for *miR-148a* (pre-miR-148a) and quantification of tubulin-corrected gp130 western blot signals. **(e)** Design of the study: two month-old mice were subjected to sham or TAC surgery for 2, 4, 6 or 8 weeks. Mice were subjected to echocardiographic evaluation and hearts harvested at indicated time points. **(f)** RT-PCR analysis of *miR-148a-3p* expression at indicated time points. **(g-i)** Echocardiographically determined LV mass/BW, EF or LVIDs, respectively. **(j)** Western blot analysis of myocardial CT-1 expression and quantification at indicated time points. **(k)** Western blot analysis of myocardial gp130 expression and quantification at indicated time points. **(l)** Western blot analysis of myocardial phosphorylated and unphosphorylated forms of STAT3 and quantification at indicated time points.
Data information: Data are means ± SEM. One-way ANOVA with Bonferroni's or Newman-Keul's multiple comparison test was used to compare groups. *n*, number of transfection experiments **(c)**, number of transfected wells **(d)**, number of mice **(f-l)**. TAC, transverse aortic constriction; LV mass/BW, left ventricular mass to body weight ratio; EF, ejection fraction; LVIDs, left ventricular internal diameter in systole; RT-PCR, real-time-polymerase chain reaction. *$P < 0.05$ vs corresponding control group.

Figure 3. *miR-148a* silencing promotes spontaneous eccentric hypertrophic remodeling and dilated cardiomyopathy *in vivo*. (a) Design of the study. Two-month-old wild-type mice were injected with a

control antagomir targeting *C. elegans miR-39* (antagomir-*Cel-39*) or antagomir against *mmu-miR-148a-3p* and subjected to sham or TAC surgery. Cardiac geometry and function was determined by serial Doppler echocardiography at 3 weeks and 6 weeks after surgery. **(b)** RT-PCR analysis of *miR-148a-3p* and unrelated *let-7b* expression in hearts from mice receiving control antagomir (antagomir-*Cel*-39) or antagomir against *miR-148a*. **(c)** Representative images of whole hearts (top panel), H&E-stained sections of four-chamber view (second panel), high-magnification H&E-stained sections (third panel), Sirius-red-stained sections (fourth panel) and WGA-stained (fifth panel) histological sections. **(d)** Measurement of LV mass/BW ratio, **(e)** LVPWs, **(f)** LVIDs or **(g)** EF by echocardiography in antagomir control and antagomir-148a treated mice after sham or TAC surgery. Measurements of **(h)** fibrotic area (sirius red staining) and **(i)** cell surface area in control and antagomir-148a treated mice after sham or TAC surgery. **(j)** RT-PCR analysis of transcript abundance of the hypertrophic stress marker genes *Nppa*, *Nppb*, *Acta1* and *Myh7* in hearts from control antagomir or antagomir-148a treated mice after sham or TAC surgery. **(k-m)** Western blot analysis and quantification of myocardial gp130 or phosphorylated and unphosphorylated forms of STAT3 in hearts from mice subjected to sham or TAC surgery and receiving antagomir-148a or a control antagomir (antagomir-*Cel*-39).

Data information: Data are means ± SEM. One-way ANOVA with Bonferroni's or Newman-Keuls multiple comparison test was used to compare groups. *n*, number of hearts; C. elegans, Caenorhabditis *elegans ;* TAC, transverse aortic constriction; RT-PCR, real-time-polymerase chain reaction; H&E, hematoxylin & eosin; WGA, wheat germ agglutinin; LV mass/BW, left ventricular mass to body weight ratio; LVPWs, left ventricular posterior wall end systole; LVIDs, left ventricular internal diameter in systole; EF, ejection fraction; *Nppa,* natriuretic peptide type A; *Nppb*, natriuretic peptide type B ; *Acta1*, alpha skeletal actin ; *Myh7*, beta myosin heavy chain. **P < 0.05* vs corresponding control group.

Figure 4. Cardiac AAV9-miR-148a overexpression protects the heart against eccentric hypertrophy, chamber dilation and systolic dysfunction. (a) Design of the study. Two-month-old mice were injected with control AAV9 (AAV9-MCS) or an AAV9 designed to overexpress *mmu-miR-148a-3p* (AAV9-148a) and subjected to sham or TAC surgery. Cardiac geometry and function was determined by serial Doppler echocardiography at 3 and 6 weeks after surgery. **(b)** RT- PCR analysis of *miR-148a-3p* expression in hearts from mice receiving AAV9-MCS or AAV9-148a virus. **(c)** Representative images of whole hearts (top panel), H&E-stained sections of four-chamber view (second panel), high-magnification H&E-stained sections (third panel), Sirius-red-stained sections (fourth panel) and WGA-stained (fifth panel) histological sections. **(d)** Measurements of LV mass/BW ratio, **(e)** LVPWs, **(f)** LVIDs, **(g)** EF, **(h)** fibrotic area (sirius red staining) and **(i)** cell surface area in AAV9-CMV and AAV9-148a treated mice after sham or TAC surgery. **(j)** RT- PCR analysis of transcript abundance of hypertrophic stress marker genes *Nppa*, *Nppb*, *Acta1* and *Myh7* in hearts from AAV9-MCS and AAV9-148a treated mice after sham or TAC surgery. **(k-m)** Western blot analysis and quantification of myocardial gp130 or phosphorylated and unphosphorylated forms of STAT3 in hearts from mice subjected to sham or TAC surgery and receiving AAV9-148a or AAV9-MCS (MCS; multiple cloning site, empty vector).

Data information: Data are means ± SEM. One-way ANOVA with Bonferroni's or Newman-Keul's multiple comparison test was used to compare groups. *n*, number of hearts; AAV9, adeno-associated virus serotype 9*;* TAC, transverse aortic constriction; RT-PCR, real-time-polymerase chain reaction;

H&E, hematoxylin & eosin; WGA, wheat germ agglutinin; LV mass/BW, left ventricular mass to body weight ratio; LVPWs, left ventricular posterior wall end systole; LVIDs, left ventricular internal diameter in systole; EF, ejection fraction; *Nppa,* natriuretic peptide type A; *Nppb*, natriuretic peptide type B ; *Acta1*, alpha skeletal actin ; *Myh7*, beta myosin heavy chain.. *$P < 0.05$ vs corresponding control group; #$P < 0.05$ vs experimental group.

Figure 5. *miR-148a* overexpression prevents the transition of pressure-overload induced concentric hypertrophic remodeling towards eccentric hypertrophy.
(a) Design of the study. Two-month-old mice were subjected to sham or TAC surgery and 4 weeks later injected with control AAV9 (AAV9-CMV) or AAV9-148a. Cardiac geometry and function was determined by serial Doppler echocardiography at 3, 5 and 7 weeks after surgery. **(b)** RT- PCR analysis of *miR-148a-3p* expression in hearts from mice receiving AAV9-CMV or AAV9-148a virus. **(c)** Representative images of H&E-stained sections of four-chamber view (top panel), high-magnification H&E-stained sections (second panel), Sirius-red-stained sections (third panel) and WGA-stained (fourth panel) histological sections. **(d)** Measurements of LV mass/BW ratio, **(e)** LVPWs, **(f)** LVIDs, **(g)** EF, **(h)** fibrotic area (sirius red staining) and **(i)** cell surface area in AAV9-CMV and AAV9-148a treated mice after sham or TAC surgery. **(j)** RT- PCR analysis of transcript abundance of hypertrophic stress marker genes *Nppa*, *Nppb*, *Acta1* and *Myh7* in hearts from AAV9-CMV and AAV9-148a treated mice after sham or TAC surgery. **(k)** Model depicting the influence of *miR-148a* on the CT-1 - gp130 – STAT3 signaling axis in cardiac stress situations, resulting in differential activation of STAT3 signaling and either concentric or eccentric remodeling.
Data information: Data are means ± SEM. One-way ANOVA with Bonferroni's multiple comparison test was used to compare groups. *n*, number of hearts; AAV9, adeno-associated virus serotype 9; TAC, transverse aortic constriction; RT-PCR, real-time-polymerase chain reaction; H&E, hematoxylin & eosin; WGA, wheat germ agglutinin; LV mass/BW, left ventricular mass to body weight ratio; LVPWs, left ventricular posterior wall end systole; LVIDs, left ventricular internal diameter in systole; EF, ejection fraction; *Nppa,* natriuretic peptide type A; *Nppb*, natriuretic peptide type B ; *Acta1*, alpha skeletal actin ; *Myh7*, beta myosin heavy chain. *$P < 0.05$ vs corresponding control group; #$P < 0.05$ vs experimental group.

Supplementary Figure 1. *miR-148a* differentially regulates ERK5, ERK1/2, Akt downstream signaling in concentric and eccentric cardiac remodeling. **(a)** Western blot analysis of myocardial LIFR expression and quantification at indicated time points. **(b-d)** Western blot analysis of phosphorylated and unphosphorylated forms of Akt, Erk5 or Erk1/2 and quantification at indicated time points. **(e-h)** Western blot analysis of myocardial LIF, CNTF, IL-6 or OSM expression and quantification at indicated time points. **(i-k)** Western blot analysis of phosphorylated and unphosphorylated forms of Akt, Erk5 or Erk1/2 and quantification in hearts from mice subjected to sham or TAC surgery and receiving antagomir-148a or a control antagomir (antagomir-*Cel*-39). **(l-n)** Western blot analysis of myocardial gp130 or phosphorylated and unphosphorylated forms of Akt, Erk5 or Erk1/2 and quantification in hearts from mice receiving AAV9-148a or AAV9-MCS.
Data information: Data are means ± SEM. One-way ANOVA with Newman-Keuls multiple comparison test was used to compare groups. *n*, number of independent WB experiments; AAV9, adeno-associated virus serotype 9; TAC, transverse aortic constriction. *$P < 0.05$ vs corresponding control group.

Supplementary Figure 2. CT-1 infusion results in cardiac dilation. (a-b) Evolutionary conservation of the other two *mmu-miR-148a* seed regions on gp130 3'UTR. In mouse they are respectively located on the nucleotide position 6150-6156 and 8532-8538 [ENSMUST00000183663.7]. **(c)** Study design of mice receiving continuous infusion of CT-1 (20 µg/kg/day) or isoproterenol (60 mg/kg/day). **(d)** Representative image of whole hearts (top panels), H&E-stained cardiac sections (second panels), high magnification H&E-stained sections (third panels), or Sirius Red stained (lower panels) histological sections of hearts from saline, CT-1 infused and isoproterenol-infused mice. Measurements of **(e)** LV mass, **(f)** EF **(g)** IVSs in saline, CT-1-treated or isoproterenol-treated mice. **(h)** Confocal microscopy images of neonatal rat cardiomyocytes treated with scrambled or precursor-148a miR-148a with or without CT-1 stimulation. **(i)** Cell surface measurements from conditions in (**f**).

Data information: Data are means ± SEM. One-way ANOVA with Bonferonni's multiple comparison test was used to compare groups. *n*, number of mice CT-1, cardiotrophin 1; LV, left ventricular; EF, ejection fraction; IVSs, Interventricular septum in systole. **P < 0.05* vs corresponding control group; #*P < 0.05* vs experimental group.

Supplementary Figure 3. Immune response in hearts from mice with altered *miR-148a* expression. (a) Representative confocal images of CD45 labeling in hearts after sham-operation or aortic banding in the presence of control antagomir targeting *C. elegans miR-39* (antagomir-*Cel-39*) or antagomir against *mmu-miR-148a-3p* (top and second panel), with CD45 positive cells (red), cardiomyocytes visualized with sarcomeric actin (green) and nuclei visualized with Hoechst (blue). Blood clot into the left ventricular chamber (left-bottom panel) and spleen (right-bottom panel) were used as internal and external staining positive controls.

Supplementary Figure 4. Apoptotic events in hearts from mice with altered *miR-148a* expression. (a) Representative confocal images of TUNEL labeling in hearts after sham-operation or aortic banding in the presence of AAV9-MCS or AAV9-148a, with TUNEL positive nuclei (red) and cardiomyocytes visualized with sarcomeric actin (green). **(b)** Quantification of TUNEL positive cardiomyocytes in experimental groups demonstrates a higher percentage of TUNEL positive myocytes after TAC compared to sham.

Data information: Data are means ± SEM. One-way ANOVA with Bonferroni's multiple comparison test was used to compare groups. *n*, number of mice; AAV9, adeno-associated virus; MCS, multiple cloning site; TAC, transverse aortic constriction. **P < 0.05* vs corresponding control group.

Supplementary Figure 5. Characterization of AAV9 transduction treatment. (a) RT- PCR analysis of viral genome copy numbers in 20ng of total DNA in hearts from mice receiving AAV9-148a virus. **(b)** RT-PCR analysis of *miR-148a-3p* expression in diverse organs from mice receiving AAV9-MCS or AAV9-148a virus.

Data information: Data are means ± SEM. One-way ANOVA with Bonferroni's multiple comparison test was used to compare groups. *n*, number of mice; AAV9, adeno-associated virus; MCS, multiple cloning site. **P < 0.05* vs corresponding control group.

Figure 1

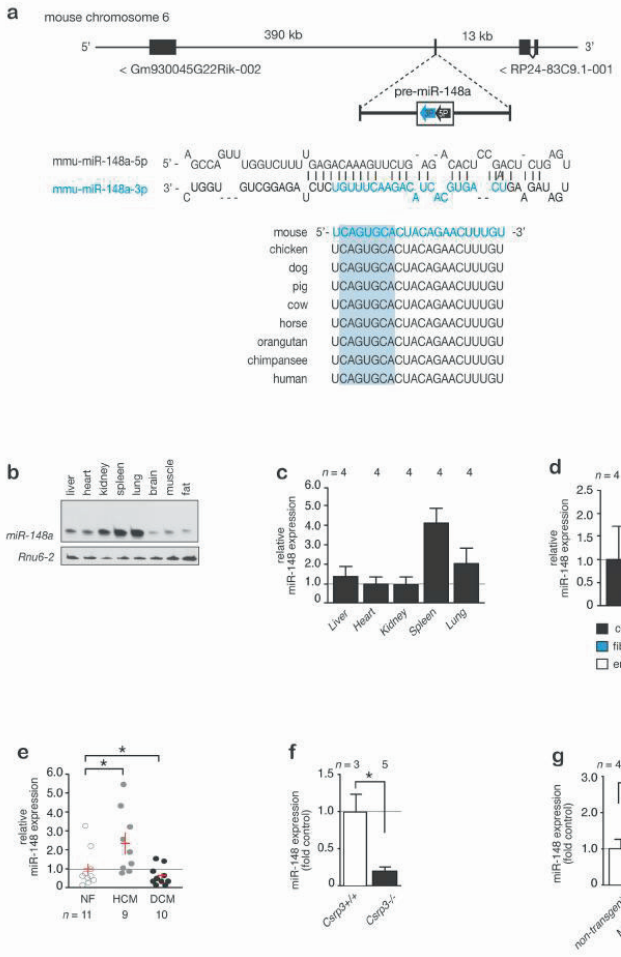
a
mouse chromosome 6
390 kb
13 kb
5'
3'
< Gm930045G22Rik-002
< RP24-83C9.1-001
pre-miR-148a
mmu-miR-148a-5p
mmu-miR-148a-3p
mouse 5'- UCAGUGCACUACAGAACUUUGU -3'
chicken UCAGUGCACUACAGAACUUUGU
dog UCAGUGCACUACAGAACUUUGU
pig UCAGUGCACUACAGAACUUUGU
cow UCAGUGCACUACAGAACUUUGU
horse UCAGUGCACUACAGAACUUUGU
orangutan UCAGUGCACUACAGAACUUUGU
chimpansee UCAGUGCACUACAGAACUUUGU
human UCAGUGCACUACAGAACUUUGU
b
liver
heart
kidney
spleen
lung
brain
muscle
fat
miR-148a
Rnu6-2
c
n = 4 4 4 4 4
relative miR-148 expression
Liver
Heart
Kidney
Spleen
Lung
d
n = 4 4 4
relative miR-148 expression
cardiomyocytes
fibroblasts
endothelial cells
e
relative miR-148 expression
NF
HCM
DCM
n = 11
9
10
f
n = 3 5
miR-148 expression (fold control)
Csrp3+/+
Csrp3-/-
g
n = 4 4
miR-148 expression (fold control)
non-transgenic
Myh6-CnA

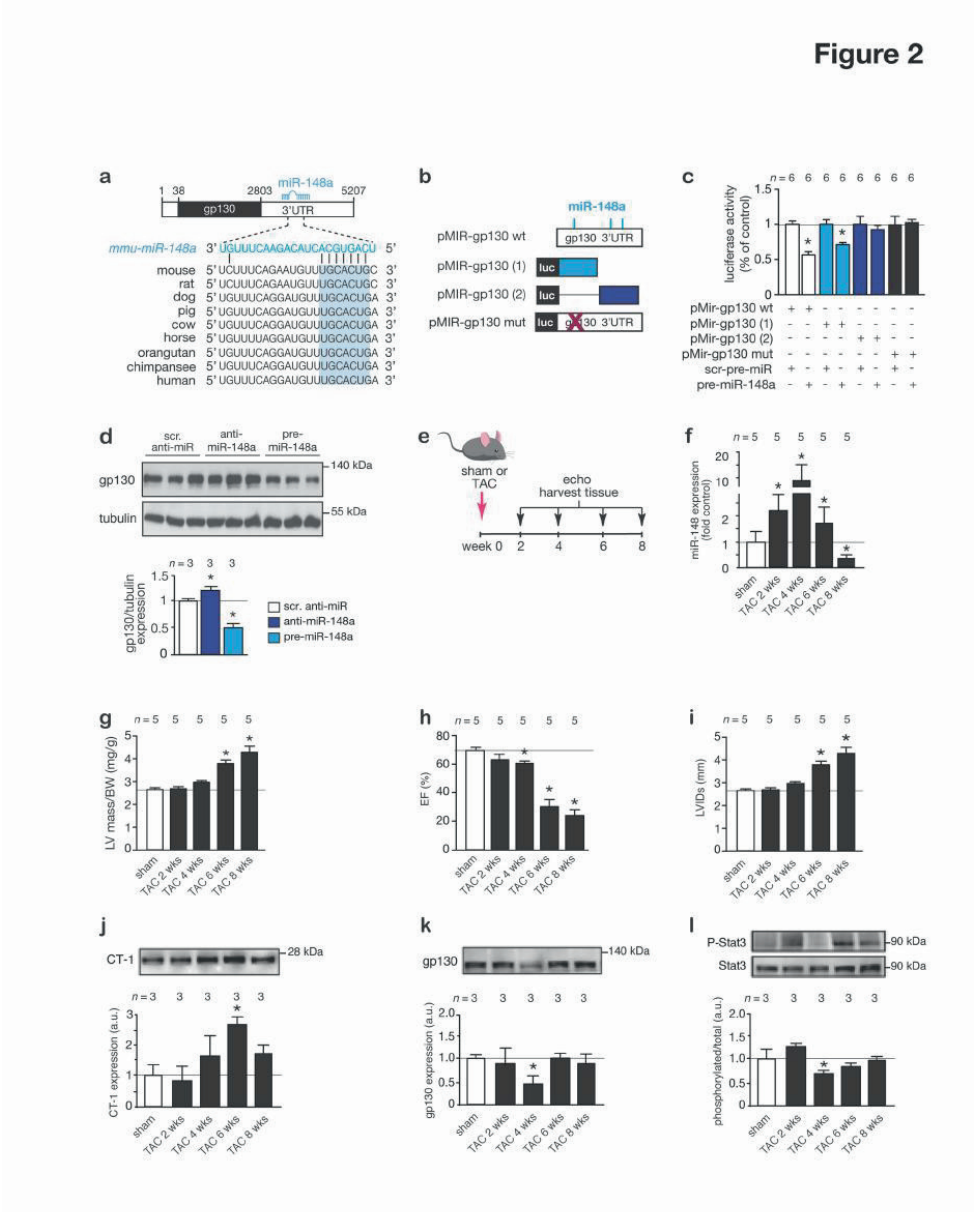
Figure 2
a
1 38
2803
miR-148a
5207
gp130
3'UTR
mmu-miR-148a 3' UGUUUCAAGACAUCACGUGACU 5'
mouse 5' UCUUUCAGAAUGUUUGGCACUGC 3'
rat 5' UCUUUCAGAAUGUUUGGCACUGC 3'
dog 5' UGUUUCAGGAUGUUUGGCACUGA 3'
pig 5' UGUUUCAGGAUGUUUGGCACUGA 3'
cow 5' UGUUUCAGGAUGUUUGGCACUGA 3'
horse 5' UGUUUUAGGAUGUUUGGCACUGA 3'
orangutan 5' UGUUUCAGGAUGUUUGGCACUGA 3'
chimpansee 5' UGUUUCAGGAUGUUUGGCACUGA 3'
human 5' UGUUUCAGGAUGUUUGGCACUGA 3'
b
miR-148a
pMIR-gp130 wt
gp130 3'UTR
pMIR-gp130 (1)
luc
pMIR-gp130 (2)
pMIR-gp130 mut
c
n = 6 6 6 6 6 6 6 6
luciferase activity (% of control)
pMir-gp130 wt
pMir-gp130 (1)
pMir-gp130 (2)
pMir-gp130 mut
scr-pre-miR
pre-miR-148a
d
scr. anti-miR
anti-miR-148a
pre-miR-148a
gp130
tubulin
140 kDa
55 kDa
n = 3 3 3
gp130/tubulin expression
scr. anti-miR
anti-miR-148a
pre-miR-148a
e
sham or TAC
echo
harvest tissue
week 0 2 4 6 8
f
n = 5 5 5 5 5
miR-148 expression (fold control)
sham
TAC 2 wks
TAC 4 wks
TAC 6 wks
TAC 8 wks
g
n = 5 5 5 5 5
LV mass/BW (mg/g)
h
n = 5 5 5 5 5
EF (%)
i
n = 5 5 5 5 5
LVIDs (mm)
j
CT-1
28 kDa
n = 3 3 3 3 3
CT-1 expression (a.u.)
k
gp130
140 kDa
n = 3 3 3 3 3
gp130 expression (a.u.)
l
P-Stat3
Stat3
90 kDa
90 kDa
n = 3 3 3 3 3
phosphorylated/total (a.u.)

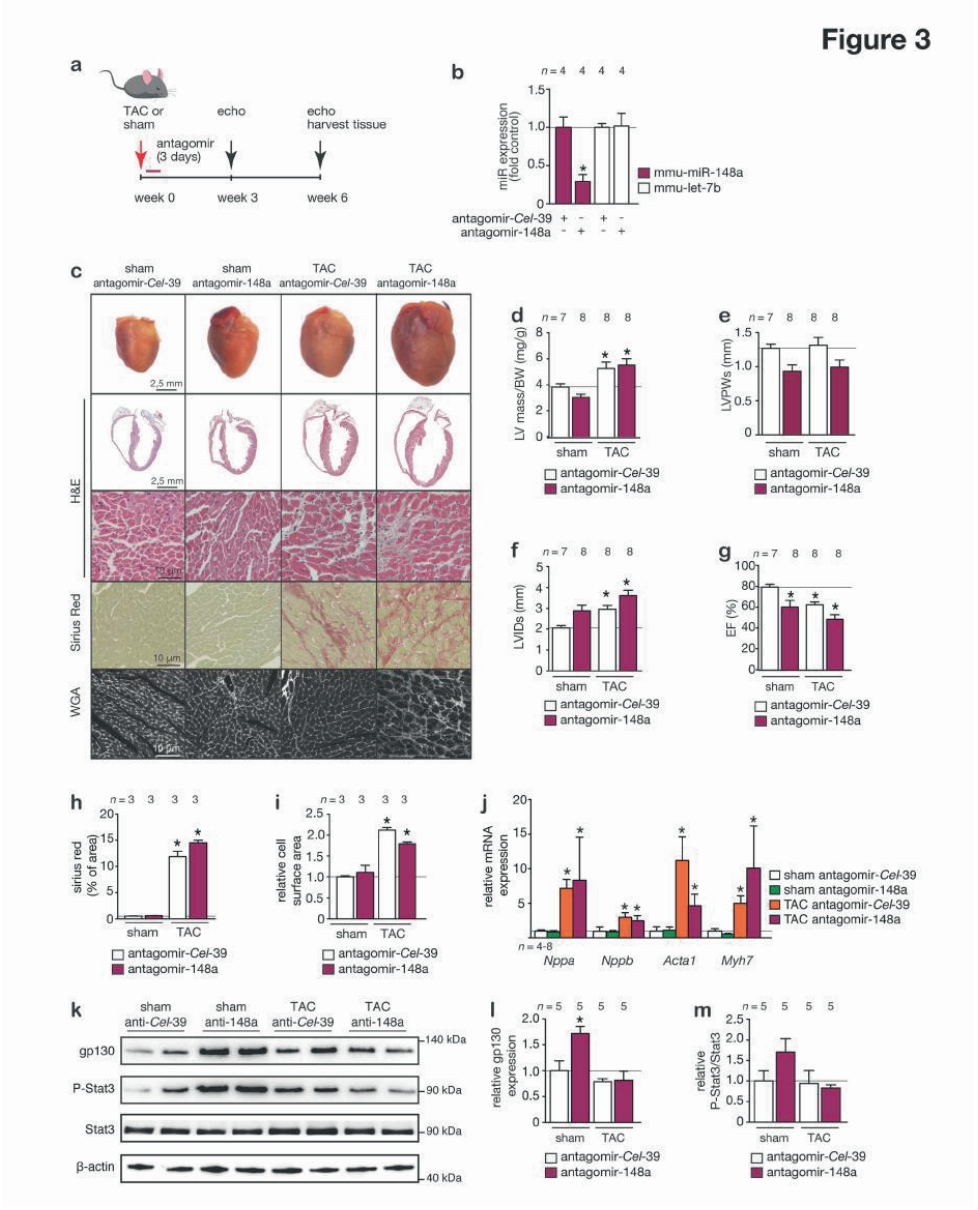
Figure 3
a
TAC or sham
echo
echo harvest tissue
antagomir (3 days)
week 0
week 3
week 6
b
n = 4 4 4 4
miR expression (fold control)
mmu-miR-148a
mmu-let-7b
antagomir-Cel-39
antagomir-148a
c
sham antagomir-Cel-39
sham antagomir-148a
TAC antagomir-Cel-39
TAC antagomir-148a
H&E
Sirius Red
WGA
d
LV mass/BW (mg/g)
e
LVPWs (mm)
f
LVIDs (mm)
g
EF (%)
h
sirius red (% of area)
i
relative cell surface area
j
relative mRNA expression
Nppa
Nppb
Acta1
Myh7
k
anti-Cel-39
anti-148a
gp130
P-Stat3
Stat3
β-actin
140 kDa
90 kDa
40 kDa
l
relative gp130 expression
m
relative P-Stat3/Stat3

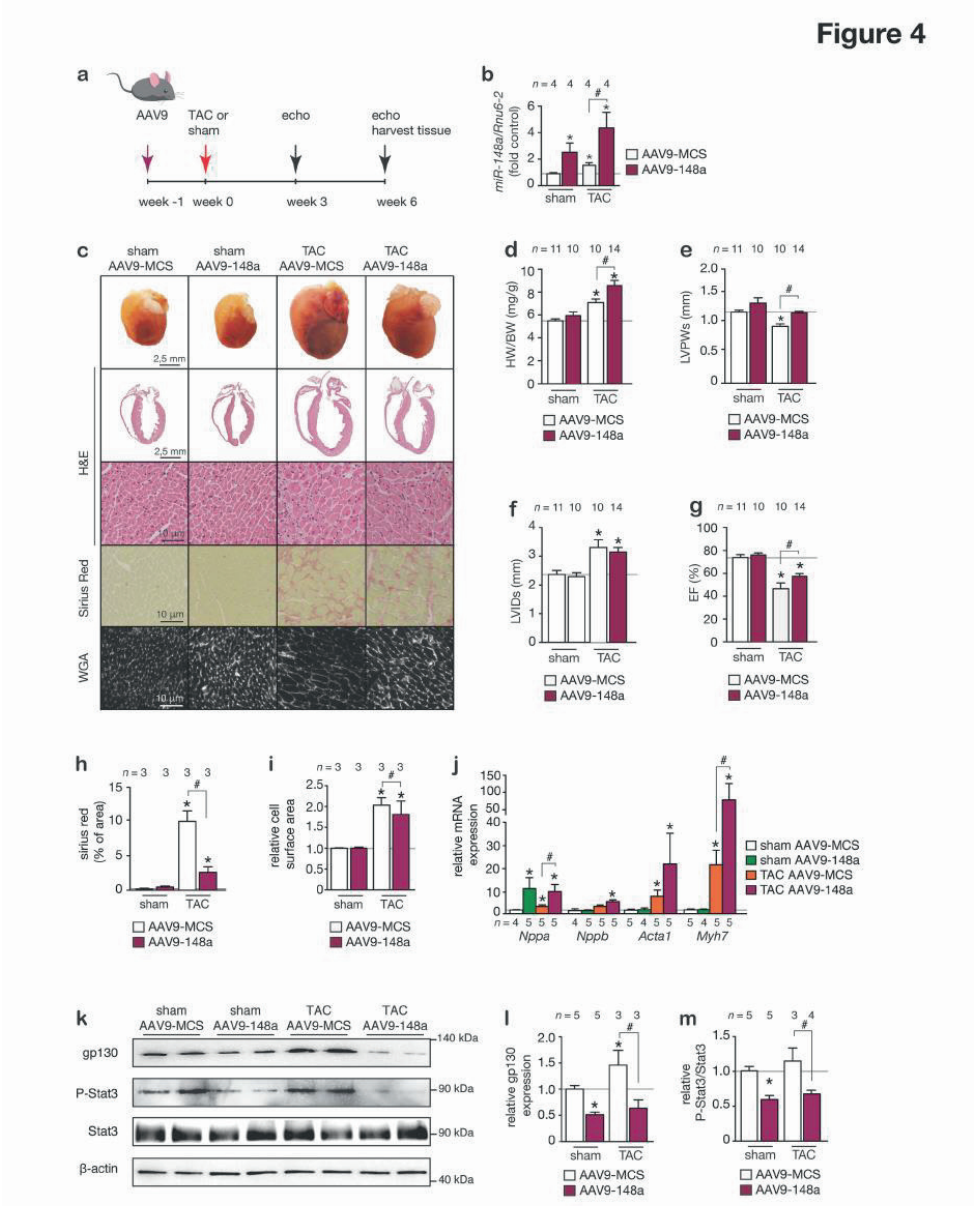
Figure 4
a
AAV9
TAC or sham
echo
echo harvest tissue
week -1
week 0
week 3
week 6
b
miR-148a/Rnu6-2 (fold control)
AAV9-MCS
AAV9-148a
sham
TAC
c
sham AAV9-MCS
sham AAV9-148a
TAC AAV9-MCS
TAC AAV9-148a
H&E
Sirius Red
WGA
2,5 mm
10 µm
d
HW/BW (mg/g)
e
LV/PWs (mm)
f
LVIDs (mm)
g
EF (%)
h
sirius red (% of area)
i
relative cell surface area
j
relative mRNA expression
Nppa
Nppb
Acta1
Myh7
k
gp130
P-Stat3
Stat3
β-actin
140 kDa
90 kDa
90 kDa
40 kDa
l
relative gp130 expression
m
relative P-Stat3/Stat3

Figure 5

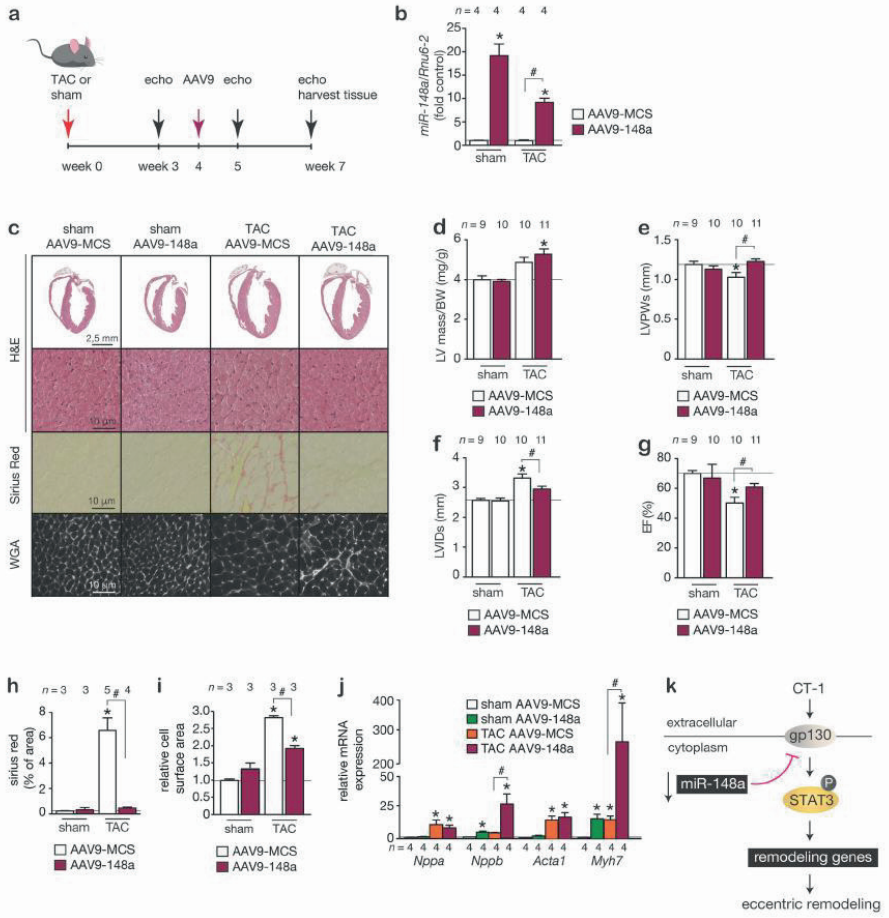
a
TAC or sham
echo
AAV9
echo
echo harvest tissue
week 0
week 3
4
5
week 7
b
n = 4 4 4 4
miR-148a/Rnu6-2 (fold control)
AAV9-MCS
AAV9-148a
sham
TAC
c
sham AAV9-MCS
sham AAV9-148a
TAC AAV9-MCS
TAC AAV9-148a
H&E
Sirius Red
WGA
2.5 mm
10 μm
d
n = 9 10 10 11
LV mass/BW (mg/g)
e
LVPWs (mm)
f
LVIDs (mm)
g
EF (%)
h
n = 3 3 5 4
sirius red (% of area)
i
n = 3 3 3 3
relative cell surface area
j
sham AAV9-MCS
sham AAV9-148a
TAC AAV9-MCS
TAC AAV9-148a
relative mRNA expression
Nppa
Nppb
Acta1
Myh7
k
CT-1
extracellular
cytoplasm
gp130
miR-148a
P
STAT3
remodeling genes
eccentric remodeling

Supplemental Figure 1

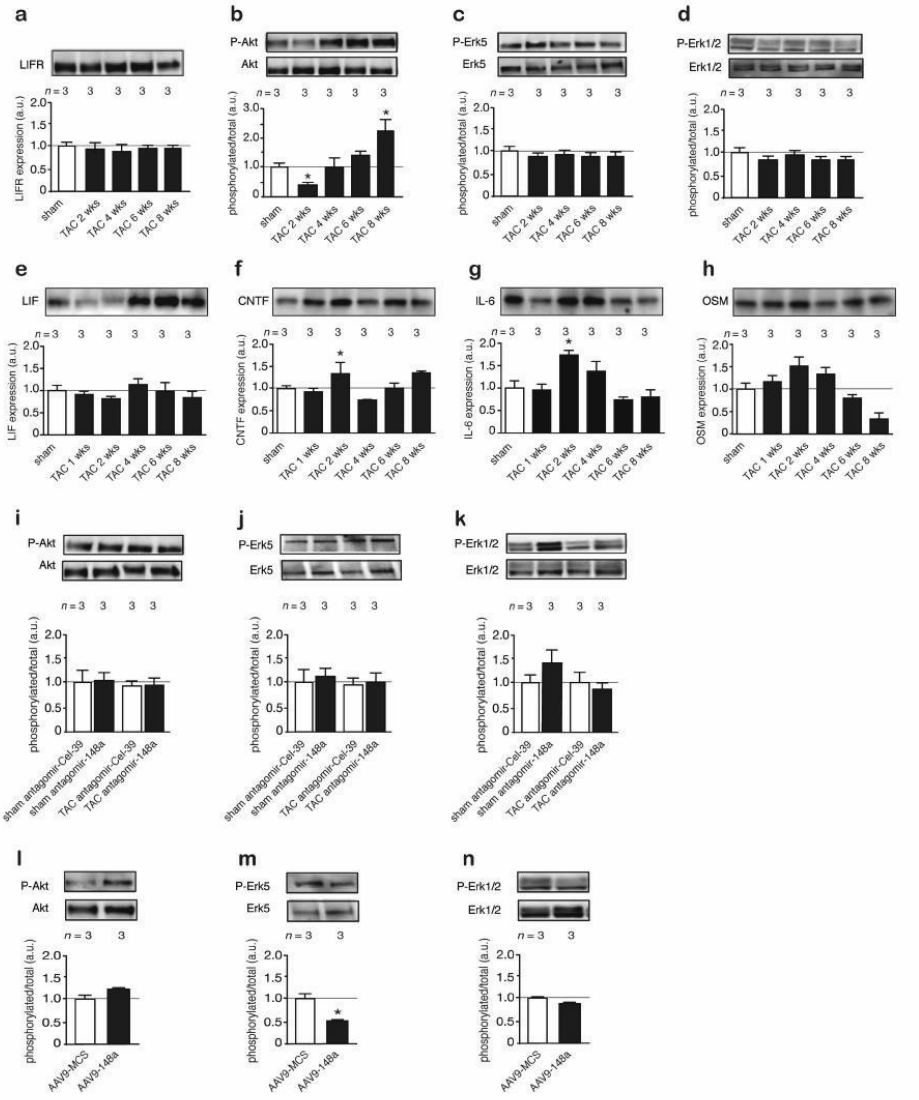

Supplemental Figure 2

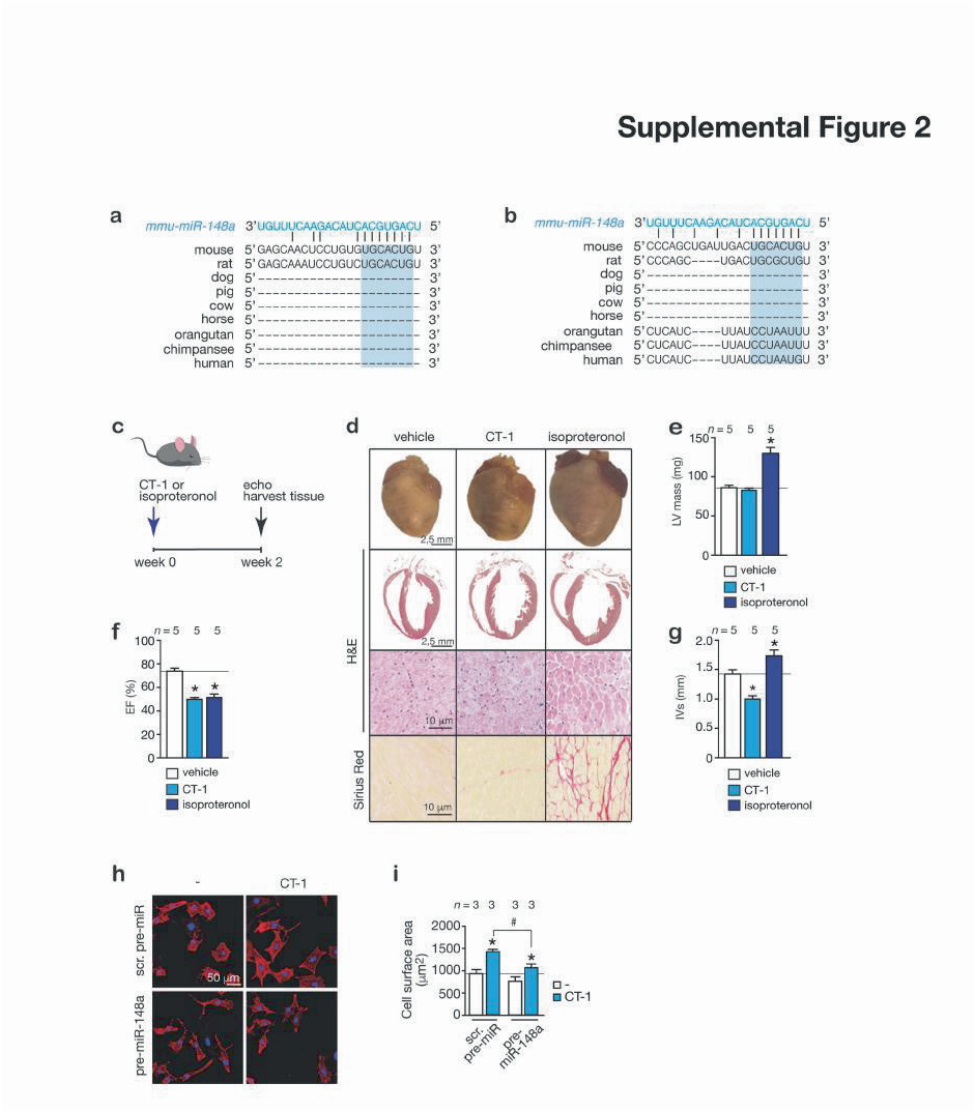

Supplemental Figure 3

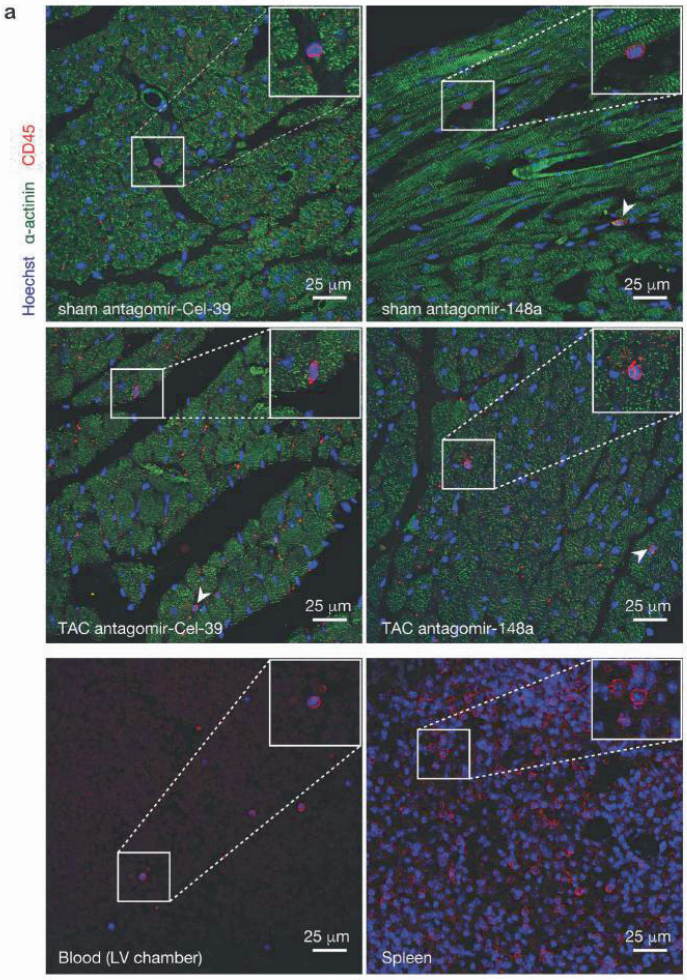

Supplemental Figure 4

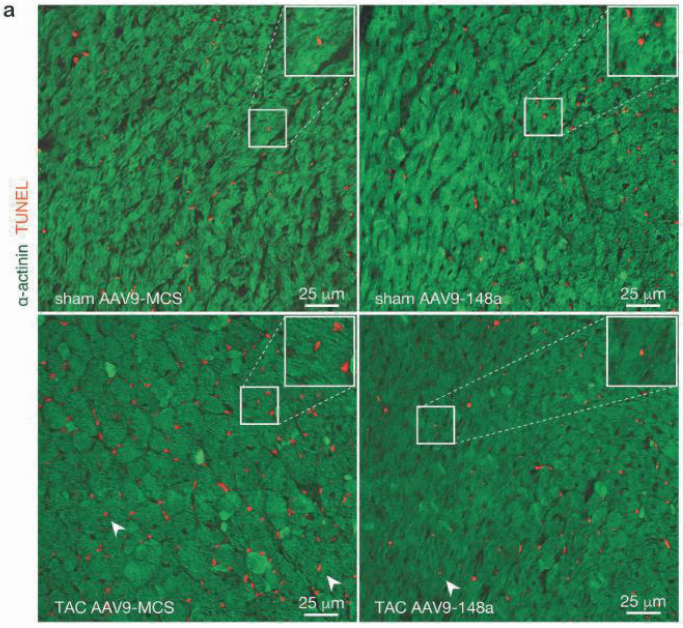

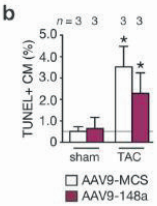

Supplemental Figure 5

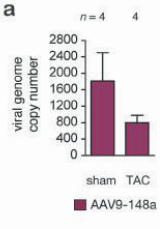

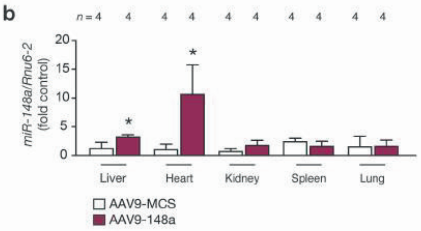

Table 1. Morphometric and echocardiographic characteristics of mice subjected to sham or TAC surgery and treated for 3 weeks with control (Ctrl) antagomir or antagomir-148a.

	Sham		TAC	
	Ctrl Antagomir	Antagomir-148a	Ctrl Antagomir	Antagomir-148a
n	5	5	8	8
BW (g)	22.8±2.1	25.3±2.0	23.8±1.5	24.3±1.7
LV mass (mg)	73±1	104±18*	120±19*	121±26*
LV mass/BW (mg/g)	3.2±0.2	3.8±0.4	5.2±0.4*	6.4±1.0*
IVSd (mm)	0.87±0.03	0.84±0.06	0.89±0.14	0.87±0.13
IVSs (mm)	1.42±0.01	1.33±0.10	1.03±0.16*	1.17±0.17
LVIDd (mm)	3.39±0.10	3.57±0.25	3.66±0.54	3.62±0.57
LVIDs (mm)	2.06±0.16	2.49±0.26	2.76±0.43*	2.78±0.50*
LVPWd (mm)	0.76±0.06	1.08±0.12*	0.87±0.15	0.86±0.14
LVPWs (mm)	1.12±0.09	1.18±0.15	0.96±0.14	1.07±0.16
EF (%)	77±4	66±5*	57±3*	56±5*
FS (%)	39±3	31±3*	25±2*	25±3*
E/A (mm/s)	1.16±0.04	1.23±0.08	1.65±0.13*	1.57±0.24*

Data are expressed as means ± SEM. BW, body weight; LV, left ventricular; IVSd, interventricular septal thickness at end-diastole; IVSs, interventricular septal thickness at end-systole; LVIDd, left ventricular internal dimension at end-diastole; LVIDs, left ventricular internal dimension at end-systole; LVPwd, left ventricular posterior wall thickness at end-diastole; LVPws, left ventricular posterior wall thickness at end-systole; EF, ejection fraction; FS, fractional shortening; E/A, Doppler E/A ratio. *, indicates $P<0.05$ vs sham group subjected to treatment with a control antagomir; #, indicates $P<0.05$ vs experimental group.

Table 2. Morphometric and echocardiographic characteristics of mice subjected to sham or TAC surgery and treated for 6 weeks with control (Ctrl) antagomir or antagomir-148a.

	Sham		TAC	
	Ctrl Antagomir	Antagomir-148a	Ctrl Antagomir	Antagomir-148a
n	7	8	8	8
BW (g)	22.5±1.6	25.6±1.6	25.6±1.2	24.0±1.6
LV mass (mg)	84±3	77±11	135±26*	135±20
LV mass/BW (mg/g)	3.8±0.3	4.0±0.2	4.8±0.4*	6.1±0.5*
IVSd (mm)	0.87±0.03	0.72±0.05	0.88±0.05	1.00±0.04
IVSs (mm)	1.39±0.05	1.08±0.10*	1.13±0.06	1.22±0.11
LVIDd (mm)	3.44±0.07	3.93±0.34	4.06±0.29	4.47±0.21*
LVIDs (mm)	2.07±0.16	2.90±0.36	2.97±0.33*	3.62±0.25*
LVPWd (mm)	0.89±0.03	0.69±0.04	1.04±0.12	0.85±0.08
LVPWs (mm)	1.28±0.09	0.94±0.09	1.33±0.11	1.00±0.11
EF (%)	78±4	59±6*	61±4*	47±4*
FS (%)	40±4	27±4*	27±2*	20±2*
E/A (mm/s)	1.33±0.13	1.32±0.17	1.52±0.17	1.27±0.04

Data are expressed as means ± SEM. BW, body weight; Ctrl, control; LV, left ventricular; IVSd, interventricular septal thickness at end-diastole; IVSs, interventricular septal thickness at end-systole; LVIDd, left ventricular internal dimension at end-diastole; LVIDs, left ventricular internal dimension at end-systole; LVPwd, left ventricular posterior wall thickness at end-diastole; LVPws, left ventricular posterior wall thickness at end-systole; EF, ejection fraction; FS, fractional shortening; E/A, Doppler E/A ratio; TAC, transverse aortic constriction. *, indicates $P<0.05$ vs sham group subjected to treatment with a control antagomir; #, indicates $P<0.05$ vs experimental group.

Table 3. Morphometric and echocardiographic characteristics of mice subjected to sham or TAC surgery and treated with AAV9-MCS or AAV9-miR-148a for 3 weeks.

	Sham		TAC	
	AAV9-MCS	**AAV9-miR148a**	**AAV9-MCS**	**AAV9-miR148a**
n	8	5	10	14
BW (g)	20.8±0.6	21.6±1.4	20.5±2.3	24.0±0.7
LV mass (mg)	69±6	77±6	125±10*	118±6*
LV mass/BW (mg/g)	3.3±0.03	3.6±1.8	5.7±0.56*	5.0±0.22*
IVSd (mm)	0.75±0.03	0.81±0.04	0.94±0.06*	0.94±0.04*
IVSs (mm)	1.13±0.04	1.19±0.05	1.24±0.07	1.33±0.04*
LVIDd (mm)	3.61±0.10	3.67±0.10	4.07±0.12*	3.98±0.06*
LVIDs (mm)	2.47±0.10	2.54±0.10	3.10±0.17*	2.97±0.11*
LVPWd (mm)	0.68±0.06	0.72±0.03	0.97±0.05	0.96±0.03*
LVPWs (mm)	1.03±0.05	1.03±0.02	1.24±0.05*	1.25±0.03*
EF (%)	67±2	69±1	53±5*	58±3*
FS (%)	31±1	31±1	23±2*	26±2*

Data are expressed as means ± SEM. AAV, adeno-associated virus; BW, body weight; LV, left ventricular; IVSd, interventricular septal thickness at end-diastole; IVSs, interventricular septal thickness at end-systole; LVIDd, left ventricular internal dimension at end-diastole; LVIDs, left ventricular internal dimension at end-systole; LVPwd, left ventricular posterior wall thickness at end-diastole; LVPws, left ventricular posterior wall thickness at end-systole; EF, ejection fraction; FS, fractional shortening; MCS, multiple cloning site; TAC, transverse aortic constriction. *, indicates $P<0.05$ vs AAV-MCS sham group; #, indicates $P<0.05$ vs experimental group.

Table 4. Morphometric and echocardiographic characteristics of mice subjected to sham or TAC surgery and treated with AAV9-MCS or AAV9-miR-148a for 6 weeks.

	Sham		TAC	
	AAV9-MCS	**AAV9-miR148a**	**AAV9-MCS**	**AAV9-miR148a**
n	11	10	10	14
BW (g)	19.1±0.5	23.8±1.0	22.6±1.2	25.1±0.9
LV mass (mg)	82±3	99±8	102±7*	116±5*
LV mass/BW (mg/g)	3.9±0.1	4.1±0.2	4.6±0.4*	4.6±0.2*
IVSd (mm)	0.84±0.02	0.93±0.02*	0.85±0.02	0.91±0.02*#
IVSs (mm)	1.21±0.05	1.39±0.03*	1.17±0.05	1.26±0.03
LVIDd (mm)	3.57±0.07	3.58±0.08	4.06±0.14*	4.09±0.08*
LVIDs (mm)	2.27±0.10	2.22±0.09	3.23±0.19*	3.08±0.11*
LVPWd (mm)	0.82±0.02	0.95±0.10	0.79±0.03*	0.92±0.02#
LVPWs (mm)	1.23±0.03	1.38±0.09	1.00±0.04*	1.22±0.03#
EF (%)	74±2	76±2	46±5*	57±3*#
FS (%)	37±2	38±2	19±2*	26±2*#
E/A (mm/s)	1.24±0.04	1.25±0.05	1.35±0.03	1.19±0.02

Data are expressed as means ± SEM. AAV, adeno-associated virus; BW, body weight; LV, left ventricular; IVSd, interventricular septal thickness at end-diastole; IVSs, interventricular septal thickness at end-systole; LVIDd, left ventricular internal dimension at end-diastole; LVIDs, left ventricular internal dimension at end-systole; LVPwd, left ventricular posterior wall thickness at end-diastole; LVPws, left ventricular posterior wall thickness at end-systole; EF, ejection fraction; FS, fractional shortening; E/A, Doppler E/A ratio; MCS, multiple cloning site; TAC, transverse aortic constriction. *, indicates $P<0.05$ vs AAV-MCS sham group; #, indicates $P<0.05$ vs experimental group.

Table 5. Morphometric and echocardiographic characteristics of mice subjected to sham or TAC surgery for 3 weeks, before treatment with AAV9-MCS or AAV9-miR-148a at 4 weeks after surgery.

	Sham		TAC	
	AAV9-MCS	**AAV9-miR148a**	**AAV9-MCS**	**AAV9-miR148a**
n	9	10	10	11
BW (g)	21.1±0.18	21.2±0.3	19.4±0.3	19.5±0.4
LV mass (mg)	79±3	85±4	97±3*	101±5*
LV mass/BW (mg/g)	3.7±0.12	4.0±0.22	5.0±0.17*	5.2±0.25*
IVSd (mm)	0.68±0.02	0.71±0.08	0.90±0.03*	0.94±0.03*
IVSs (mm)	0.99±0.04	1.05±0.10	1.23±0.04*	1.32±0.05*
LVIDd (mm)	3.31±0.06	3.39±0.34	3.69±0.06*	3.72±0.06*
LVIDs (mm)	2.14±0.06	2.15±0.21	2.59±0.05*	2.59±0.11*
LVPWd (mm)	0.72±0.04	0.77±0.09	0.92±0.02*	0.90±0.06*
LVPWs (mm)	1.03±0.02	1.08±0.10	1.22±0.03*	1.20±0.06*
EF (%)	73±2	74±3	65±2*	65±3*
FS (%)	35±1	37±2	30±2*	30±3*

Data are expressed as means ± SEM. AAV, adeno-associated virus; BW, body weight; LV, left ventricular; IVSd, interventricular septal thickness at end-diastole; IVSs, interventricular septal thickness at end-systole; LVIDd, left ventricular internal dimension at end-diastole; LVIDs, left ventricular internal dimension at end-systole; LVPwd, left ventricular posterior wall thickness at end-diastole; LVPws, left ventricular posterior wall thickness at end-systole; EF, ejection fraction; FS, fractional shortening; MCS, multiple cloning site; TAC, transverse aortic constriction. *, indicates $P<0.05$ vs AAV-MCS sham group; #, indicates $P<0.05$ vs experimental group.

Table 6. Morphometric and echocardiographic characteristics of 3 weeks sham and TAC surgery followed by a 1 week post-treatment with AAV-MCS or AAV9-miR-148a.

	Sham		TAC	
	AAV9-MCS	**AAV9-miR148a**	**AAV9-MCS**	**AAV9-miR148a**
n	9	10	10	11
BW (g)	21.2±0.22	21.3±0.35	20.7±0.47	20.91±0.34
LV mass (mg)	80.5±4	89.2±3	101±7*	102±5*
LV mass/BW (mg/g)	3.7±0.16	4.2±0.13	4.7±0.25*	4.9±0.27*
IVSd (mm)	0.73±0.03	0.78±0.03	0.83±0.04*	0.89±0.04*
IVSs (mm)	1.19±0.04	1.10±0.03	1.14±0.04	1.22±0.03*
LVIDd (mm)	3.83±0.04	3.91±0.09	4.03±0.08*	3.91±0.07*
LVIDs (mm)	2.52±0.06	2.75±0.11	3.14±0.10*	2.88±0.09*^
LVPWd (mm)	0.78±0.04	0.81±0.04	0.85±0.06	0.87±0.05
LVPWs (mm)	1.11±0.03	1.13±0.56	1.02±0.05	1.18±0.04^
EF (%)	72±2	65±9	53±2*	59±3*
FS (%)	34±1	30±2	23±2*	26±2*

Data are expressed as means ± SEM. AAV, adeno-associated virus; BW, body weight; LV, left ventricular; IVSd, interventricular septal thickness at end-diastole; IVSs, interventricular septal thickness at end-systole; LVIDd, left ventricular internal dimension at end-diastole; LVIDs, left ventricular internal dimension at end-systole; LVPwd, left ventricular posterior wall thickness at end-diastole; LVPws, left ventricular posterior wall thickness at end-systole; EF, ejection fraction; FS, fractional shortening; TAC, transverse aortic constriction. *, indicates $P<0.05$ vs AAV-MCS sham group; #, indicates $P<0.05$ vs experimental group.

Table 7. Morphometric and echocardiographic characteristics of mice subjected to 7 weeks of sham or TAC surgery and treated AAV9-MCS or AAV9-miR-148a for 3 weeks.

	Sham		TAC	
	AAV9-MCS	**AAV9-miR148a**	**AAV9-MCS**	**AAV9-miR148a**
n	9	10	10	11
BW (g)	22.0±0.3	22.0±0.5	21.2±0.3	22.0±0.5
LV mass (mg)	88±4	86±3	105±6*	116±5*
LV mass/BW (mg/g)	4.0±0.2	3.9±0.1	4.8±0.3*	5.3±0.3*
IVSd (mm)	0.73±0.03	0.79±0.04	0.83±0.05*	0.90±0.03*
IVSs (mm)	1.07±0.03	1.07±0.06	1.15±0.05	1.20±0.04*
LVIDd (mm)	3.85±0.04	3.79±0.06	4.20±0.10*	4.02±0.08*
LVIDs (mm)	2.62±0.04	2.59±0.08	3.31±0.15*	2.90±0.08*#
LVPWd (mm)	0.89±0.08	0.84±0.04	0.80±0.05	0.94±0.05#
LVPWs (mm)	1.17±0.05	1.13±0.04	1.01±0.06	1.23±0.05#
EF (%)	70±2	68±9	50±4*	61±2*#
FS (%)	32±1	31±2	21±2*	27±1#

Data are expressed as means ± SEM. AAV, adeno-associated virus; BW, body weight; LV, left ventricular; IVSd, interventricular septal thickness at end-diastole; IVSs, interventricular septal thickness at end-systole; LVIDd, left ventricular internal dimension at end-diastole; LVIDs, left ventricular internal dimension at end-systole; LVPwd, left ventricular posterior wall thickness at end-diastole; LVPws, left ventricular posterior wall thickness at end-systole; EF, ejection fraction; FS, fractional shortening; MCS, multiple cloning site; TAC, transverse aortic constriction. *, indicates $P<0.05$ vs AAV-MCS sham group; #, indicates $P<0.05$ vs experimental group.

Table 8. Patient characteristics

	Gender	Age at HTx (yrs)	LVAD	LVEF %	LV ED/ES (mm)	LVPWT (mm)
DCM 1	female	48	yes	10	68/65	7
DCM 2	male	55	no	10	69/65	8
DCM 3	male	57	yes	10	47/43	10
DCM 4	male	47	no	10	51/49	10
DCM 5	male	66	no	10	58/54	10
DCM 6	female	21	yes	10	61/54	6
DCM 7	female	58	yes	10	65/57	8
DCM 8	male	36	yes	10	69/63	8
DCM 9	female	58	yes	10	67/62	6
DCM 10	male	61	yes	10	62/60	7
HCM 1	male	57	no	55	43/42	16
HCM 2	male	31	no	15	85/81	13
HCM 3	male	37	no	20	66/54	13
HCM 4	male	36	no	25	47/39	15
HCM 5	female	31	no	50	29/10	18
HCM 6	female	36	no	40	45/20	14
HCM 7	male	25	no	45	40/20	20
HCM 8	female	36	no	45	45/28	15
HCM 9	female	34	no	20	52/40	13
control 1	unknown	unknown	no	-	-	-
control 2	unknown	unknown	no	-	-	-
control 3	male	65	no	-	-	-
control 4	female	72	no	-	-	-
control 5	male	39	no	-	-	-
control 6	female	48	no	-	-	-
control 7	male	38	no	-	-	-
control 8	female	53	no	-	-	-
control 9	male	32	no	-	-	-
control 10	male	43	no	-	-	-
control 11	male	48	no	-	-	-

DCM, dilated cardiomyopathy; HCM, hypertrophic cardiomyopathy; LVAD, patient received left ventricular assist device;. LVEF, left ventricular ejection fraction; LV ED, left ventricular end-diastolic dimension; LV ES, left ventricular end-systolic dimension; LVPWT, left ventricular posterior wall thickness; yrs, years; mm, millimeter; -, information not available.

CHAPTER 5

SUMMARY
and
GENERAL DISCUSSION

The events leading the cardiac muscle towards sustained dysfunction, which could precipitate in the HF syndrome, have a wide range of origins. We described the variety of heart diseases causing pathological remodeling through recognized molecular pathways **(chapter 1)**. However, we are still far from having a complete picture of the effectors responsible of the orchestration and coordination of these processes. An attractive research field is the one that deals with non-coding RNA. In particular miRNAs represent versatile tools able to efficiently regulate the gene expression underlining specific cellular responses. Once we are able to recognize the role of these molecular players, this would give us the knowledge to produce gene modulatory therapies aimed to target defined pathological conditions.

Acting with this purpose, we started reviewing the recent and most relevant findings on miRNAs-based treatments inducing heart tissue regeneration and cardiac function improvement specifically after myocardial injury **(chapter 2)**. We addressed in detail the three possible strategies for myocardial regeneration: cardiac stem/progenitor cell differentiation, fibroblast reprogramming and cardiomyocyte proliferation. Moreover, we reported the interesting achievements obtained by consolidated or emerging therapeutic heart delivery strategies such as rAAV-vectors and nanoparticles. Furthermore, we indicated possible future research directions in order to improve their specificity.

From hyperplasia to hypertrophy and back

The heart is endowed with a remarkable capacity of increasing its size during its entire life span. This process is governed by the increase of cardiomyocyte number (hyperplasia) during the embryonic/fetal phase, while it moves to an increase of cardiomyocyte size (hypertrophy) after birth and for the rest of life. Precisely, even in humans, cardiomyocytes keep a limited, but still present, proliferative/regenerative ability for a short time span after birth [1, 2]. After this short period they enter in cell cycle arrest and acquire a hypertrophic and polyploid phenotype in response to overload or myocardial insults [3]. This reduced cellular plasticity is at the basis of the higher vulnerability of the heart when faced with pathological conditions with the effects of extended cell death and pathological hypertrophy [4]. The resulting clinical consequence is HF. In this work we described the potential of an evolutionary conserved miRNA cluster miRNA-106b~25 that is operative in this pathological condition **(chapter 3)**. We reported that miRNA-106b~25 is highly expressed in the heart during the early phases of post-natal life, then the expression levels of all three miRNAs decrease in the following days and remain low during adulthood. This dynamic is in accordance with the mentioned reported trend of cardiomyocyte proliferation. Remarkably, in murine models, the complete knockout of miRNA-106b~25 results in cardiomyocyte hypertrophy and

eccentric remodelling. This phenotype matches with the even further reduction of expression in human cardiac biopsies of end-stage heart failure patients. The molecular result of this pathological condition is a derepression of the pro-hypertrophic target bHLH transcription factor Hand2[5]. Moreover, we detected myocyte enhancer factor-2 d (MEF2d) as an additional downstream target of miRNA-106b~25. In accordance, MEF2d overexpression was reported to be responsible of reprogramming gene expression towards pathological cardiac remodeling [6]. Conversely, miRNA-106b~25 overexpression, using adeno-associated virus vector serotype 9 (AAV9), enhanced cardiomyocyte proliferation targeting a network of genes involved in cell cycle progression such as the E2F5, Cdkn1c, Ccne1 and Wee1. These findings reflect the reported observations of expression, both during fetal and neonatal life, of proto-oncogenes, specific cyclins and cyclin-dependent kinases, while, in adulthood, cell cycle inhibitors are more predominant [7, 8]. Taken together, our results suggest a molecular explanation for the underlining mechanism driving cardiomyocytes towards cell cycle arrest and terminal differentiation. In the early phase of life, miRNA-106b~25 is higher expressed and consequently down-regulates several cell cycle inhibitors and pro-hypertrophic effectors promoting a phenotype of cardiomyocyte hyperplasia. On the contrary, moving towards adulthood and in conditions of cardiac damage, the lower expression of miRNA-106b~25 no longer represses the mentioned targets resulting in a phenotype of cardiomyocyte hypertrophy. Guided by this knowledge, we treated a mouse model of chronic ischemic injury with the administration of AAV9-miRNA-106b~25, resulting in the regeneration of the injured adult myocardium and the conservation of heart function. In conclusion, all these findings demonstrate the possibility of using an endogenous epigenetic mechanism as a therapy able to induce cardiac regeneration.

Between concentric and eccentric hypertrophy

We already discussed how, on the cellular and morphological level, a certain kind of pathological hypertrophy can arise from specific heart insults (chapter 1). Pressure overload is the main origin of concentric hypertrophy, while volume overload conditions tend to display eccentric hypertrophy [9]. Here, using samples from HF patients and HF mouse models, we reported a differential expression of the evolutionary conserved miRNA-148a showing higher level in concentric remodelling and lower expression in conditions with eccentric remodelling **(chapter 4)**. Our data also shows that miRNA-148a is able to regulate the cardiac IL-6 superfamily signalling cascades by targeting the co-receptor gp130. In line, miRNA-148a down-regulation, using a specific antagomir approach, resulted in increased expression of gp130 in the heart and the coupled intracellular signalling combined with a maladaptive cardiac phenotype characterized by worsened function, wall thinning and chamber

dilatation following stress conditions. Conversely, cardiac-restricted miRNA-148a overexpression, by AAV9-148a delivery, resulted in reduced gp130 expression with a protective effect promoting wall thickness towards concentric remodelling. These data give indications of molecular events underling distinct forms of cardiac hypertrophy and able to balance the morphological remodelling of the heart.

The activation of these cardiac pathological mechanisms should be connected with agonists enhanced in the stress response. Cardiotropin-1 (CT-1), a member of the IL-6 cytokine superfamily, acts via gp130 homodimer or gp130/leukemia inhibitory factor receptor-β (LIFRβ) heterodimer interaction [10]. In cultured cardiomyocytes, it is described to promote the assembly of sarcomeres in series. The consequence is the hypertrophic increase in cell length but not a significant modification of cell width, and this longitudinal elongation involves the intercellular signal transducers STAT3 and ERK5 [11]. In accordance, we performed a study with continuous CT-1 infusion at a dose of 20 μg/kg/day resulting in an eccentric hypertrophic phenotype with reduced cardiac function and wall thinning. The transfection of miRNA-148a precursor on CT-1 treated cardiomyocytes induced a reduction of the hypertrophic effect indicating the interaction between CT-1 signalling and miRNA-148a. Regarding the involvement of the subunit gp130, it is described to be pivotal in a variety of signalling events activated by the IL-6 cytokine superfamily [12, 13]. In particular, on one side gp130-signaling is necessary for cardiomyocyte survival pathways but on the other side it allows for the transmission of pro-hypertrophic signals. In fact, mice with ventricular-restricted deficiency of gp130 demonstrate a rapidly progressing heart failure phenotype driven by a massive cardiomyocyte apoptosis [14]. On the contrary, over-activation of the transducer MEK5 in the murine heart results in severe eccentric cardiac hypertrophy progressing towards dilated cardiomyopathy and sudden death [15]. Taken together these observations suggest that the IL-6 cytokine/gp130 signalling plays an important and modulatory role in the regulation of distinct subtypes of cardiac hypertrophic. In this scenario, our work provides a framework to understand the action of miRNA-148a and reveals a biphasic mechanistic regulation that can shed new light on the clinical observation of the transition from a compensatory, early stage hypertrophic response to later stage dysfunctional heart failure.

Concluding remarks and future perspectives

Despite a variety of different heart diseases driving to HF syndrome, there is still a lack of specific treatments able to efficiently cure the injured heart. The precise action of these future therapies will become reality through a better understanding of the molecular mechanisms regulating the different morphological modifications of the heart. In this thesis we presented examples indicating the involvement of

specific miRNAs, a defined class of the non-coding RNAs, to regulate processes in these mechanisms. Specifically, our data show how the miRNA106b~25 cluster enhances cardiomyocyte hyperplasia instead of cardiomyocyte hypertrophy by targeting a network of cell cycle inhibitors and pro-hypertrophic factors. Moreover, we reported how the overexpression of miRNA106b~25 is able to promote cardiac regeneration and heart function in a model of permanent myocardial infarction. In the second part, we focused on the dynamic of expression and regulation of miRNA-148a in the concentric and eccentric hypertrophy response. We showed how miRNA-148a exerts a protective effect against eccentric remodelling progression. Our findings support the idea that miRNA-148a can target the co-receptor gp130 and participates at the modulation of the biphasic-regulating mechanism represented by the IL-6 cytokine/gp130 signalling cascades. In conclusion, and recognizing that further tests and trials are needed, we consider our work a valid contribution aimed to expand the concept of tailored, more personalized medicine by using microRNAs as therapeutic targets in the treatment of heart diseases.

References

1. Porrello, E.R., et al., *Transient regenerative potential of the neonatal mouse heart.* Science, 2011. **331**(6020): p. 1078-80.
2. Haubner, B.J., et al., *Functional Recovery of a Human Neonatal Heart After Severe Myocardial Infarction.* Circ Res, 2016. **118**(2): p. 216-21.
3. Brodsky, V., et al., *Polyploidy in cardiac myocytes of normal and hypertrophic human hearts; range of values.* Virchows Arch, 1994. **424**(4): p. 429-35.
4. Olson, E.N. and M.D. Schneider, *Sizing up the heart: development redux in disease.* Genes Dev, 2003. **17**(16): p. 1937-56.
5. Dirkx, E., et al., *Nfat and miR-25 cooperate to reactivate the transcription factor Hand2 in heart failure.* Nat Cell Biol, 2013. **15**(11): p. 1282-93.
6. Kim, Y., et al., *The MEF2D transcription factor mediates stress-dependent cardiac remodeling in mice.* J Clin Invest, 2008. **118**(1): p. 124-32.
7. Busk, P.K., et al., *Involvement of cyclin D activity in left ventricle hypertrophy in vivo and in vitro.* Cardiovasc Res, 2002. **56**(1): p. 64-75.
8. Pasumarthi, K.B., et al., *Targeted expression of cyclin D2 results in cardiomyocyte DNA synthesis and infarct regression in transgenic mice.* Circ Res, 2005. **96**(1): p. 110-8.
9. Gaasch, W.H. and M.R. Zile, *Left ventricular structural remodeling in health and disease: with special emphasis on volume, mass, and geometry.* J Am Coll Cardiol, 2011. **58**(17): p. 1733-40.
10. Wollert, K.C., et al., *Cardiotrophin-1 activates a distinct form of cardiac muscle cell hypertrophy. Assembly of sarcomeric units in series VIA gp130/leukemia inhibitory factor receptor-dependent pathways.* J Biol Chem, 1996. **271**(16): p. 9535-45.
11. Lopez, N., J. Diez, and M.A. Fortuno, *Differential hypertrophic effects of cardiotrophin-1 on adult cardiomyocytes from normotensive and spontaneously hypertensive rats.* J Mol Cell Cardiol, 2006. **41**(5): p. 902-13.
12. Heineke, J. and J.D. Molkentin, *Regulation of cardiac hypertrophy by intracellular signalling pathways.* Nat Rev Mol Cell Biol, 2006. **7**(8): p. 589-600.
13. Sugden, P.H. and A. Clerk, *"Stress-responsive" mitogen-activated protein kinases (c-Jun N-terminal kinases and p38 mitogen-activated protein kinases) in the myocardium.* Circ Res, 1998. **83**(4): p. 345-52.
14. Hirota, H., et al., *Loss of a gp130 cardiac muscle cell survival pathway is a critical event in the onset of heart failure during biomechanical stress.* Cell, 1999. **97**(2): p. 189-98.
15. Nicol, R.L., et al., *Activated MEK5 induces serial assembly of sarcomeres and eccentric cardiac hypertrophy.* EMBO J, 2001. **20**(11): p. 2757-67.

VALORIZATION

Contribution to society and innovation

According with the most recent report of the World Health Organization (WHO), cardiovascular disease (CVD) still represents the biggest cause of death worldwide [1]. In particular, during the last 15 years, ischemic heart disease, followed by stroke, occupied the leading positions of the global top 10 causes of death. Together they account for 15.2 million out of the 56.9 million deaths worldwide in 2016.

Interestingly, even if CVD appears to be an established health problem in the High/Upper-middle-income countries, it shows an incidence spike in the Low/lower-middles-income countries. This effect is ascribable to the globalization of westernized life style conjointly with a more limited access to CVD treatments [2].

Among the different heart diseases, ischemic heart disease is a major cause of heart failure (HF). Moreover, regardless the causing reasons, a diagnosis of HF results in patient death for up to 50% in a time frame of 5 years [3, 4]. Recent observations report that HF incidence appears to be stable in High/Upper-middle-income countries, yet in more recent years its prevalence showed an increase due to improvement on stabilizing treatment and ageing of population [5]. Unfortunately, increased hospitalization and health care costs are predicted to grow more in future decades. For these reasons, truly curative therapies that can effectively lead to a better health state of HF patients is a pivotal goal of cardiovascular research.

In this context, the findings reported in this thesis add a new piece of knowledge to better understand the molecular response to cardiac injury. Moreover, by focusing on the involvement of miRNAs, our work proposes new possibilities of therapeutic targets for cardiac therapies.

Target groups and implementation

The involvement of miRNAs in heart diseases shows a potential benefit for HF patients. In particular, it opens new therapeutic strategies to treat cardiac remodeling. Even though we recognize that further investigations are still needed, with our work we suggest patient target groups that may have beneficial effect from the results provided in this thesis.

Specifically, the described role of the cluster miRNA-106b~25 in the regulation of cardiomyocyte hyperplasia and hypertrophy is giving new insight on the control of anti-cell-cycling and pro-hypertrophic factors responsible for the switch of these phenotypes from pre- to postnatal life. In line, its reported regenerative action draws a clear link to a potential application on patients afflicted from a new acute myocardial infarction (AMI) or any injury causing a widespread loss of cardiomyocytes and the consequent compensatory hypertrophic response of the surviving myocardium. In addition, if the regenerative therapy would show clinical benefit, this patient target group can be potentially extended to

patients that have experienced older myocardial injuries that have now been converted to stable scars.

With regards to miRNA-148a, its modulation between conditions of concentric and eccentric hypertrophic remodeling could offer benefit to delay or block the dilation of the heart. Patients affected by high blood pressure or dilated cardiomyopathy may take advantage by a therapy able to reduce or stop the disease progression.

As we said, further investigations have to clarify the concrete potential application of our findings on therapeutic strategies aimed to cure cardiac patients inducing cardiac function conservation or rescue. Still in the preclinical phase, the validation of our findings in larger animal models is a mandatory step. Studies using porcine models represent the ideal option due to their anatomical and physiological similarities to humans. There are several types of porcine models with cardiac pathologies, nowadays widely used by research groups from all over the world. For example, the transient occlusion of the left anterior descending artery (LAD) through the inflation-deflation of an angioplasty catheter can better mimic the ischemia-reperfusion condition to which AMI patients are subjected as a consequence of the reperfusion treatment they receive in coronary care units [6].

At this preclinical level, it will also be important to develop the delivery route of therapies together with the vehicle used to carry miRNAs to the heart. For both these points, recent works of Catalucci's group suggests an interesting approach [7, 8]. Treating patients with an aerosol of bio-inspired nanoparticles loaded with miRNAs could avoid invasive procedure of administration and increase the safety of the treatment. In fact, as already discussed in the chapter 2, the use of some AAV serotypes represents a powerful tool that we cannot completely control yet.

A second and mandatory feature of drug development that needs precise investigation is the non-toxicity of the treatment, usually represented by dose-escalation studies in two species, for example one rodent and one non-rodent species such as non-human primates. This point is linked with the two mentioned before in terms of level of miRNA overexpression and timing of the therapy. Being able to discriminate the effects on the short- and long-term of the treatment will give a solid basis to move to clinical studies.

Finally, the three phases of the clinical trial are the more challenging and historically more failure-prone parts of the entire research & development path. At this level the acquired knowledge of molecular reasoning, pharmacodynamics properties and safety of the proposed therapy should help us to better identify the sample of patients to include in our study. Fundamental in this part is the definition of the expected results/objectives depending on the phase of the trial. This careful planning will increase the chance of an efficient interpretation of the resulting experimental outputs and hopefully will offer successful therapeutic achievements also in terms of the cost-benefit ratio of the costs of the new therapeutic modality and patient benefit.

Activities and dissemination

The findings reported in this thesis are the result of the work of an international network composed by motivated and committed scientists collaborating from different international scientific centers. These data have been presented and discussed in international conferences from the European Society of Cardiology, the American Heart Association, EMBO organization, Keystone meetings, as well as more specialized conferences on noncoding RNA. Moreover, the scientific outputs have been submitted and published on international peer-reviewed journals with a proactive approach of sharing our findings to the entire scientific community.

References

1. https://www.who.int/news-room/fact-sheets/detail/the-top-10-causes-of-death, W.H.O. *The top 10 causes of death*. 24 May 2018.
2. Agyemang, C. and B.J. van den Born, *Limited access to CVD medicines in low-income and middle-income countries: poverty is at the heart of the matter.* Lancet Glob Health, 2018. **6**(3): p. e234-e235.
3. Greenberg, B., *Gene therapy for heart failure.* Trends Cardiovasc Med, 2017. **27**(3): p. 216-222.
4. Ammar, K.A., et al., *Prevalence and prognostic significance of heart failure stages: application of the American College of Cardiology/American Heart Association heart failure staging criteria in the community.* Circulation, 2007. **115**(12): p. 1563-70.
5. Savarese, G. and L.H. Lund, *Global Public Health Burden of Heart Failure.* Card Fail Rev, 2017. **3**(1): p. 7-11.
6. Wei, K., et al., *Epicardial FSTL1 reconstitution regenerates the adult mammalian heart.* Nature, 2015. **525**(7570): p. 479-85.
7. Miragoli, M., et al., *Inhalation of peptide-loaded nanoparticles improves heart failure.* Sci Transl Med, 2018. **10**(424).
8. Di Mauro, V., et al., *Bioinspired negatively charged calcium phosphate nanocarriers for cardiac delivery of MicroRNAs.* Nanomedicine (Lond), 2016. **11**(8): p. 891-906.

ACKNOWLEDGEMENTS

I took the decision of performing my PhD abroad with the ambitious aim of evolving my professional profile towards a more international status, having the opportunity to join a scientific top-level environment.

What it comes out has been an experience that overcomes the expectations.

A surprising and more complex adventure, full of exiting events and demanding challenges. The new step in the travel of my life able to shape me not only as a scientist but specially as a man.

Physically I moved further to north, to the Netherlands, to Maastricht, but in reality I mainly had to travel deeper in my own personality. I tasted the bitter of putting in discussion my beliefs and faced the scary occasion of moving to a next unexpected level.

The result is a new me, the product of the support, fair exchange and collaboration with a lot of people that have surrounded me during this period.

MY DEEP GRATITUDE GOES TO ALL OF YOU!!!!

Leon, you have been an exceptional mentor, the one to refer in the difficulties and with whom I shared enthusiasm and push-forward attitude. I felt supported and respected. Thanks for the trust and the friendship you have granted to me.

Ellen, there are no words to define what you have been for me, the angel that introduced me to this extraordinary experience, the first to believe in my skills.

From you I learnt what commitment, ambition but also right priority means. Thanks for the good caring and clear teachings you have given.

Lara, in you I found an anchor. The estimated colleague to consult about work issues and the sweet friend where to ran in any desperate moments. Thanks for your authentic loyalty.

Paula, Martina, Servé, Lilian and **Barbara** but also **Mora, Hamid, Nicole, Julie, Antonio, Ella, Rio** and **Burcu,** you are the seniors that have been daily happily tormented by me during this long period. It is difficult to deal with a subject like me but I truly appreciate your understanding. Thanks for the tutorials, scientific discussions and strong exchanges of opinions; for the morning chats, coffee and vlaai in the kitchen and travels we have experienced together. I feel enriched by what you have done for me.

To all my PhD mates, with you time in the lab and around in the city was priceless. **Vasculino**, I will keep in my heart the runs to Chateaux and all the conversations we had. **Marida,** thanks for the laughs and the fresh southern air you have gifted to me. **Federica,** It was nice to make fun of each other especially during our “archaeological” researches. **Indira,** girl from the island, I appreciate your tenacity

and kindness. **Raquel**, the one that mostly put me in discussion, I have seen a different me in you, thank you. **Zenab,** funny girl, thanks for the serenity you transmit. **Nicolò,** a hurricane that pleasantly upset our days, well done! **Ricardiño** and **Andreia,** examples of perseverance and professional attitude. All the new PhD-students **Robin**, **Jana** and **Jordi,** time together was short, I wish you success in your objectives and to find the satisfaction I had in my time.

To all the former and current members of the Cardiology Department, especially to **Stephane, Blanche, Marc, Paul, Rick, Wouter, Paolo**, **Roel, Sandrine, Emma, Vincenza, Joyce, Cristina, Robin, Monika, Steffie, Lena, Michiel, Annika** and **Quentin.** Thanks for all the moments we shared in the lab, offices, along the corridor and in the kitchen. With some of you I also had amazing party adventures that I will never forget. Hope to leave in all of you a good memory of this crazy Italian, from my side I will keep the precious lessons raised from this variegate meet of cultures, personalities and professionalisms.

Lauren and **Beatricelle,** two sweet hearts that make me feel part of a family (including **Lara**). Good food, vine and music were the elements characterizing our dinners, but friendship, hugs, smiles and sincerities were the glue keeping all of us together; just before of crashing into the next party with **Margaux** and **Kim**. Crazy girls, thanks to have been there!!!

To all the ones physically far away but close to me with their souls, to all **the friends spread in Italy and in Europe**. Thanks for the support and good consideration despite any difficulties.

To my **big family**, to my mamma and papà, to my brothers, sisters and their families, to my nephews and to my mother and father in law. You have been the solid base on which I am built and on which I will always grow. The ones that know me better, ready to exult for my achievements or to collect my pieces whatever is going to happen. Without you I would be lost.

To my wife **Fanj,** the perfect partner by my side. Love and friend of my life. Thanks for the understanding, the support and for the tough decision of doing this experience far from each other. All of this is shared with you because together we are one.

Biography

Andrea Raso was born the 24th of August 1988 in Polistena, (Reggio Calabria, Italy). On March 2014 he graduated cum laude at the medical biotechnology master of the University of Trieste, Italy. He spent the last year of his master working in the molecular medicine laboratory of the International Centre for Genetic Engineering and Biotechnology (ICGEB, Trieste, Italy), under supervision of Prof. Dr. Mauro Giacca and Dr. Serena Zacchigna and in collaboration with Prof. Dr. Perikles Simon, from the sports medicine department of Johannes Gutenberg University, Mainz (Germany). He focused his research on the " Characterization of different Adeno Associated Virus (AAV) serotypes as gene doping vector", a project supported by the World Anti-Doping Agency (WADA). During this period, Andrea developed a strong interest in the molecular mechanisms modulating the gene expression. Therefore, awarded of the Kootstra Talent fellowship, from October 2014 till December 2018, Andrea worked as PhD-student in the department of cardiology at Maastricht University under supervision of Prof. Dr. Leon J. de Windt. His work concentrated on non-coding RNAs controlling various cardiomyocyte phenotypes.